POLITECNICO DI MILANO

Facoltà di Ingegneria Industriale

Corso di Laurea in
Ingegneria Meccanica

Mechanical Characterization of Shape Memory Polymers

Relatore: Prof. Francesco BRAGHIN

Co-relatore: Prof. Pierre LAMBERT

Tesi di Laurea di:

Simone MARCOLINI

Matr. 782649

Anno Accademico 2012 - 2013

Table of contents

II

Index of figures

Index of figures

IV

Index of figures

Index of tables

Index of figures

Abstract

Shape memory polymers (SMPs) are smart materials that can remember a primary shape and can return to this primary shape from a deformed secondary shape when given an appropriate stimulus. Moreover, they are lightweight, have high strain/shape recovery ability, easy to process and their properties can be tailored for a wide range of applications. In most cases, they are also biocompatible. The combination of all these properties made this family of materials suitable for the application in a project (ARC PREDICTION project) to which the present work is subservient. In particular the present work was aimed to an accurate thermo-mechanical characterization of some types of thermo-activated shape memory polymers. For this purpose a tailored test bench was developed. Starting from a first hypothesis of the machine inspired by the solutions found in literature, a long optimizing process was carried out through the application of several interesting and innovative solutions. The result was a reliable and accurate machine for shape memory testing. With the aid of the assembled system a wide study on some different types of shape memory polymers was developed. The latter on the one hand made possible to identify and solve some of the residual limits of the machine, on the other hand it provided several useful information in order to identify the most suitable solution for the application in ARC PREDICTION project.

Keywords

Sommario

Il presente elaborato è la descrizione delle principali fasi e aspetti di un'attività svolta presso l'Université Libre de Bruxelles (ULB), in particolare all'interno del dipartimento BEAMS (Bio Electro And Mechanical Systems). Tale attività, asservita ad un più ampio progetto denominato ARC PREDICITON, si è svolta attraverso un lungo percorso di progettazione ed effettiva realizzazione di un banco di prova studiato per l'analisi dei polimeri a memoria di forma (Shape Memory Polymers, SMPs). Tale fase progettuale e realizzativa è stata seguita da una effettiva campagna di prove finalizzata all'ottimizzazione della macchina realizzata e alla caratterizzazione delle principali proprietà di tali materiali.

Per quanto riguarda il progetto ARC PREDICTION, quest'ultimo è nato recentemente e verrà sviluppato nei prossimi anni in collaborazione tra l'università di Mons (UMONS), il dipartimento BEAMS dell'Université Libre de Bruxelles e l'ospedale di Erasme.

L'obiettivo di tale progetto è la diagnosi real-time e minimamente invasiva del cancro ai polmoni attraverso l'uso di un bio-sensore basato sulla tecnologia della fibra ottica e applicato alla broncoscopia. Tale dispositivo risulta particolarmente sensibile e delicato all'attacco da parte di agenti esterni. In particolare, ai fini di una corretta diagnosi è necessario prevenire l'esposizione del biosensore ai fluidi corporei prima di essere arrivati a contatto con il tessuto tumorale. A tal fine il progetto prevede la realizzazione di una capsula protettiva capace di aprirsi una volta raggiunto la zona interessata dal cancro e richiudersi al termine della diagnosi.

Tra le varie ipotesi realizzative di tale componente una risultò particolarmente interessante e promettente, tanto da giustificare il presente lavoro. In particolare si tratta di realizzare la capsula protettiva utilizzando i polimeri a memoria di forma.

Questi ultimi infatti presentano una serie di caratteristiche che risultano particolarmente utili nella suddetta applicazione.

Innanzi tutto questi materiali sono in grado di deformarsi a seguito di semplici stimoli [1] [2] che possono essere il calore, la luce o più in generale l'esposizione a radiazioni di particolare lunghezza d'onda [3] [4].

In particolare, la famiglia di materiali scelta per il presente lavoro è sensibile al calore. È infatti possibile, a partire da una forma temporanea precedentemente fissata (attraverso un particolare ciclo di "programmazione" del materiale), recuperare la forma originale di cui il materiale dimostra quindi avere "memoria". Tale processo viene semplicemente attivato nel momento in cui il polimero, esposto ad una fonte di calore, viene portato ad una temperatura superiore alla così detta 'Melting Temperature'.

Quest'ultima, come molte altre caratteristiche termo meccaniche del polimero a memoria di forma può essere regolata in un ampio range attraverso la modifica

della composizione chimica del materiale [12] [20]. Tale proprietà rende ancora più affascinanti questi materiali e conferisce loro la possibilità di adattarsi alle esigenze di un progetto. Nella presente applicazione ad esempio, il valore della 'Melting Temperature' è stato fissato ad un valore basso (45°C) al fine di rendere fattibile l'attivazione di questi materiali all'interno del corpo umano.

Un'altra importante caratteristica è la biocompatibilità, fondamentale in una applicazione medica [4][10][16].

L'insieme di tutte le suddette caratteristiche rende particolarmente interessanti i polimeri a memoria di forma per la presente applicazione e giustifica il presente progetto.

Al fine di comprendere meglio i passaggi e le logiche che hanno guidato le varie fasi del progetto risulta importante introdurre alcune grandezze fondamentali e concetti basilari relativi a questa famiglia di materiali.

In particolare i polimeri a memoria di forma termo attivati sono in grado di recuperare deformazioni che vanno dal 100 al 300% della forma originale.

Come anticipato precedentemente, prima di sfruttare la proprietà di memoria di forma è necessario sottoporre i polimeri ad un particolare ciclo di "programmazione" che dal punto di vista pratico prevede di riscaldare il polimero fino ad una temperatura superiore alla 'Melting Temperature' ed applicare una particolare deformazione che si vuole 'fissare' nel materiale. In seguito raffreddando il polimero al di sotto della 'Melting Temperature' mentre se ne mantiene vincolata la forma, quest'ultima viene temporaneamente fissata nel materiale che risulta deformato anche a seguito della rimozione dei vincoli.

A questo punto il ciclo di programmazione è terminato e il materiale è pronto per l'utilizzo. Riscaldandolo infatti al di sopra della 'Melting Temperature' si induce un recupero della forma originale, precedente al ciclo di programmazione.

Al fine della caratterizzazione di tali materiali le grandezze e gli indici particolarmente rilevanti sono quelli ottenibili realizzando un ciclo termo-meccanico come quello dell'andamento teorico presentato nella

Figura I [5]-[9] [17]. In particolare quest'ultimo prevede una fase di trazione (da 1 a 2) ad alta temperature. Lo sforzo raggiunto al termine di questa fase è il massimo sforzo e viene definito σ_{max} ed è legato alle proprietà meccaniche del materiale ad alta temperatura (in particolare il modulo di Young). A tale livello di sforzo corrisponde la massima deformazione del ciclo ε_{max}. La fase successiva consiste nel raffreddare il materiale mantenendolo ad un livello di deformazione costante (da 2 a 3) e pari a ε_{max}. In seguito il materiale viene liberato e raggiunge la condizione di sforzo nullo (da 3 a 4) a cui corrisponde una deformazione ε_{fix} che normalmente risulta leggermente inferiore a quella massima. Il materiale infatti non riesce a fissare la deformazione imposta in modo completo. Per quantificare l'abilità del polimero

a fissare una certa deformazione si introduce l'indice 'strain fixity rate' (R_f) definito come rapporto tra ε_{fix} e ε_{max}. Attraverso queste prime tre fasi si è ripercorso il ciclo di "programmazione" del materiale.

A questo punto il ciclo si divide in due possibili soluzioni. La prima consiste nel recuperare la forma originale portando il materiale ad una temperatura superiore alla 'Melting Temperature' (da 4 a 5a). Un ciclo che termina secondo questa modalità prende il nome di 'strain recovery cycle'. Al termine di questa fase si riscontra normalmente una deformazione residua ε_{res} che il polimero non è stato in grado di recuperare. Per quantificare la capacità del polimero di recuperare la forma originale, si introduce l'indice 'strain recovery rate' (R_r), definito come rapporto tra la differenza ($\varepsilon_{fix} - \varepsilon_{res}$) e e ε_{fix} stesso.

La seconda soluzione con cui è possibile concludere il ciclo consiste nel vincolare nuovamente il polimero e riportare la temperatura al di sopra della 'Melting Temperature' (da 4 a 5b). Viene così attivato il recupero della forma del materiale che però risulta inibita dall'applicazione dei vincoli. Il risultato è lo sviluppo di uno sforzo. Quest'ultimo raggiunge un livello al termine di questa fase che normalmente è inferiore a σ_{max} e viene definito $\sigma_{recovery}$. Il rapporto tra $\sigma_{recovery}$ e σ_{max} rappresenta la percentuale dello sforzo massimo che è stato possibile recuperare ed è un importante indice della capacità del polimero di sviluppare un certo livello di sforzo quando attivato. Un ciclo che termina secondo questa modalità prende il nome di 'stress recovery cycle'.
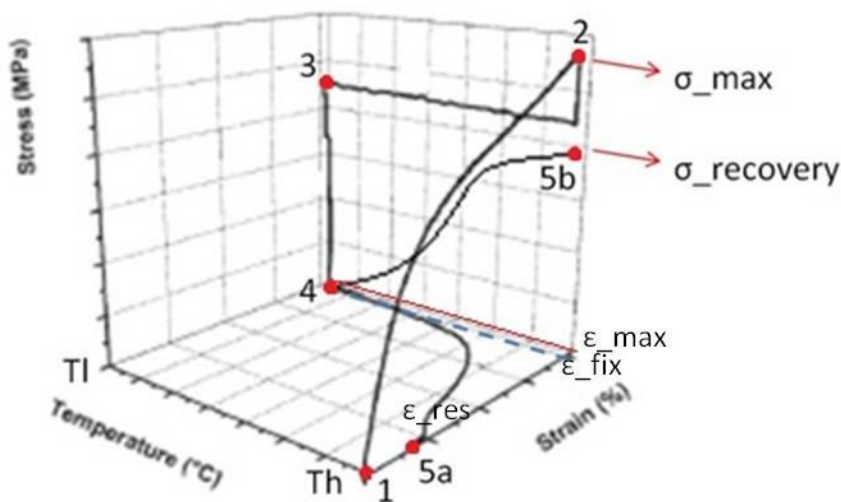
Figura I. Andamento teorico finalizzato alla caratterizzazione dei materiali polimerici a memoria di forma termo-attivati

Alla luce di questi concetti basilari il presente progetto si propone di sviluppare un sistema che permetta la valutazione accurata e affidabile di tutte le proprietà e gli indici introdotti. Ciò si traduce nella progettazione e realizzazione di un banco di prova per i materiali polimerici a memoria di forma.

In particolare, il primo step di questa fase di progettazione ha portato ad una prima ipotesi realizzativa di questo 'banco di prova' di cui si riporta una riproduzione CAD in

Figura II. Tale ipotesi si basa su diversi spunti rinvenuti nello studio della letteratura relativa alla caratterizzazione dei materiali polimerici a memoria di forma [6] [7]. In particolare, facendo riferimento alla

Figura II, il campione di polimero (film con forma a osso di cane in conformità con le specifiche di [18]) viene fissato alla macchina tramite i due dispositivi di afferraggio (numero 7). In seguito la trazione viene applicata tramite un attuatore lineare (numero 1). L'allungamento imposto viene monitorato tramite un dispositivo laser (numero 3) che punta contro una barretta solidale con l'albero del motore (numero 8). La forza sviluppata durante la trazione viene monitorata tramite un'apposita cella di carico (numero 2) posta tra il provino e l'albero motore. La temperatura del provino è misurata tramite una convenzionale termocoppia (numero 4) mentre la sorgente di calore è rappresentata da lampade a infrarossi (numero 6). Infine il sistema è contenuto da un cilindro di Plexiglass trasparente (numero 9) che funge da schermo termico verso l'esterno e trattiene il calore nella zona centrale della macchina. Una telecamera (numero 5) è prevista al fine di riprendere lo svolgimento del test.
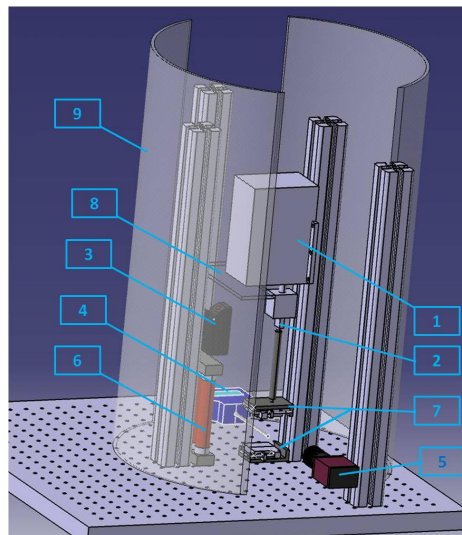
Figura II. Prima ipotesi realizzativa del banco di prova per materiali polimerici a memoria di forma

Sommario

A tale progetto preliminare non è seguita una effettiva realizzazione per via di una serie di limiti e problematiche rinvenute in questo assieme. Al fine di superare queste ultime è stato intrapreso un percorso di ottimizzazione del sistema che ha portato fino all'attuale versione del banco di prova di cui si riporta un'immagine in
Figura III.
In particolare le modifiche più consistenti hanno riguardato il sistema di misura della deformazione imposta al provino e la modalità di riscaldamento e controllo della temperatura.
In estrema sintesi si può dire che la prima ipotesi di monitoraggio della deformazione faceva coincidere lo spostamento del albero motore con l'allungamento del provino. Tale soluzione è quella normalmente utilizzata e presentata nella letteratura relativa alla caratterizzazione dei polimeri a memoria di forma [6] [7].
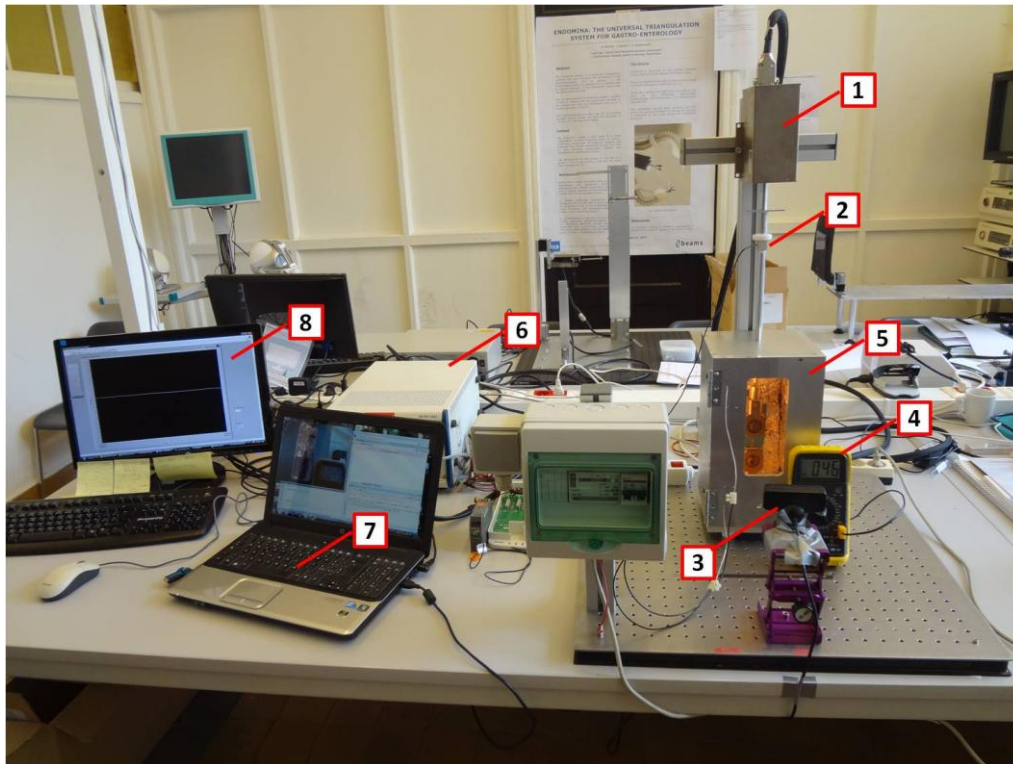
Figura III. Versione definitiva del banco di prova per i materiali polimerici a memoria di forma

Tuttavia, nel momento in cui si adottano provini con una sezione sensibile ristretta (come suggerito da [18]) lo spostamento dell'albero motore tiene conto anche della deformazione delle zone di maggiore larghezza che in realtà non dovrebbero essere contemplate. A questo punto la soluzione più immediata

sarebbe l'applicazione di un estensometro alla zona sensibile del provino. Tuttavia tale soluzione non è percorribile per via delle temperature a cui il materiale viene esposto (anche superiori ai 100°C).

La soluzione che è stata pensata nel presente progetto, di cui rappresenta uno degli aspetti più innovativi, consiste nell'adozione di un sistema a non-contatto che insegue e registra lo spostamento di due linee stampate sul provino agli estremi della zona sensibile. Tale sistema si avvale di una telecamera gestita da uno script Python che fotografa il provino a intervalli regolari di tempo. In seguito, attraverso un altro script Python è possibile rielaborare manualmente le immagini registrate, ricostruendo in questo modo l'andamento della deformazione della sola zona sensibile in funzione del tempo.

Per quanto riguarda la modalità di riscaldamento e la misurazione e controllo della temperatura si è pensato di sostituire il sistema a lampade a infrarossi e termocoppia con una camera climatica progettata su misura per la presente applicazione. Si riporta una riproduzione CAD di tale componente in Figura IV.
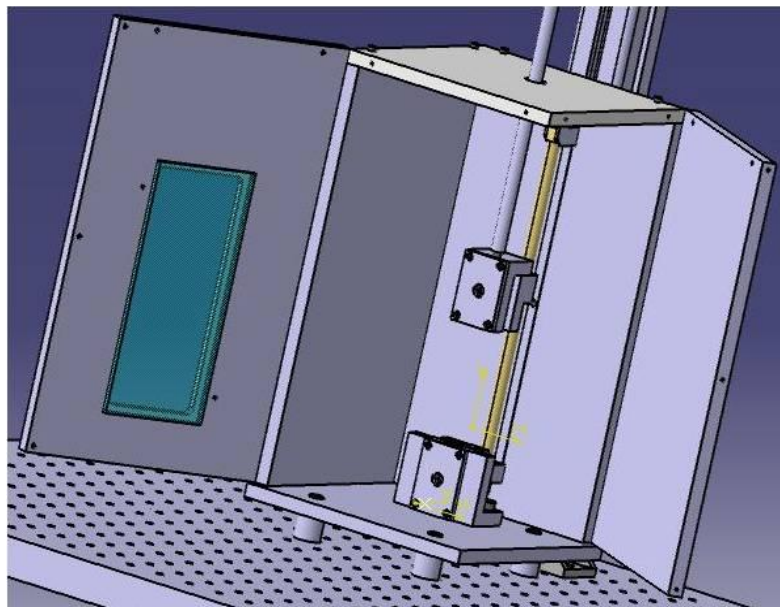
Figura IV. Riproduzione CAD della camera climatica adottata nella versione definitiva del banco di prova

La sorgente di calore in questo caso è una lampada alogena di intensità regolabile posizionata all'interno della camera climatica. La temperatura interna viene monitorata tramite una convenzionale termocoppia. Attraverso questo genere di soluzione è possibile portare l'ambiente circostante al provino ad una desiderata temperatura e mantenerla costante. Dopo un breve intervallo di tempo è possibile assumere che sia la termocoppia che il provino siano in equilibrio

Sommario

con l'ambiente circostante e avere dunque un affidabile feedback rispetto alla temperatura raggiunta dal materiale. Tutto questo non sarebbe possibile con la soluzione precedente. La misurazione e il controllo della temperatura interna al provino non sarebbe infatti stata altrettanto affidabile ed efficace. Quindi, nonostante nella letteratura si riscontrino applicazioni del riscaldamento a raggi infrarossi per i polimeri a memoria di forma

[19] [20] [21] la prima ipotesi realizzativa è stata abbandonata.

Oltre queste due importanti modifiche, molti altri aspetti di minore entità sono stati curati in questo processo di ottimizzazione del sistema.

In particolare una grande attenzione è stata dedicata alla scelta della cella di carico e al condizionamento del suo segnale. Tale componente infatti deve monitorare carichi estremamente contenuti, soggetti a variazioni minime. La gran parte dei materiali polimerici presenta infatti un modulo di Young molto basso ad alte temperature. È quindi fondamentale avere un segnale privo di ogni rumore o disturbo e allo stesso tempo si necessità di un dispositivo estremamente sensibile. Inoltre nel momento in cui si voglia studiare il polimero a temperatura ambiente o nello specifico caso di materiali con proprietà meccaniche elevate anche ad alta temperatura, è necessario assicurare un capacità sufficiente della cella di carico.

Il risultato di questo processo di ottimizzazione è una macchina funzionale ed affidabile nel riprodurre il reale comportamento dei materiali studiati svolgendo dei cicli come quello presentato in

Figura I.

Attraverso tale sistema è stata svolta una campagna di prove sui materiali polimerici a memoria di forma disponibili. Per quanto riguarda questi ultimi, sei tipologie di polimeri a memoria di forma termo attivati sono stati forniti dall'università di Mons.

Lo studio rispetto a tali materiali si è sviluppato come segue. Il primo step è stato svolgere un primo gruppo di 'strain recovery cycles' e 'stress recovery cycles' per la maggior parte dei materiali disponibili, imponendo un deformazione relativamente bassa. Nelle successive

Figura V e

Figura VI sono riportati degli esempi di risultati di tipo grafico ottenuti per un certo materiale in entrambe le modalità di ciclo.
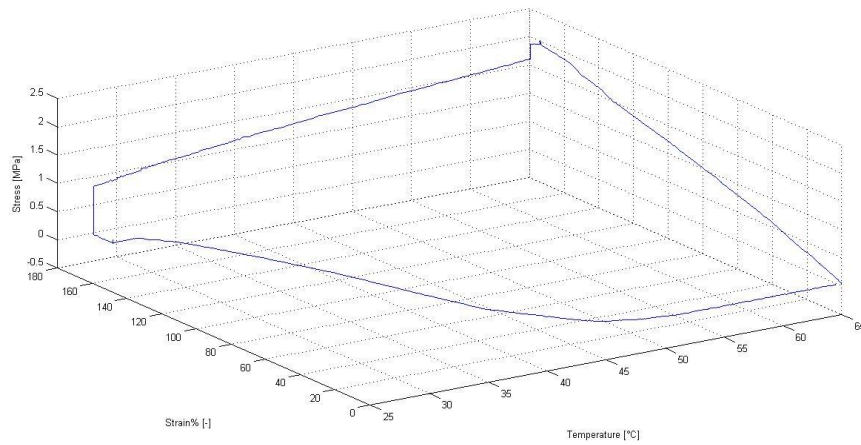
Figura V. Andamento tipico ottenuto durante lo svolgimento di uno 'strain recovery cycle'
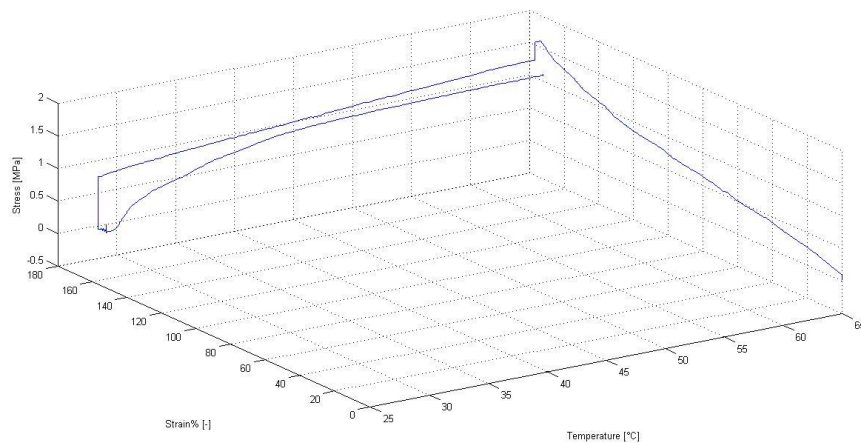
Figura VI. Andamento tipico ottenuto durante lo svolgimento di uno 'stress recovery cycle'

A partire da questo primo set di risultati è stato possibile concludere che il sistema assemblato era efficace nel sottoporre il materiale ai cicli di prova adottati in letteratura e nel monitorare fedelmente le principali variabili in gioco. A partire da tali risultati è quindi possibile valutare i più importanti indici di prestazione legati a questa famiglia di materiali.

Tuttavia, dai primi cicli svolti sono emersi alcune problematiche legate al sistema. È stato così possibile identificare i limiti ancora presenti nel sistema e procedere al loro superamento attraverso un breve processo di ottimizzazione e messa a punto della macchina che ha concluso questa prima fase della campagna di prove sui materiali.

Sommario

Il passaggio successivo è consistito in uno studio sulla ripetibilità dei risultati ottenuti con il banco di prova. In particolare, a parità di condizioni del test (deformazione imposta, range di temperatura) per alcune delle tipologie di materiali disponibili sono stati testati diversi provini ripetendo la stessa tipologia di test. Gli andamenti e indici ottenuti sono stati quindi confrontati da un test all'altro e quello che si è osservato è che i risultati mostravano una buona ripetibilità. Nonostante dunque le differenze presenti tra un provino e l'altro a causa della qualità del processo di fabbricazione, la macchina restituiva dei risultati caratterizzati da una bassa dispersione.

In seguito, come passo successivo di questo studio, sono stati svolti 'strain recovery cycles' e 'stress recovery cycles' per tutte le tipologie di materiali disponibili aumentando da una coppia di cicli all'altra l'allungamento imposto al provino. Non tutti i materiali analizzati sono stati in grado di sopportare le più ampie deformazioni. Durante lo svolgimento di questa fase del lavoro è stato possibile, anche attraverso il calcolo dei principali indici di prestazione dei materiali polimerici a memoria di forma, identificare i materiali più performanti e adatti per l'applicazione medica del progetto ARC PREDICTION.

Infine, al termine di questo lavoro di caratterizzazione, i materiali che nelle prime fasi si sono dimostrati più performanti sono stati selezionati e sottoposti ad uno studio di fatica, volto alla valutazione dell'eventuale deterioramento delle proprietà di memoria di forma a seguito dello svolgimento di diversi cicli. Quello che si è evinto è che tali materiali godono di una certa stabilità nelle delle proprietà anche dopo diversi utilizzi.

In conclusione, il presente lavoro ha prodotto un sistema efficace, affidabile e per diversi aspetti innovativo per valutare le prestazioni di questa famiglia relativamente nuova di materiali "smart". Inoltre, tramite un'ampia campagna di prove, ha fornito diverse informazioni utili all'identificazione del materiale più adatto per una applicazione all'interno di un progetto più ampio, il progetto ARC PREDICTION.

Parole chiave

Polimeri a memoria di forma · caratterizzazione termo meccanica · dispositivo ottico di misura dello spostamento · Scienza dei materiali

Introduction

The present work is the description of the main aspects and results of an activity held at Université Libre de Bruxelles (ULB) in particular in the environment of BEAMS (Bio Electro And Mechanical Systems) department. This activity was subservient to a larger project named ARC PREDICTION, and consisted in a large design and realization path of a tailored test bench for the study of Shape Memory Polymers (SMPs) followed by an actual work of characterization of these materials.

All the main steps of this activity are accurately described in the following pages. In particular the present work is divided in four chapters.

The first one is a brief introduction to shape memory polymers. All the main features and characterizing indexes are introduced and explained, making also reference to the normally adopted tests procedures.

In the second chapter, all the steps that led to the assembly of the final version of the machine are described. In particular, starting from the first hypothesis of the machine inspired by the information found in literature several innovative and effective solutions were introduced.

Chapter three presents all the details related to tests types, materials and methods adopted making also a brief overview of shape memory polymers types investigated.

In conclusion, chapter four describes all main results obtained during this study about shape memory polymers that led to characterize these materials in order to provide useful information to ARC PREDICTION project.

Chapter 1

Shape Memory Polymers

This first chapter consists in a synthetic introduction of fundamental concepts regarding Shape Memory Polymers. The aim of the following sections is to provide the reader with the basic notions regarding these family of materials and to introduce the important concepts necessary to understand all the procedures and data treatment methods during the experimental section.

In particular in section 1.1 the ARC PREDICTION project will be briefly introduced while section 1.2 exposes the reasons that justified the present work. Finally, section 1.3 is a broad overview about the family of SMPs adopted for this project.

1.1 The ARC PREDICTION project

ARC PREDICTION project started recently and will be developed in the following years in collaboration between Mons University, ULB's BEAMS department and ULB Erasme hospital. The aim of the project is the real-time and minimally invasive diagnostic of lung cancer through optical fiber detection applied to bronchoscopy.

1.2 The choice of the actuation

The hypothesis of device tough to achieve ARC project's goal provides a biosensor with a protective packaging that should protect it until it is not exactly in proximity of cancer. Once the tumor tissue is reached the biosensor should be exposed to it.

Among the various hypothesis proposed for the realization of bio-sensor's protective packaging, one resulted particularly interesting and justified the present work. It consisted in adopting Shape Memory Polymers (SMPs) and taking advance of their "smart" properties that make them suitable for this kind of application.

First of all they are able to strain themselves by mean of simple stimuli [1] [2]. For example the family of materials adopted for this project is sensitive to heat but there exist also shape memory polymers sensitive to light or radiations in general [3] [4].

Regarding heat actuated shape memory polymers, starting from a previously fixed temporary shape, it is possible to recover an original permanent contracted or elongated shape simply heating the material above a specific temperature [5] [6] [7] [8] [9] [17]. The name used for the latter is 'melting temperature' and it changes from a material to another. It was then tough that this behaviour could be used to realize the opening-closing mechanism of bio-sensor's protective case. Another important feature is the bio-compatibility of most of these materials, which is an essential aspect for a medical application. As a matter of fact several medical applications of shape memory polymers can be found in literature [4][10][16].

The combination of these and other characteristics, made the hypothesis of adopting Shape Memory Polymers more and more attractive. Consequently it was tough that a wide characterization study on these materials could result really useful in order to fulfil the objectives of the project. This is what justifies the present work, which consists in an extensive characterization procedure on Shape Memory Polymers aimed to define as completely as possible their thermo-mechanical properties. In order to do that it was necessary to design and assemble a tailored test bench, as it will be described in the following chapters.

1.3 Principal features of Shape Memory Polymers

Shape memory polymers (SMPs) are a new family of materials qualified as "smart" due to the impressive features they offer. Light weight, low cost, simple functioning principle and high strain capability make the SMPs ideal for a wide variety of applications [10]-[12] [14]-[17].

One classification criterion of the materials belonging to this large family is based on the activation principle. Among the existing families, the one of heat actuated SMPs is particularly important and attractive. This family is the object of the present work and will be widely exposed in the following steps.

1.3.1 Heat actuated Shape Memory Polymers

1.3.1.1 Main features and functioning principle

Literature about heat actuated shape memory polymers features and properties is not rich [5]-[9] [17].

Polymers belonging to this family can be strained up to $100 - 300$ % at elevated temperatures [5] [11] [12] [17].

Cooling down the material with the active constraints fixes the induced strain in the polymer. The original shape can be recovered when the material is heated back above a critical level, without any constraint applied. This phenomenon is

the shape memory effect. On the other side, if the material is kept constrained while heating, it will exert a recovery force on bonds. This phenomenon is known as constrained recovery.

As the other polymers SMPs are characterized by glass temperature T_g, around which they pass from a glassy state to a rubbery one. However, they show another important characteristic temperature, that is melting temperature T_m. The latter is related to shape memory behaviour. All recovery phenomenon take place around T_m. Above T_m Young Modulus decreases and the material becomes softer. The higher elasticity of the material at this state is due to the ability of polymer's chains to form freely in this high entropy state. At this juncture the latter could be defined as a measure of the disorder or randomness in a closed system. Without any force applied, the polymer chains assume the most probable random shape in this high entropy state. However, when a tensile force is applied, the chains stretch into a less favourable formation with lower entropy. If the tensile force is removed while the temperature is above T_m, the chains are unable to hold their deformed shape and the polymer displays elastic behaviour, because the entropy is high enough to overcome the intermolecular forces and the more probable shape tends to be recreated. On the other hand, if the polymer, deformed at high temperature, is cooled down below T_m under strain constraint and then released, the deformation will now be locked in because the low entropy is unable to overcome the intermolecular forces between the polymer chains. If the shape memory polymer, with the locked in strains is reheated above the glass transition temperature, the increasing entropy overcomes the intermolecular forces and results in recovery of the original shape[1] [4] [9].

Even inside heat actuated SMPs it is possible to make a distinction between thermoplastic and thermoset SMPs [20]. Thermoplastic have no chemical crosslinks. Consequently, they are easy to reshape or reform. However, they can potentially melt at excessive temperatures and they can lose their memory properties over time. In contrast, thermoset SMPs have chemical crosslinks, and they soften but do not melt at elevated temperatures. Generally thermoset SMPs have higher stiffness and lower strain capability than thermoplastic SMPs. Another characteristic is tunable actuation temperature (e.g., glass transition temperature of thermally responsive SMPs) and glassy elastic modulus [12] [20]. By modifying the chemical composition, the thermomechanical properties of SMPs can be tailored for specific applications. For example, thermally responsive SMPs with a glass transition temperature below 37°C are more compliant (i.e., have a lower glassy elastic modulus and recovery force) and self-actuate at body temperature, while SMPs with a higher glass transition temperature accompanied by an extrinsic heating source provide higher recovery force and explicit control of the actuation. The latter property is particular important in order to meet specific requirements.

1.3.1.2   Common characterizing procedure and cycle

Since shape memory polymers are relatively new in the smart materials family, one can find just few references to them in literature [5]-[9] [17]. Comprehensive test data sets characterizing the complex thermo-mechanical behavior over a broad range of strain and temperature would enable a better understanding of the material behavior and allow the development of constitutive models. This would promote the increased use of SMPs in practical applications.

The usual way adopted to characterize shape memory polymers behavior is a thermo-mechanical cycle that can be well described by the theoretical trend of Figure 1.1.
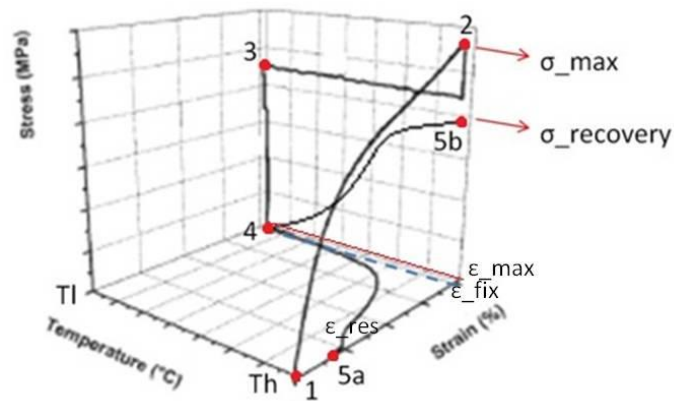
Figure 1.1. Theoretical trend of typical shape memory polymer material thermo-mechanical cycles showing the shape memory effect and the constrained recovery

Making reference to

Figure 1.1, the material is initially heated at a temperature, T_h, above T_m, is deformed to a prescribed strain ε_{max} (path 1➔2). Next, it is cooled to a low temperature, T_l, while holding the strain at ε_{max} (path 2➔3). Thereafter, the sample is released from one of the grippers in order to reach zero stress condition (path 3➔4). The corresponding strain at unloading (point 4) is the amount of strain stored in the material, ε_{fix}. The test can thereafter be continued in one of the following two ways: (1) heating the SMP without any constraints (path 4➔5a) in which case the polymer tends to recovers the original shape, displaying the shape memory effect, even if a residual strain ε_{res} is always observable; or (2) heating the SMP while holding the strain at ε_{fix} (path 4➔5b), in which case the polymer develops a recovery stress. From the tests, critical stress and strain values corresponding to specific points on the thermo-

mechanical cycle can be obtained. This includes the stress value, σ_{max} , at the end of the high temperature loading (σ corresponding to ε_{max} and T_h, point 2 in Figure 1.1), the strain value, ε_{fix} , stored at unloading (ε at T_l and $\sigma = 0$, point 4), and the stress $\sigma_{recovery}$, when the SMP is reheated while constrained (σ at T_h and ε_{fix}, point 5b). In addition to the strain and stress values, Young's modulus at high temperature, E_{rubber} , which is the slope of the first linear part in loading path (path 1➔2) can be obtained. According to literature [5]-[9] [17], shape memory properties are finally evaluated through the following two indexes at the N-th cycle:

Strain fixity rate:

$$R_f(N) = \frac{\varepsilon_{fix}(N)}{\varepsilon_{max}}$$ (1.1)

Strain recovery rate:

$$R_r(N) = \frac{\varepsilon_{fix}(N) - \varepsilon_{res}(N)}{\varepsilon_{fix}(N)}$$ (1.2)

Table 1.1 resumes the previously exposed typical thermo-mechanical testing procedure

Table 1.1. Typical thermo-mechanical testing procedure

Path	Description	Variables achievable
Path 1➔2	SMP at an elevated temperature T_h (above T_m) strained to a value ε_{max}	E_{rubber} ; σ_{max}
Path 2➔3	SMP cooled to a low temperature T_l (below T_m) while holding strain at ε_{max}	-
Path 3➔4	SMP released at T_l , stress reduces to zero, stored strain at zero stress is ε_{fix}	ε_{fix} strain at unloading; $R_f(N)$
Path 4➔5a	SMP heated unconstrained to a temperature above T_m. Tends to recover original shape (shape memory effect)	Residual strain ε_{res}; $R_r(N)$
Path 4➔5b	SMP heated to a temperature above T_m while holding strain (at ε_{fix}). It Develops a recovery stress	$\sigma_{recovery}$

Chapter 2

Test bench design path

2.1 Introduction and involved variables

The design path of testing bench was extremely articulated and long. As in most cases, when dealing with a real problem, the process you follow is not linear, but rather a sort of loop made up of several iterations that lead to a definitive solution. The latter is a kind of compromise between different exigencies of the project. This was the way to proceed followed during the present work. Indeed, starting from the first realization hypothesis of the testing bench, the final solution was reached passing through several changes, optimizations and intuitions. Step by step it was realized that some solutions were more effective than others. This whole dynamics took a lot of time but led to a good and for some aspects innovative solution but above all, satisfactory from the point of view of project's needs.

As already said, the project consisted in a study about Shape Memory Polymers, in order to characterize their thermo-mechanical behaviour. Starting from literature it was possible to assume that the thermo-mechanical cycle exposed in section 1.3.1.2 could be a very efficient way to gather several information about SMPs. All the indexes and variables achievable from this particular cycle make possible to estimate some important features of the studied material and the performances it is able to provide [1] [4]-[9]. It was then decided to adopt this characterization procedure also for the present work.

In order to perform this cycle, the variables to be monitored are basically three: force, elongation and temperature. As it was necessary to achieve comparable results among tests, the first two variables were normalized to stress and strain, taking in account the dimensions of the samples [4]-[9] [22].

Regarding stresses, that means that the value of the force, during tests, was divided by the area of sample's normal section. For example, assuming to deal with a rectangular sample, characterized by a width *w* and thickness *t* (as the one illustrated in

Figure 2.1), the normal section is the result of the following simple computation:

$$Normal\ Section = A = w \cdot t \qquad (2.1)$$

And finally it is possible to obtain stress as follows.

$$Stress = \sigma = \frac{F}{A}$$

<div align="right">(2.2)</div>

Where *F* is force applied to sample's extremities.
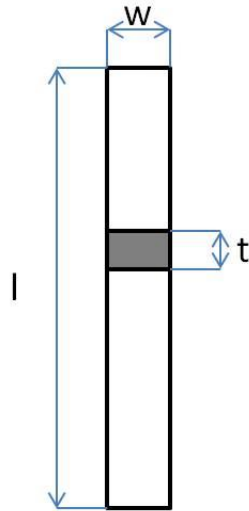
Figure 2.1. General rectangular sample

At the same time, the elongation was continuosly normalized to a strain dividing it by the value of the initial length l_{in}, as showed in the following equation.

$$Strain = \varepsilon = \frac{Elongation}{Initial\ length} = \frac{l - l_{in}}{l_{in}}$$

<div align="right">(2.3)</div>

where *l* is sample's actual length.

In the next chapters all technical solutions tough and adopted for the control or measuring of the mentioned variables will be explained widely. It will be then clearer why this phase has been one of the major challenges of the project. The first step will be the description of the initial constructive hypothesis developed for the bench in section 2.2 while last version of the machine will be accurately presented with all its details in section 2.3.

2.2 First design solution and limits

The first step made in this project consisted in a wide overview of literature about Shape Memory Polymers. Several papers, articles and thesis were carefully analyzed during this important phase [5]-[9] [17]. This procedure was very useful either to become more familiar with this family of materials or to get an overview about the testing procedure normally adopted to study them and all the technical solution already developed in this field. Several hints emerged during this phase were effectively adopted in the project while others were just the foundation for subsequently developed ideas. As a matter of fact this project was not limited to a reproduction or a combination of solutions already existing in literature, but it brought some innovative aspects aimed to improve the reliability and effectiveness of tests performed on SMPs, as it will be explained later. In this section, the first hypothesis of the machine will be introduced in a general way at the beginning. Afterwards, each component will be analyzed in detail.

The first step was to realize a simple block diagram representing approximately what was tough to be the most effective combination of components in order to obtain a machine suitable with the object of the study. The previous mentioned block diagram is reported in Figure 2.2.
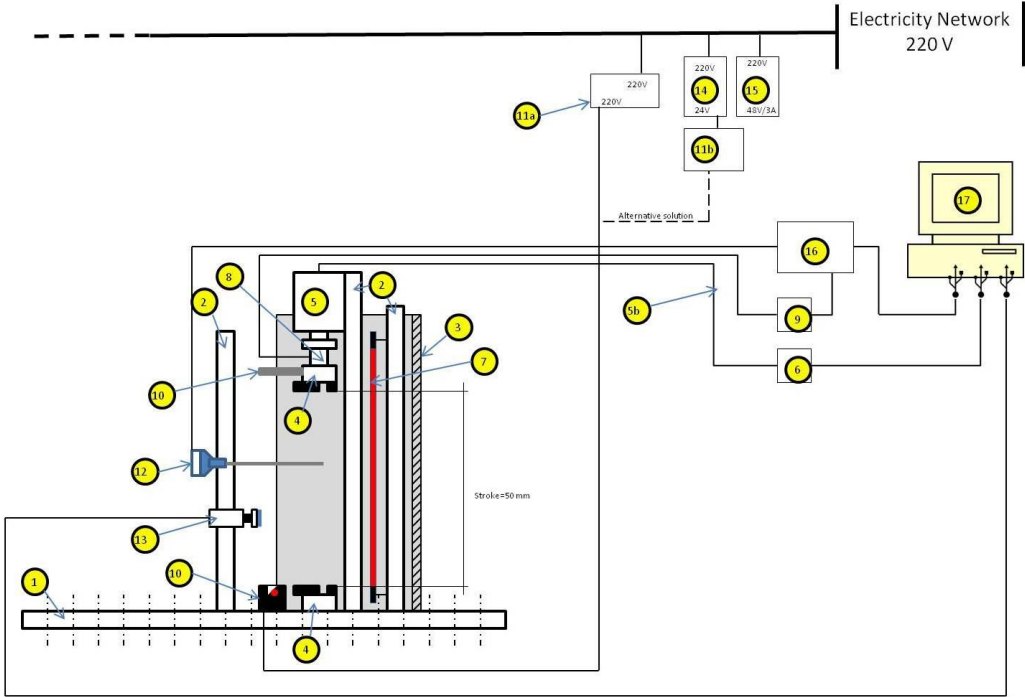
Figure 2.2. Block diagram of test bench's first version. An increasing numbering is assigned to components

This representation arises from the need to have a clearer idea of the final assembly and the exigency to identify better all the devices necessary. As a matter of fact, an increasing numbering is assigned to main components. In this way it was simpler to draw up an ideal inventory which associated to the generic type of component an already available solution in the department or a purchasing hypothesis. At the same time, the block diagram resulted very useful and clear in order to expose this idea of realization to project managers, whose approval was necessary for the continuation of the project.
Making reference to
Figure 2.2, a general idea of the machine will be now introduced. Table 2.1 is a legend of the numbers listed in
Figure 2.2. In the same table some suitable devices already available in the laboratory at that time are proposed for many of the needed components. For other components the realization hypothesis is just explained.

Table 2.1. Legend of components introduced by
Figure 2.2. Next to some numbers, already available components at the beginning of the project are mentioned

Number 1: Base plate: Newport M-B-2B
Number 2: Supporting columns: aluminium profile
Number 3: Cylindrical thermal shield
Number 4: Gripping devices
Number 5: Actuator: SMAC LAL-095-050-71-FS.
Number 5b: Connecting cable: SMAC LAH-LAD-03
Number 6: Controller: SMAC LAC-1 (Controller with integrated amplifier)
Number 7: Infra red lamp
Number 8: Load Cell: two solutions available   • Futek: capacity (0-10g)   • Festo: capacity (0-5kg)
Number 9: Isolated strain gauge input module (signal conditioner): Pimzos SG-3016
Number 10: Laser displacement meter: two solutions available   • Keyence LC2440 (Ultra high accuracy laser displacement meter)   • Keyence LK-G10 (CCD high resolution displacement meter)
Number 11a: Power supply device: 220V (adopted only with Keyence LC2440)
Number 11b: Controller for displacement detector: Keyence LK-G3001 PV   (adopted only with Keyence LK-G10)
Number 12: Thermocouple
Number 13: Supporting video device (camera)
Number 14: Transformer, RS components; 220V ➔ 24V
Number 15: Transformer, RS components TIS 150-148; 220V➔ 48V/3A DC
Number 16: Data acquisition system, National Instruments NI-DAQ 6024E ;

(Low cost E series multifunction DAQ
Number 17: PC + National Instruments LabView (data managing software)

Among the components listed in the diagram, there are some particularly interesting, either because they were kept in machine's last version or because they represent a first idea that was optimized or changed subsequently.

Once this first preliminary draft of the machine was approved, the following step consisted in a CAD reproduction of each components and in an assembly simulation.

The CAD software adopted was Catia v5 (Dassault Systèmes). A license was available for this software in the department.

Figure 2.3 is an overview of the machine in which all main components are associated to a number. Figure 2.4 focuses on the machine central area and shows where polymeric samples are positioned during tests.

The CAD design phase resulted really useful for several reasons. First of all, the assembly simulation, allowed to evaluate the dimensions of each component and the compatibility with the others, making possible to avoid eventual interferences in the real final assembly. In particular for machine's moving parts. Furthermore, it gave a realistic overview of the final result. In the end it resulted very useful during a meeting with other members of ARC PREDICTION project. As a matter of fact, it was really efficient in giving an idea of the evolution of this part of the project and its prospects.
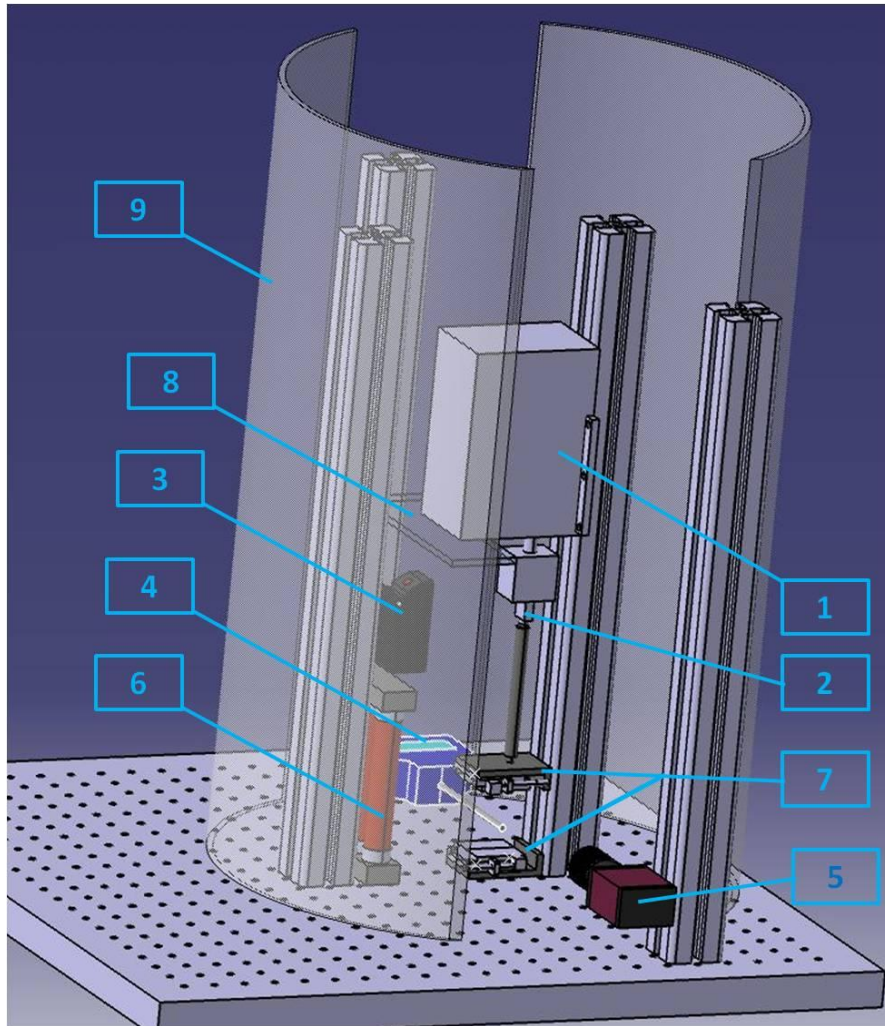
Figure 2.3. First hypothesis of test bench, CAD assembly. A number is associated to all main components. (1) Linear actuator; (2) Load cell; (3) Laser displacement meter; (4) Thermocouple; (5) Camera; (6) IR lamps; (7) Grippers; (8) Reflective mirror; (9) Thermal shield
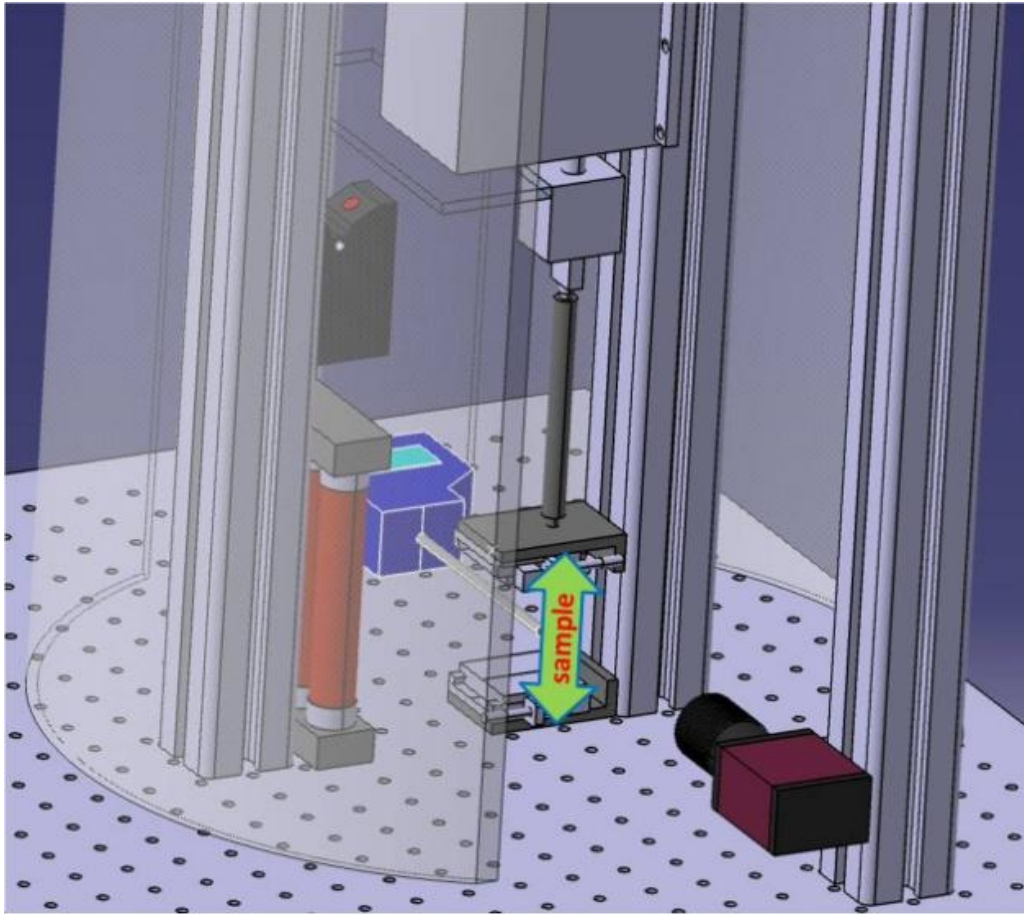
Figure 2.4. First hypothesis of bench, sample position

Starting from
Figure 2.2,
Figure **2.3** and Figure 2.4 it is possible to deduce the general idea the machine based on. A linear actuator (number 5 in
Figure 2.2 and number 1 in
Figure **2.3**) was supposed to apply a controlled strain to polymeric sample. The latter consisted in a properly cut film, positioned and fixed through two gripping devices (number 7 in
Figure **2.3**) as showed in Figure 2.4. A load cell (number 2 in
Figure **2.3**) was positioned between motor's shaft and an extension of the latter connected with the upper gripping device. A prolongation of motor shaft was retained necessary in order to keep the motor and the load cell far from infra red lamps (number 6 in

Figure **2.3**) which were supposed to heat polymer sample. In this first concept of the machine, the elongation applied to sample is measured by mean of a laser displacement meter (number 3 in
Figure **2.3**). This instrument pointed to a mirror (number 8 in
Figure **2.3**) positioned perpendicularly in respect of laser pointer and integral with motor shaft. Sample's temperature was monitored by mean of a thermocouple (number 4 in
Figure **2.3**) with the sensitive extremity very close to polymer. A camera (number 5 in
Figure **2.3**) was inserted just in order to take movies of the test and monitor its evolution. In the end, a thermal shield made up of Plexiglass® (number 9 in
Figure **2.3**), was positioned around the main area of the machine with the aim to prevent people to get in contact with the hot zone of the bench and to keep heat around sample. Two of the above mentioned components should be treated in a deeper way.

The first one is the heating principle. All the material studied during this project were provided by Mons university. During the first meeting in Mons, it was suggested to heat polymeric samples using infra red radiations. Mons researchers ensured that shape memory polymers chemical nature is not modified neither by infrared radiation nor by hot fluids, like water or oil. Moreover several reference to this heating principle adopted for SMPs were found in literature

[19] [20] [21]. Offers were then sent to several infra red lamps sellers or producers, specifying the need for a lamp able to emit inside the range of 700 nm and 1700 nm (SMPs' absorbance spectrum

[19] [20]) and with a dimmable intensity, in order to control the temperature reached inside the heated material in a range between ambient temperature and 100°C. All the producers answered and different suitable solution were proposed.

Another noteworthy component in bench's first concept are the gripping devices. At the beginning, no suitable grippers were found in the laboratory. It was then tough to manufacture this components in collaboration of ULB internal workshop. A CAD design was then developed also for this component and sent to workshop staff in order to evaluate the feasibility of the component and the time delay needed.

Figure 2.5 and
Figure 2.6 provide an overview of the component realized with CATIA v5.
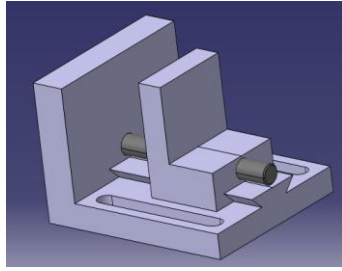
Figure 2.5. Gripping device back view
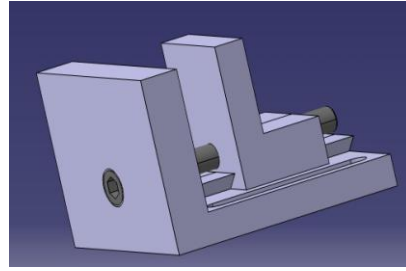
Figure 2.6. Gripping device front view

It is now important to underline the aspects that limited this first version of the bench and justified all the changes that led to bench's definitive and optimized version.

The first important limit is related to the way through which displacement is measured. As explained a laser device (number 3 in

Figure **2.3**) measured the displacement of a relatively long beam provided with a reflective surface and fixed to motor's shaft (number 8 in

Figure **2.3**). This solution even if really simple, imply three important negative aspects.

The first is related to beam's dimension. In order to expose the reflective surface to laser, it was necessary to design a beam going from motor's shaft to the zone above laser device. Starting from the assembly simulation, it was noticed that this distance was consistent. Furthermore, as the beam was moved by motor, it was retained important to reduce the weight of this component in order not to reduce excessively actuator's force range. In conclusion the beam was designed long but thin. Such kind of component is subjected to not negligible vibrations on the side opposite to the one from which it is moved. A qualitative description of this phenomenon is showed in

Figure 2.7.
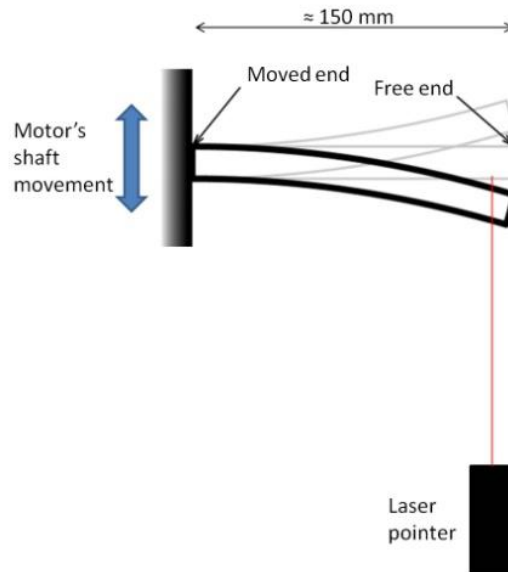
Figure 2.7. Reflective beam's deflection during motor movement

The deflection of the beam is read by laser device which moreover is very sensitive. This vibration compromises the signal recorded that is no more representative of the elongation imposed to sample.

Another important negative aspect related to this solution is the fact that through this system what is measured is basically shaft's displacement and it doesn't correspond exactly to sample's elongation. As it will be exposed in section 3.2 during the project a regulation was adopted for the shape of samples. The latter is ASTM D638 [18] about polymer testing and it suggests to use dogbone shaped samples. Such kind of shape has two wider extremities and a sensitive central zone, the narrower one, as showed in

Figure **2.8**.
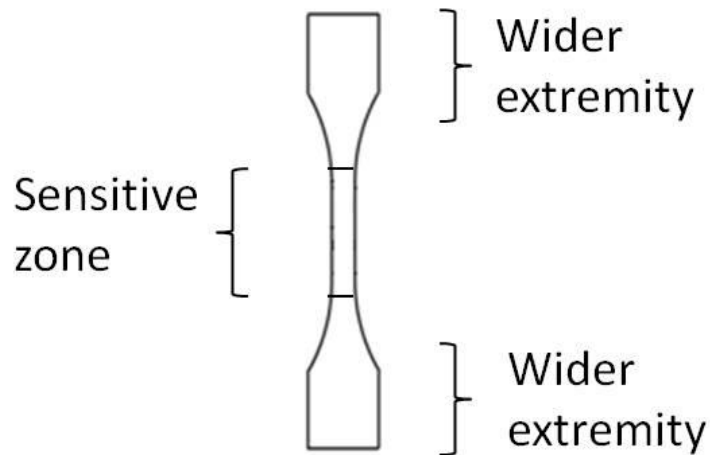
Figure 2.8. Dogbone shaped sample

The initial and actual length considered for measuring strain as introduced in equation (2.3) should be the ones of this sensitive zone. However, measuring the displacement of motor's shaft, the deformation of the wider extremities will be took in account. This problem made necessary to find a way to measure only sensitive zone's deformation.

The last problem related to this measuring solution is related to laser device capacity. As a matter of fact, the model available in the laboratory (Keyence LK-G10) provided a measuring range of 10 mm. This range is shorter than actuator's stroke (50 mm) and extremely limitative considering that SMPs are able to recover very large imposed strains.

For all these reasons, finding an alternative measuring solution for elongation became necessary.

Another important problematic aspect of this machine's first version is related to heating principle. Using IR lamps as suggested at Mons and in
[19] [20] [21], seemed to be a charming and effective solution. However it imply some problems.

The first one is the fact that a thermal shield like the one designed (number 9 in Figure 2.3) is not really effective in keeping the heat around the working area. Furthermore such a thermal shield doesn't provide a protection for all measuring instruments and heat sensitive components of the bench.

A further problem related to this solution is that controlling temperature reached inside samples results very complicated. As already explained sample's temperature is measured through a conventional thermocouple positioned as close as possible to polymer. This measuring method is not really reliable and probably not exactly representative of the actual temperature inside sample.

An alternative solution became necessary also for this part of the machine.

In the following section a wide description of machine's definitive version will be presented and all the alternative solutions introduced to face previously underlined problems will be exposed.

2.3   Final design solution

The version of test bench presented in this section is an evolution of the one described in section 2.2 and its design path, as the previous one, passed through a CAD reproduction of all components and an assembly simulation.
Figure 2.9 and
Figure 2.10 show the result of this step. Already from these images is possible to sense some important differences compared to the precious version. However, also in this representation there are some features that were finally modified in machine actual assembly and some fundamental components are missing.
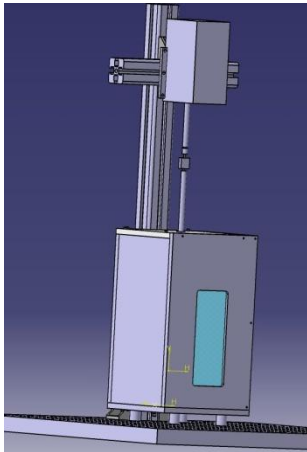
Figure 2.9. Assembly simulation through CATIA v5 of machine definitive version. Climatic chamber closed
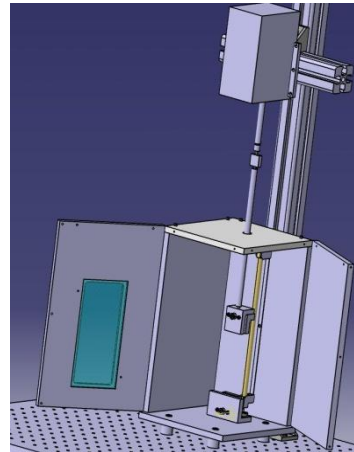
Figure 2.10. Assembly simulation through CATIA v5 of machine definitive version. Climatic chamber open

Figure 2.11 is a photo of the bench took at the end of its assembly. Several components were not present in CAD reproduction.
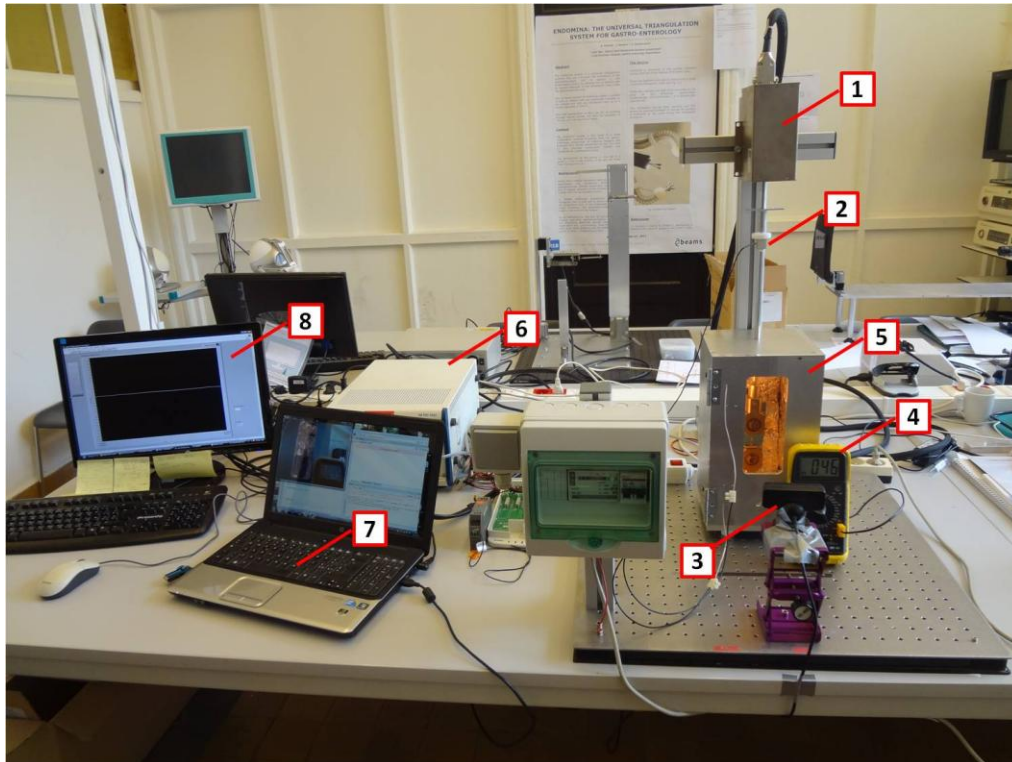
Figure 2.11. Test bench definitive version. A number is associated to each main component. (1) Linear actuator; (2) Load cell; (3) Camera; (4) Thermocouple; (5) Climatic chamber; (6) DAQ - computer; (7) Computer 2; (8) DAQ - computer interface

Making reference to
Figure 2.9,
Figure 2.10 and
Figure 2.11 main differences between first and last versions of the machine will be now explained.

The first important difference is related to the way adopted for sample's elongation measurement. In the previous version a laser displacement meter measured motor shaft's displacement.

As already explained in section 2.2 this measuring system implied several problems. It was then tough to substitute it with a contactless measuring systems based on the usage of a camera (number 3 in
Figure 2.11) associated to three Python scripts.

The second important difference is the heating principle. In order to overtake the problems related to IR lamps, it was tough to assemble a tailored climatic chamber (number 5 in
Figure 2.11) heated by a dimmable halogen lamp. Both these optimizing systems and all the other main components of this bench will be deeply explained in the next sections of this chapter.

2.3.1 Components description

2.3.1.1 National Instruments software and hardware

When working with measuring instruments, it is necessary to have a interface that makes possible to communicate with them and read the output signal. A normally adopted solution is to connect all the instruments to a data acquisition system and afterwards plug the latter to a personal computer. For this project it was not necessary to use a personal computer, because in the department a National Instruments computer with an integrated acquisition board was already available. The latter can hardly be seen in

Figure 2.11 (number 6) Because hidden by a laptop.

Figure 2.12 shows the device better.
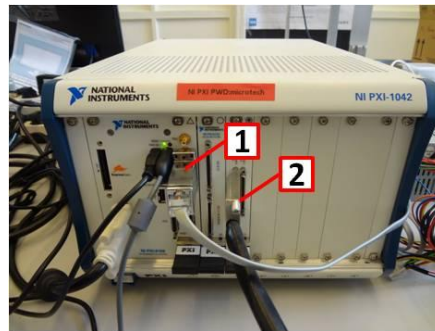
Figure 2.12. National Instruments NI PXI-1042 computer with integrated acquisition board

This hardware system is very powerful and performing. It provides numerous analog and digital input/output channels. Among these only one analog channel has been used and dedicated to the load cell. The device has still several available channels for the connection of eventual further instruments dedicated to the test bench, in order to optimize it in future. From

Figure 2.12 it could be noticed that two connectors are plugged in NI PXI-1042 computer. The first one (number 1 in

Figure 2.12) is the cable coming from linear actuator controller, while the second one (number 2 in

Figure 2.12) is related to a connecting board through which it is possible to connect the devices or measuring instruments to NI PXI-1042 computer.

The software running on this computer and aimed to data acquisition and treatment is National Instruments Labview. A tailored script was developed in this programming environment and it was tough to acquire a voltage signal coming from the load cell, convert it into force and filter it through a software filter. All these aspects will be explained in section 2.3.1.3 about load cell.

In conclusion, in order to interact with NI PXI-1042 computer, a interface set was connected to it (screen, keyboard and mouse, number 8 in Figure 2.11).

2.3.1.2   Linear actuator and controller

Starting from literature, one can assume that SMPs are able to recover every kind of deformation. For example it is possible to recover either a twisted shape or an elongated one. In order to induce a twisted shape in a polymeric sample, it would be necessary to adopt a motor able to provide a linear and an angular motion. For this reason, at the beginning of the project it was hypothesized to purchase a linear-rotary actuator. Some manufacturers were investigated and suitable solutions found. Afterwards, it was realized that in order to perform the thermo-mechanical cycle presented in section 1.3.1.2 a linear actuator was enough. Extending the study also to torsional deformations would have been incompatible with the timeframes available and furthermore, not particularly useful for the aim of ARC project. Moreover, the solutions found in literature for this component have just a linear dynamics. In particular either [6] or [7] use a screw-driven actuator which is able to develop high levels of force at the expense of accuracy.

Regarding the present work, a suitable model of actuator was already available in the laboratory. The brand of the latter is SMAC, model LAL95-050-7. It was then decided to adopt this component for the application of a controlled force and deformation to polymeric samples. This kind of actuator doesn't provide high levels of force, but is very accurate.

Figure 2.13 is an image of the previously mentioned motor, while Table 2.2 lists the main features of the component.

Figure 2.13. SMAC LAL95-050-7; actuator adopted for the assembly of test bench

Table 2.2. SMAC motor main features

Model	SMAC LAL95-050-7
Voltage [V]	48
Stroke [mm]	50
Maximum force [N]	65
Size LxWxH [mm]	147x70x95
Maximum current [A]	1.7

As it could be noticed by Table 2.2 this model of actuator provides a maximum stroke of 50 mm. With such stroke it is possible to impose deformation of considerable magnitude to a sample with contained dimensions like the ones adopted for this study.

Another important feature is the maximum force provided. Starting from the results obtained in preliminary traction tests at ambient temperature performed on simple rectangular samples (1 mm thick and 5mm width), it was observed that, despite sample's small dimensions, the force needed to deform it was very high. This polymeric material shows indeed a really high Young's modulus at ambient temperature and results very hard to deform. The value reached during traction was slightly above 100 N. SMAC LAL95-050-7 was hence not suitable to perform traction tests at ambient temperature. However, in thermo-mechanical cycle presented in section 1.3.1.2, traction phase is performed at a temperature above melting temperature T_m. As already explained in section

1.3.1.1, when these materials are heated above T_m their mechanical properties change substantially and, in particular, Young's Modulus is subjected to a strong decrease. That means that with the same dimensions of the sample, the force to be exerted in order to deform it is largely below 65 N provided by SMAC LAL95-050-7 (in particular, during tests, the maximum force value reached was around 5 N at a strain of almost 180%, as it will be explained in Chapter 4). Therefore it was decided not to purchase a new actuator and to adopt the one already available.

SMAC LAL95-050-7 is connected to its own controller (SMAC LAC-1).

Figure 2.14 shows the device.

The latter connects motor to an interface (National Instruments NI PXI-1042 computer; see section 2.3.1.1) and at the same time to power line.

This model of actuator is powered by a voltage of 48V. SMAC LAC-1 controller has an internal transformer (220V – 48V). Moreover the controller offers a connection to all the digital channels coming out from the actuator.

In order to manage the actuator, a Matlab script able to communicate with these channels was developed. This script allows to move motor shaft specifying speed, acceleration and relative or absolute displacement.

Figure 2.14. SMAC LAC 1 actuator controller with internal transformer

The feedback for the control of all these variables is provided by an internal potentiometer through which acceleration, speed and position of the shaft are known.

It is noteworthy that the internal potentiometer could be used in order to measure shaft displacement. As a matter of fact, making reference to motor shaft displacement is a common adopted solution in literature. For example in [6] the displacement of screw driven testing machine's crosshead is assumed as representative of sample elongation. Also in [7] the motor shaft's movement is associated to sample elongation. In this case an optical system (VIC) helps in measuring the whole field of deformation on sample's surface, but the actual measurement of the elongation is deduced from motor internal potentiometer.

All these kind of solutions would be really similar to the one tough in machine first version, but at the same time, they would solve at least the problem related to reflective beams vibrations (see section 2.2). However using the internal potentiometer would imply all the other problems related to the usage of shaft's displacement for sample's strain measuring (see section 2.2). Furthermore, in order to synchronize data coming from all measuring instruments, it would be desirable to manage them through one only software. As load cell is connected to National Instruments acquisition board which communicates with Labview, it would be necessary to make Matlab script related to motor run inside Labview environment, and monitor in this way the variable associated to shaft displacement. Even if this solution is feasible, it results particularly complicated and difficult. For these reasons, the usage of the internal potentiometer was limited to motor control.

2.3.1.3   Load cell and signal conditioning

This section is dedicated to a device whose importance is particularly high. In order to measure force, a strain gauge based load cell was chosen. The application of this component in such a project results particularly complicated because of the need to measure a broad range of force keeping a good resolution at low levels. Force values to be measured while working at high temperature with some polymers are indeed really low. It was then necessary to resolve slight variations of a very low force signal. All this issues will be described in the following sections.

2.3.1.3.1   Futek LSB 200

The solutions presented in literature about this component are not various and for this reason they don't provide effective guidelines for the selection of a proper device. In particular in [6] and [7] the same type of samples (bigger than the ones studied in the present work) was adopted. Despite the analogy between samples' dimensions the load cells used are completely different. A 1000 N load cell was chosen in [7] while in [6] the capacity of the load cell adopted was lower and equal to 10 N.

As exposed in Table 2.1, two load cells were already available at the beginning of the project in the laboratory. The first one (Futek load cell) has a capacity of 10 g. This value is too low either for tests above melting temperature (T_m) or for ambient temperature tests. As already introduced in section 2.3.1.2 about linear actuator, the force range while working with SMPs goes from few Newton above melting temperature (T_m) up to more than 100 Newton at ambient temperature. Futek 10g load cell was then discarded. The second one (Festo load cell) shows a capacity of 5 kg ($\approx 50\,N$) which is more than enough for tests

above melting temperature (T_m) but too low for ambient temperature tests. Furthermore, the device itself was damaged and didn't ensure a reliable behaviour. As it was retained important to have a well functioning device and at the same time, the possibility to keep opened the eventuality to perform tests at ambient temperature, it was decided to purchase a new load cell. The latter was supposed to have a larger capacity but at the same time a good resolution.

As the already available devices resulted not suitable for this application, it was decided to purchase a new one. Several manufacturers were investigated and all the specifications needed were exposed to each one.

It was retained that a capacity around 200 N was enough for every kind of test. Among all the offers made by manufacturers one brand resulted particularly interesting. The latter is Futek, whose measuring instruments are slightly more expensive than the average but they ensure a very good and reliable functioning and provide very high performances. The device that was finally purchased is Futek LSB200 50 lb (222.4 N).

Figure 2.15 is a photo of the load cell while Table 2.3 lists all its main features.
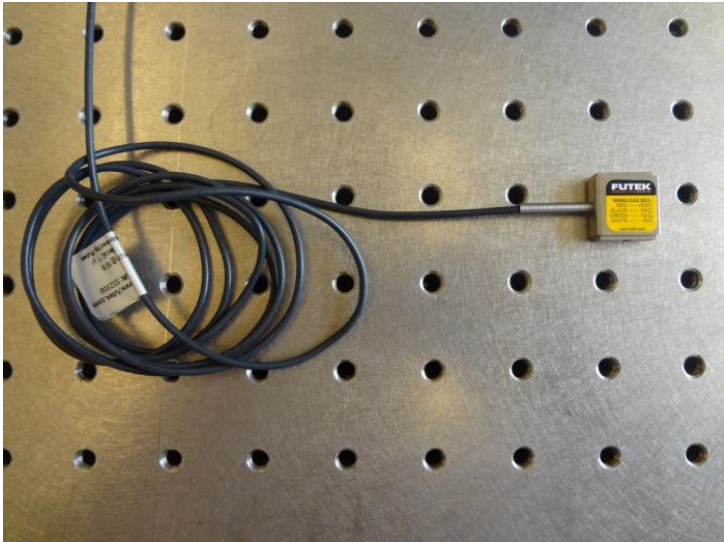
Figure 2.15. Futek LSB200 50 lb (222.4 N)

Table 2.3. Futek LSB200 50 lb (222.4 N) load cell main features

Model	Futek LSB200

Dimensions	
Capacity [lb] ([N])	50 (222.4)
Rated Output [mV/V]	2
Bridge resistance [Ω]	350 (nom)
Safe overload	1000% of R.O.
Excitation (VDC or VAC)	10 max
Weight [g]	9
Compensated Temp. [°C]	15 to 72
Operating Temp. [°C]	-50 to 93
Material	Stainless steel

The capacity of this device could seem even excessive and not compatible with an high resolution. However we were ensured by the seller that this device is extremely performing and provides a very good resolution. As a matter of fact using the load cell, we verified that it is able to provide a resolution of few grams which is perfectly suitable with the final application.

Another important feature to be underlined are the dimensions of the device. The compatibility between this load cell's high capacity and its contained dimensions is a further confirmation of the high performances offered by this device. As a consequence of its small dimensions, this measuring instrument has a very low weight, which is an important feature for an object hanging from motor shaft (as explained in section 2.2). Moreover, despite its dimensions, the safe overload offered is really high.

In conclusion, a mention must also be made about the operating temperature. The available range goes indeed from -50°C to 93°C. As it will be explained in the following sections, the materials studied have all a melting temperature T_m around 45°C. Moreover starting from literature [5]-[9] [17], it is possible to assume that increasing too much the temperature of samples above T_m, doesn't affect shape memory behaviour. Then, as T_m is around 45°C, it was decided to adopt $T_{max} = 70$°C as maximum temperature reached by the system during sample heating phase. This not excessive maximum value is also imposed by the fact that some of the studied materials are sensitive to high temperature. Heating

them above 100°C could compromise their shape memory properties. For these reasons the working range covered during tests goes from ambient temperature ($T_m \approx 25$°C) to $T_{max} = 70$°C. This range is not only comprehended inside operating temperature allowed by load cell but also in compensated temperature range. Furthermore, as it was in machine's first version, an extension of motor shaft was put between heating zone and load cell in order to keep the device and the motor far from high temperatures. This obviously decrease the level of temperature to which all sensitive components are exposed.

2.3.1.3.2 Conditioning module and electrical devices

As already said, force signal while working with polymers at high temperature is really low. This means that if load cell signal is not well conditioned it is possible that electrical noise becomes comparable with it.
It is then practically impossible to distinguish the actual signal from what is just noise.
Conditioning load cell meant basically two things:
- Stabilization of load cell alimentation
- Stabilization of load cell output

Load cell output signal is proportional to the input value of the alimentation. In particular, this load cell model works with a full Wheatstone bridge taking advance of internal beam's flexion. A simple scheme of Wheatstone bridge in this configuration ([23] [24] [25]) is reported hereunder in
Figure 2.16.
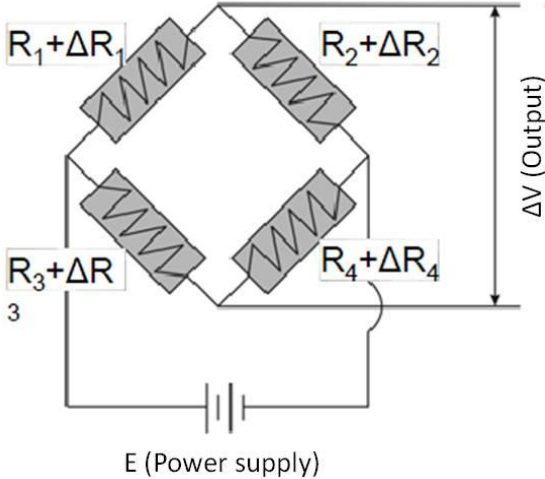
Figure 2.16. Full Wheatstone bridge

The disposition of the resistances on the internal beam and the working principle will be now simplified as shown in
Figure 2.17.
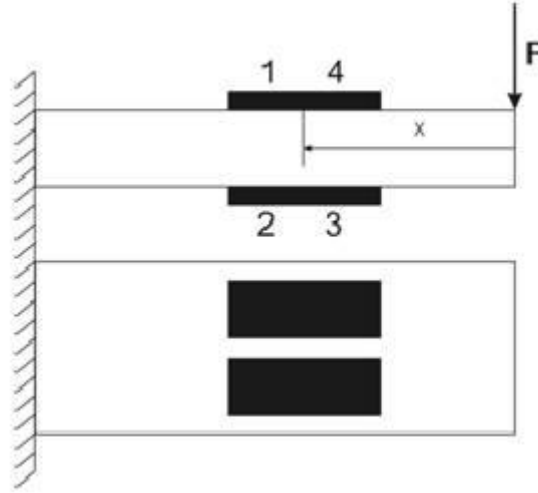
Figure 2.17. Qualitative scheme of resistances' disposition inside the load cell and working principle

Making reference to
Figure 2.16 and
Figure 2.17 it is possible to write:

$$\Delta V = \frac{E}{4}\left(\frac{\Delta R_1}{R_1} - \frac{\Delta R_2}{R_2} + \frac{\Delta R_4}{R_4} - \frac{\Delta R_3}{R_3}\right) \tag{2.4}$$

$$M_f = F \cdot x \tag{2.5}$$

$$\varepsilon_1 = \varepsilon_4 = -\varepsilon_3 = -\varepsilon_2 = \frac{M_f}{E \cdot W} \tag{2.6}$$

where ε_i is the elongation related to i-th resistance.

$$W = \frac{1}{6}bh^2 \tag{2.7}$$

$$\Delta V = \frac{V_0}{4}K(\varepsilon_1 + \varepsilon_4 - \varepsilon_2 - \varepsilon_3) = \frac{V_0}{4}K4\varepsilon_1 \tag{2.8}$$

Equation (2.4) shows that load cell's output is proportional to the value of power supply while Equation (2.8) shows that this configuration is particularly sensitive. As a matter of fact the gauge factor obtained is equal to 4.

As load cell output signal is proportional to the input value of the alimentation, if the latter is not stable the output of load cell won't be stable too, and it will be disturbed.

That's why it is impossible to power a load cell through a 220V-10V transformer connected directly to the mains. As a matter of fact, power distribution network trend is not stable and affected by all the electrical utilities connected. Normally, neither transformer output signal is stable. For all these reasons it was necessary to interpose a conditioning module between the mains and the device itself. The component adopted is Pimzos SG-3016 isolated strain gauge input module which is represented in

Figure 2.18, while in

Figure 2.19 a qualitative electrical diagram of the connection between the mains, conditioning module and load cell is reported. In the end

Figure 2.20 shows the internal electrical diagram of conditioning module.

Before connecting properly all the devices, a calibration procedure made up of three steps was performed on the conditioning module, as suggested by device's manual.

- Adjustment of the offset value
- Adjustment of the gain value
- Adjustment of the excitation voltage value

Each one of these steps asked for a different connecting configuration in order to monitor properly the parameters under adjustment.

At the end of this procedure the devices were connected as shown in

Figure 2.19.

Figure 2.18. Pimzos SG-3016 isolated strain gauge input module
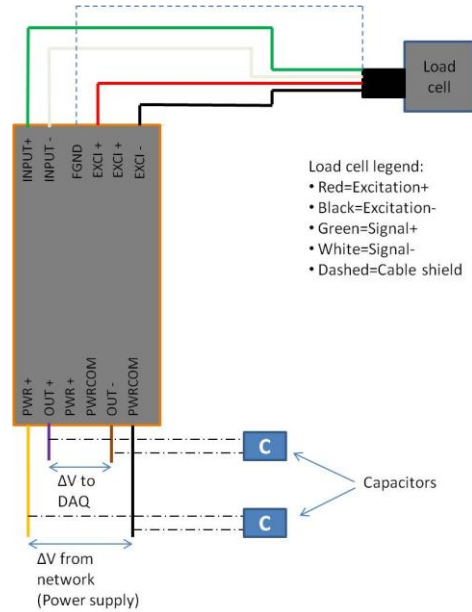
Figure 2.19. Load cell signal conditioning circuit
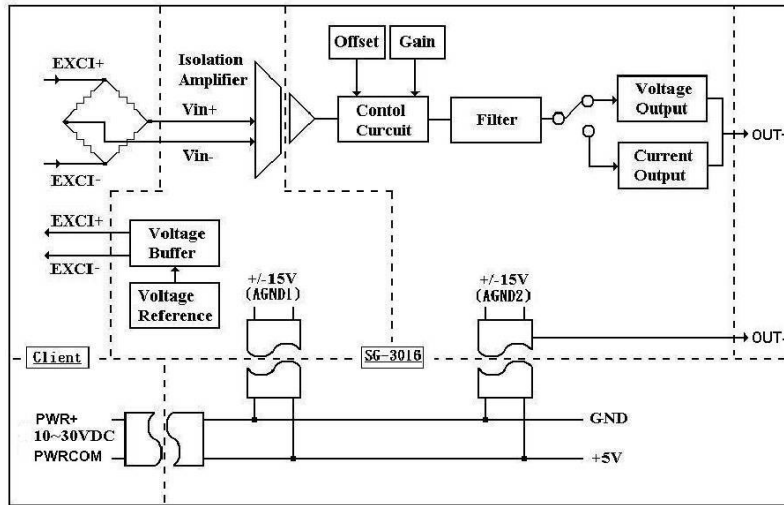
Figure 2.20. Conditioning module internal circuit

Basically conditioning module acts like a buffer that accumulate the charge coming irregularly from electrical network, absorbs peaks and valleys, and returns an average of the input. The latter is what the conditioning module uses in order to power the load cell. Afterwards, since the signal coming back from load cell is very low voltage, the conditioning module amplifies it. As a result, load cell output signal read by DAQ is perfectly stable and clean. It is then

possible to sense variations in the signal up to the maximum resolution of the instrument.

In order to make the signal even more stable two capacitors were added to the circuit. The capacitors have a capacity of 1 μF and a maximum tension of 63 V. The first one was positioned in parallel with the power supply coming from the transformer. The second one was set in parallel with the output signal going to DAQ. These components act like buffers and accumulate the charge transported by the output signal and release it gradually. In this way all the residual irregularity of the signal are deleted.

It is important to underline that both the conditioning module and the capacitors, acting like buffers, cause a little delay in the signal. It becomes then impossible to sense instant changes in the input. However, for the present application this doesn't represent a particular problem. As a matter of fact, all the thermo-mechanical cycles are performed in a really slow way, so no high frequency phenomenon have to be monitored. The slow evolution of the test allows the system to follow it properly, despite the presence of buffers.

2.3.1.3.3 Software interface and filtering

As already anticipated, the software running on National Instruments computer and adopted for signal managing is National Instruments Labview. In this programming environment a load cell dedicated script was developed. Only load cell uses this script because, as it will be explained in next sections, the other instruments were independent from data acquisition system. A snapshot of the block diagram associated to the script is reported in
Figure 2.21.
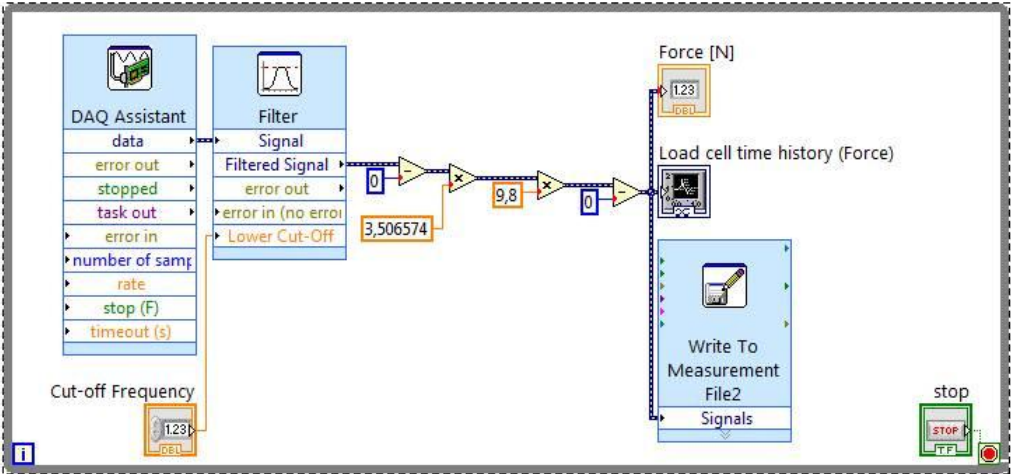
Figure 2.21. Labview block diagram dedicated to load cell

This script is pretty simple. Everything is enclosed in a while loop that may be interrupted by means of a stop button. The block 'DAQ Assistant' is associated to data acquisition system channels. It is synchronized with the channel related to the load cell. The block returns this signal from channel data. From the settings of this block it is also possible to regulate some important parameters. In particular, the acquisition frequency has been set to 100 Hz.

The output of this block enters a second block named 'Filter'. This is indeed a software filter applied to the signal coming from data acquisition system. It simply multiplies signal's spectrum by a Bessel low-pass filter, order 5, with a cut off frequency real time adjustable through a numerical control ('Cut-off Frequency' block, connected with 'Lower cut-off' channel in Figure 2.21). As already explained in section 2.3.1.3.2, the performed tests are really slow. No high frequency variations are supposed to occur. All high frequency components of signal's spectrum are then attributable to noise. For this reason, setting a very low cutting frequency doesn't compromise the signal related to the studied polymer's behaviour and cleans it up from any undesired interference and disturb. As a matter of fact the value chosen for this parameter is around 5 Hz.

The output of 'Filter' block is a voltage signal as the output of previous block was. Defining rated capacity as the maximum weight that a particular load cell can measure while meeting its specifications, the rated output is defined as difference between the value of the electrical output when the load applied is maximum (rated capacity) with the value when no load is applied. It is usually expressed in output (electrical signal when load is applied) per excitation voltage (fixed alimentation value of the load cell) [mV/V]. Starting from this index it is possible to obtain the relationship between volts and kilograms.

In order to verify load cell's good functioning and linearity, and in order set the device, a calibration procedure was performed. Increasing loads were hung to the load cell while taking note of the voltage output. The latter is in mV, but in the following steps it will be reported directly in V. In the following Table 2.4 the results obtained are listed while Figure 2.22 shows the interpolating curve.

Table 2.4. Load cell calibration numerical results

Object	Object's weight [kg]	Total load applied [kg]	Output [V]
Load free	0	0	0
Loads holding plate	0.0835	0.0835	0.0239
Weight (200g nom)	0.2005	0.284	0.08045
Weight (200g nom)	0.2015	0.4855	0.13815
Weight (500g nom)	0.5005	0.986	0.28155
Weight (1000g nom)	1.0015	1.9875	0.56905
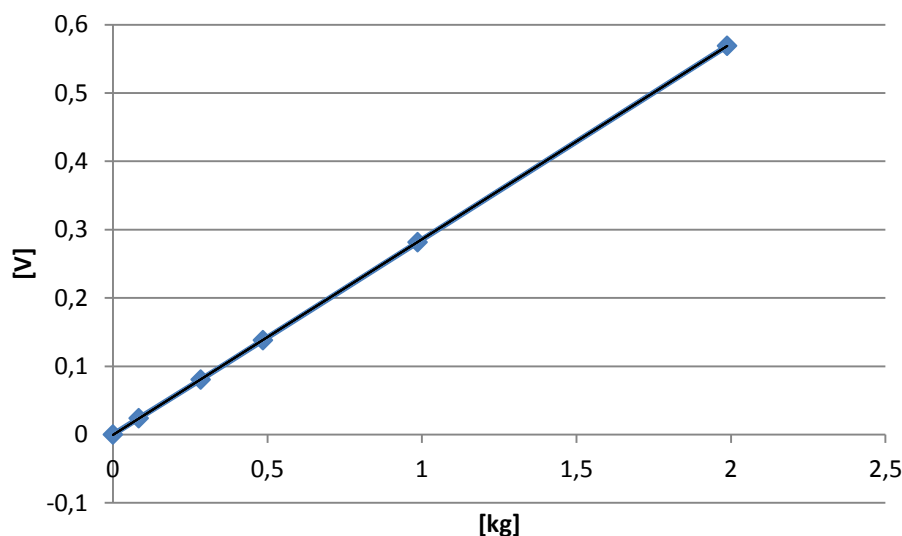
Figure 2.22. Load cell calibration interpolating curve

As one could notice, the trend obtained with calibration procedure is quite perfectly linear. The equation of the interpolating line is the following:

$$y = 0.2864\, x - 0.0005 \qquad\qquad \text{(2.9)}$$

The quite perfect linearity of this trend is further confirmed by R^2 index associated to interpolating curve. This index is indeed equal to one.

The inverse of the obtained slope is then the relationship that associates kilograms to volts. Its value is 3.506574. This explains the coefficient multiplied by the exit of the filter in Labview's script.

Afterwards the signal is multiplied by another coefficient 9.8, which represent gravitational acceleration and operates the switch from kilograms to newtons.

In conclusion, the signal is sent both to a numeric indicator and to a graph indicator which makes possible to visualize force trend during test. The last branch of block diagram leads to a block that creates a file in which all the samples took are stored in a particular structured format (.lvm), compatible with Microsoft Excel.

2.3.1.4 Climatic chamber

This component represents an important difference compared to bench's first version. As explained in section 2.2, the idea to heat polymer through IR lamps implied several issues.

The solution tough to overtake these limits and problems was basically to create a temperature-controlled environment just around sample. This meant to enclose the main area of the machine into a tailored climatic chamber. This kind of solution was inspired by literature. As a matter of fact either in [6] or in [7] a climatic chamber was adopted. In particular in [7] a thermocraft oven was used in order to heat the sample, while liquid nitrogen performed the cooling phase.

One of the main issues related to IR heating, was the difficulty in controlling samples' temperature in relationship whit power supply provided to lamps. Even if it is possible to regulate lamps power, lead sample to a desired temperature and keep it constant could be really problematic. Moreover measuring sample's internal temperature results quite impossible through a conventional thermocouple, like the one available. Even if thermocouple sensitive zone is really close to sample, the measured temperature will be probably closer to the one of the surrounding environment than to the sample's one. Through a climatic chamber, it is possible to heat the internal volume up to a desired temperature, and if chamber's dimensions are contained, this process could be really fast. In order to monitor the internal temperature, a conventional thermocouple could be adopted. If the latter is stuck in the chamber, its sensitive zone is exposed to internal heat and in few seconds it reaches thermal equilibrium conditions with the environment. The same thing happens to sample, whose really small dimensions allow it to follow quickly environment's temperature. After few seconds of exposition to heat it is possible to assume that the environment, thermocouple and sample are in thermal equilibrium. This system make then possible to monitor and control sample's temperature in a reliable way, which is impossible with IR lamps and the configuration tough for machine first version.

A particularly interesting solution regarding thermocouple position is presented in [6]. In particular, in the system presented, the device is suspended from the top gripper. In this way it is possible to keep thermocouple constantly in contact with specimen surface. In the present project, thermocouple position is fixed. In particular the device is kept as close as possible to sample's central area.

Going back to climatic chamber's advantages, this kind of device makes possible to reduce sensitive components direct exposition to heat, which is then kept close to sample, as desired.

All these advantages justified the evolution in the project regarding heating principle and temperature monitoring.

It was decided to assembly a climatic chamber from scratch because looking for a commercial suitable solution would have been more complicated and expensive. As a matter of fact, during a quick research among available solutions on the market, it was realized that none resulted suitable in terms of dimensions and other important aspects. The component searched was supposed to have some peculiarities difficult to find in commercial solutions. For example the chamber should provide an opening for motor shaft and, as it will deepen in

next section, a wide optical access on the front side. All these important particulars made impossible to find a suitable commercial solution and suggested to proceed with the design of a new climatic chamber.

The path followed was the same adopted for the whole bench. In this case, the first phase didn't consisted in a simple reproduction of components, because components did not exist yet, but more in a real design of new parts. Every piece was studied in order to fit volumetric constraints and to make the final assembly as ergonomic and safe as possible.

2.3.1.4.1 Materials and features

The general idea since the beginning was to realize the external structure of the chamber with a rigid material and possibly characterized by a low thermal conductivity. Moreover it was tough to cover the internal side using an insulating material with a reflective side. The first material tough for the external structure was Peek. It was indeed tough that a polymeric material able to resist to really high temperatures levels was something meeting perfectly all the needs of this part of the assembly. After a first search among polymers it was found Peek as perfectly suitable. This material, as all polymeric materials, has e low thermal conductivity but differently from most of other polymers, it is characterized by a very good resistance to high temperatures. Peek is a semi-crystalline thermoplastic with excellent mechanical and chemical resistance properties that are retained to high temperatures. Glass transition temperature of this material is around 143°C and it melts around 343°C. The thermal conductivity increases nearly linearly versus temperature between room temperature and solidus temperature. Moreover Peek is characterized by very good mechanical properties. Young's modulus is equal to 3.6 GPa and its tensile strength is around 100 MPa [26].

In the end, from a first contact with ULB internal workshop, it was discovered that the internal staff had already dealt with this material and had all the instruments to work with Peek.

Despite all these advantages, the idea of using Peek was finally left because of economical matters. As a matter of fact, the price of this material reflects its extremely high performances. However it should be considered that these performances were even oversized for this application. As already explained, temperature working range for SMPs testing in this project is not severe and reaches a maximum temperature which is around 75°C. For this reason the material adopted changed to aluminum.

The latter is relatively economic and diffused in ULB workshop. Despite its good thermal conductivity, the not excessive maximum temperature, the limited exposition time to high temperatures and the presence of an internal insulating layer made possible to adopt this material without any risk.

In parallel with material research, the CAD design of climatic chamber's components was carried on.

As already said, during this phase, several dimensional bounds were took in account. The chamber had to be as small as possible, in order to reduce all thermal transients. At the same time it had to allow the gripping device fixed on motor shaft to perform a full stroke of 50 mm. Furthermore, the chamber had to provide enough space, once open, for handle the sample during tests.

Figure 2.23 is an overview of the final assembly realized through CATIA v5.

Figure 2.23. Climatic chamber CAD assembly

As aluminum sheets (thickness of 10 mm) were already available in the work shop, and the staff is really specialized in aluminum processing, the time delay and the cost of the actual assembly of the component was very small.

Once individual components were manufactured, the actual assembly process started. Table 2.5 shows some of the main phases of this process.
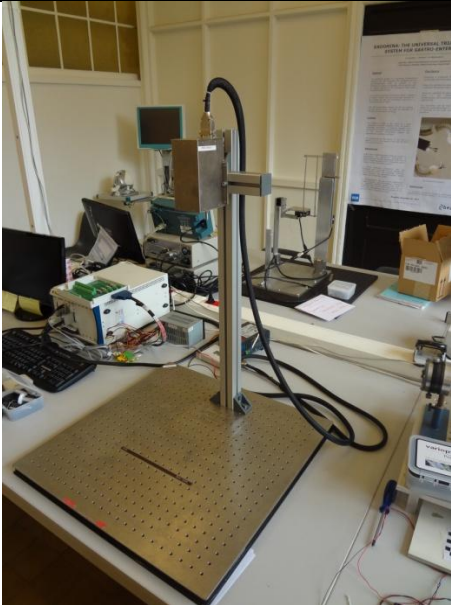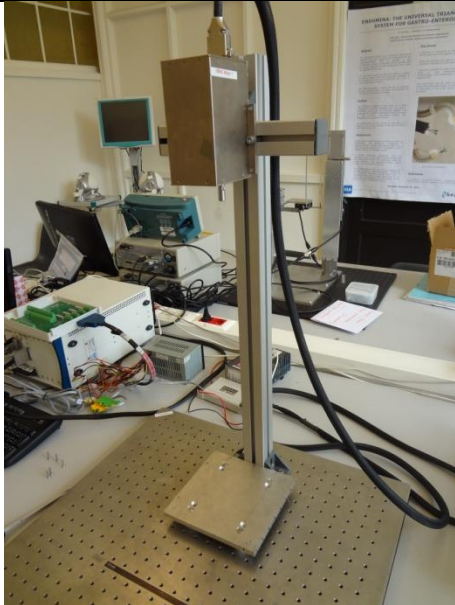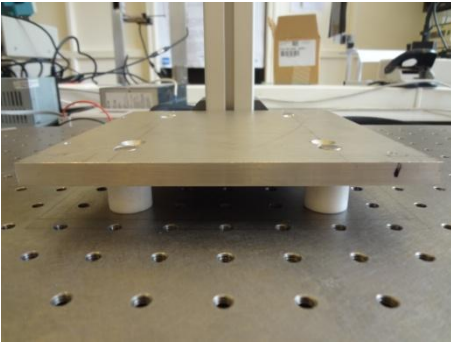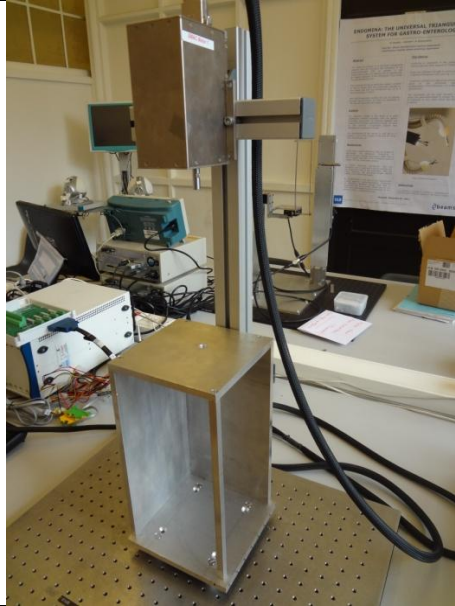
In the final assembly, hinges were added to doors, in order to realize the opening movement shown in

Figure 2.23.

The results of this first phase, was just the external structure of the component. Afterwards, several steps followed. The first one was to close the wide optical

access on the front door using a particular type of transparent material. After a quick research among commercial solutions, we were proposed to adopt a particular kind of glass, able to resist when exposed to high temperature (up to 200°C).

Table 2.5. Climatic chamber assembly phases

(1) Empty basement	(2) Climatic chamber's base
(3) Climatic chamber's Teflon feet	(4) Lateral and top panels assembled

(5) Compatibility with other test bench's components	(6) Front and lateral doors added
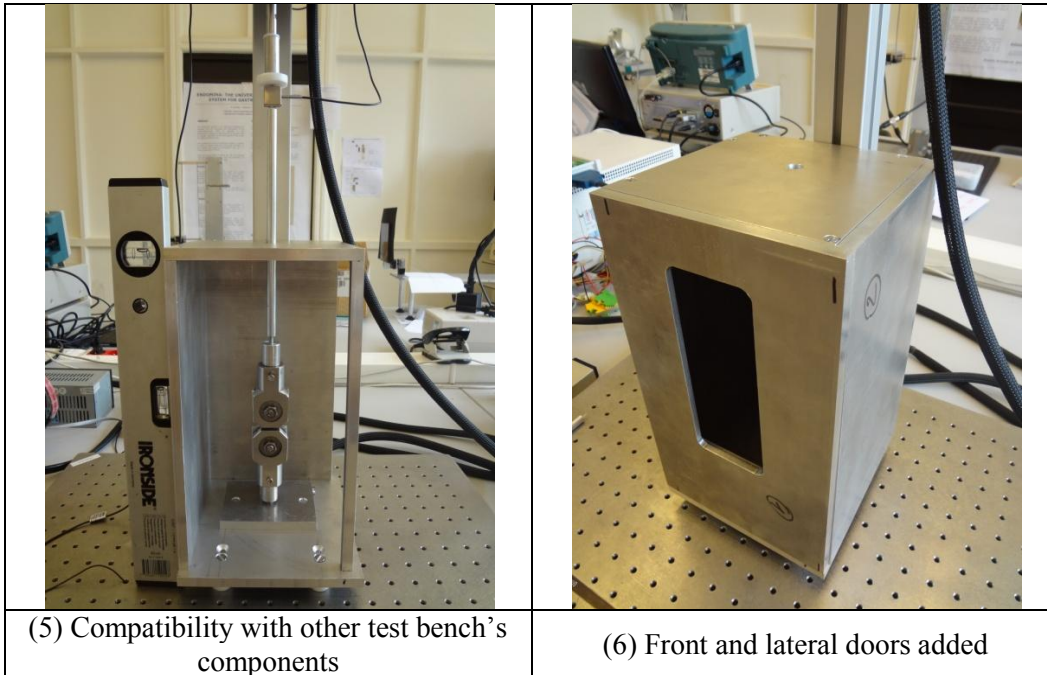
Another important step was to add an insulating layer on the inner side of the chamber. It was decided to adopt rock wool covered with a thin aluminium reflective layer. This expedient improved the ability of the chamber to keep heat and reduce its dispersion to ambient also thanks to aluminium layer that reflects radiations towards the inner part of the oven. This means also that heat transmitted through aluminium decreases and the external temperature of the chamber is even more compatible with security constraints.

Figure 2.24 is an image of the chamber after the addition of the insulating layer.
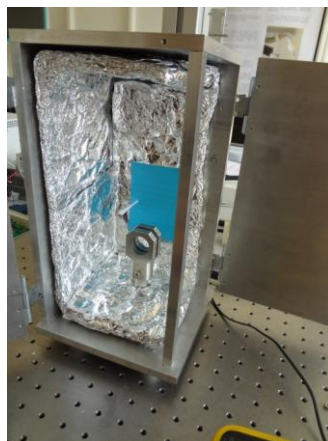
Figure 2.24. Climatic chamber main body after the addition of the insulating layer

2.3.1.4.2 Lamp and electrical circuit

At this point, the heating source was added. It was tough to use a halogen lamp for this purpose. The latter is a commercial economic device, which is available in several different configurations. In particular the one chosen for the actual work is a linear halogen lamp (Pro light lamp) providing a power of 1000W with a voltage of 230V (50/60Hz). The following
Figure 2.25 is a photo of the device itself while in
Figure 2.26 some dimensional information are reported.

Figure 2.25. Pro light halogen lamp
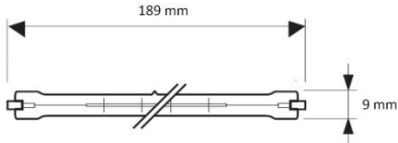
Figure 2.26. Pro light halogen lamp dimensions

Furthermore, another important feature is the fact that this lamp is dimmable from zero up to the maximum power offered by the device. This feature is particularly important as one of the main aspects of climatic chamber is the possibility to control the internal temperature. Using Pro light halogen lamp temperature can be controlled either switching the lamp on or off or taking advance of Pro light halogen lamp possibility to be dimmed. In order to use this peculiarity, a dedicated electrical circuit was realized. A schematic reproduction of the latter is shown in
Figure 2.27 while
Figure 2.28 is a photograph of the actual circuit.
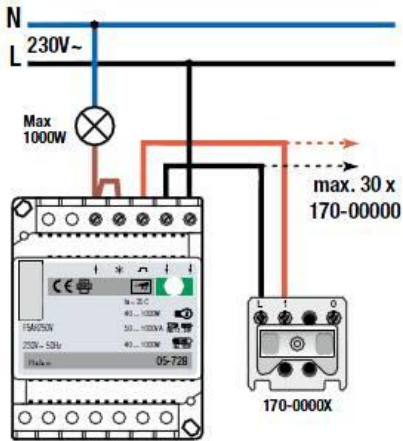
Figure 2.27. Dimmer circuit scheme
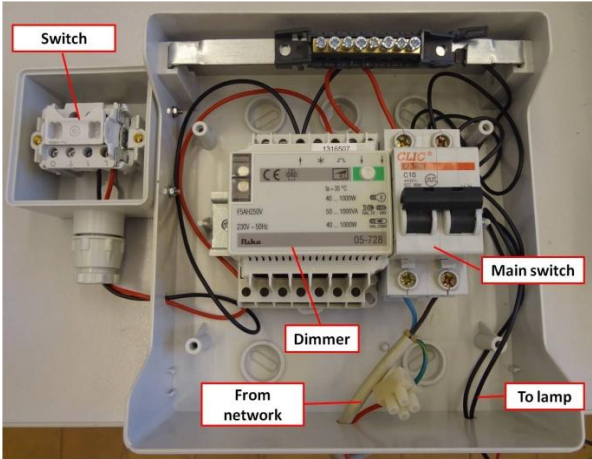
Figure 2.28. Actual dimmer circuit

As shown in

Figure 2.28, compared to the scheme in

Figure 2.27, a general switch was positioned between electrical network and the circuit. The aim of the latter was to avoid kicking the line in case of short circuit or any other problem. It is also important for users' safety.

Through this model of dimmer, power profiles like the one presented in

Figure 2.29 can be obtained. In the profiles shown the upper trend is the duration of the pressure exerted on the switch, while the second trend is the corresponding effect on power provided to lamp.
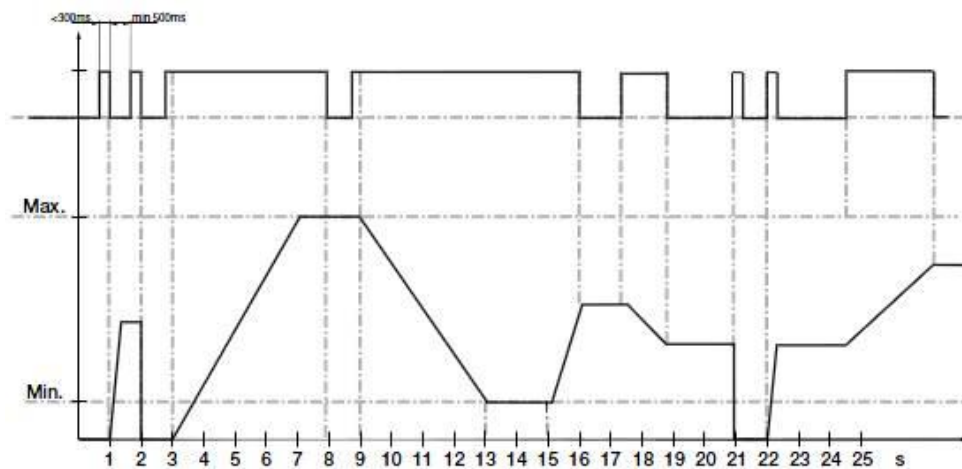
Figure 2.29. Dimmer power trend related to the duration of the pressure exerted on the switch

In the end, halogen lamp was fixed to the inner side of the front door and its extremities connected to the circuit.

Figure 2.30 shows the halogen lamp assembled on the test bench.
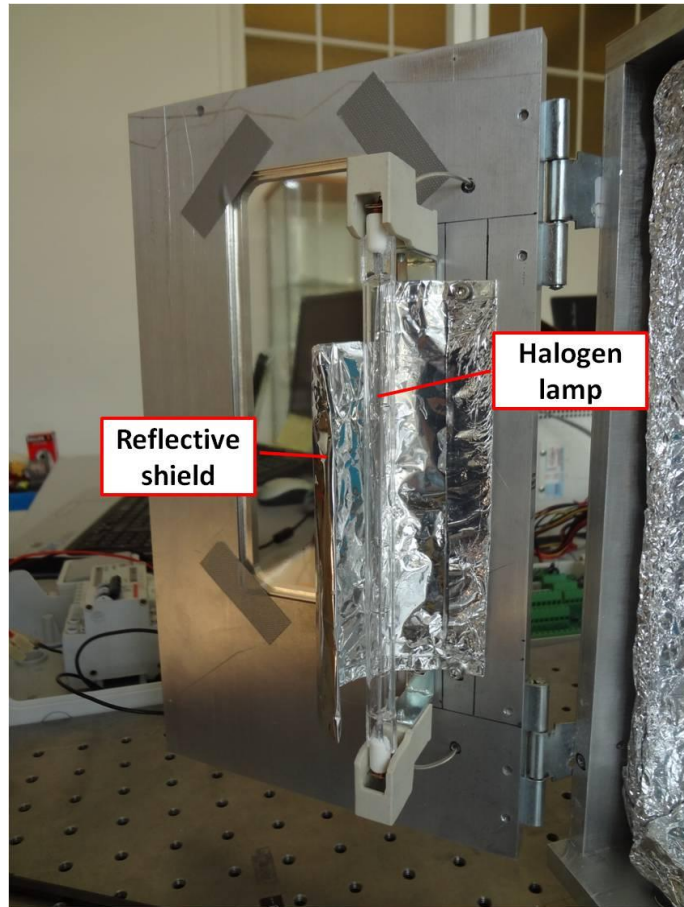
Figure 2.30. Halogen lamp fixed on the inner side of the fron door

2.3.1.4.3 Thermocouple

In order to monitor chamber's inner temperature, a conventional thermocouple was adopted. For this device, the thermocouple associated to a conventional multimeter available in the laboratory was chosen. The model is Elix My-64. A photograph of the device is shown in
Figure 2.31.
Thermocouple's sensitive extremity is stuck inside climatic chamber. In particular it is positioned in order to get as close as possible to the sample, in order to monitor the temperature of the air surrounding the object of the test.
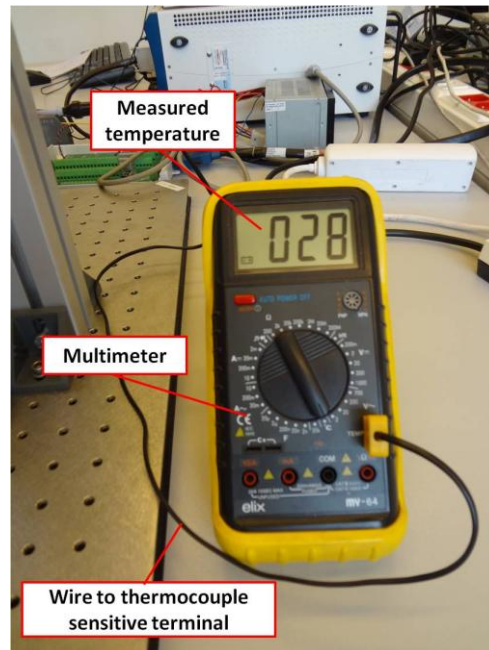
Figure 2.31. Thermocouple associated to a conventional multimeter

2.3.1.5   Camera

The last variable to be monitored is sample's elongation. As already explained in the previous sections, using motor's shaft displacement for this purpose imply several not negligible problems. However this solution was found in some systems presented in literature. In particular, [6] associates the displacement of a screw-driven testing machine's crosshead to specimens' elongation. In [7] motor's shaft movement is assumed as main reference for sample's elongation measurement and an optical system (VIC) supports the monitoring of polymer's deformation.

An alternative solution normally adopted while performing traction tests on polymers consists in adopting an extensometer as suggested by regulations [18]. Fixing the latter to the extremities of sample's sensitive zone, it is possible to track exactly the elongation of just this part, avoiding to take in account undesired deformations. However this solution can't be applied in the present work. As a matter of fact, this device should be enclosed in the climatic chamber and exposed to high temperatures. Normally this devices are characterized by a particular temperature working range which does not reach the maximum values previewed for the present work.

For this reason, even if the extensometer appears like an effective solution, an alternative hypothesis had to be worked out. Finally an idea that seemed to suite properly all project's needs came out. The latter consisted in adopting a

contactless system able to track sample's sensitive zone elongation. It was tough to manage a conventional camera through a Python script.

2.3.1.5.1 Hardware

The device managed by the above mentioned scripts is a common web cam reported in
Figure 2.32. The latter is plugged through a USB socket to a laptop which is different from the computer used for the load cell.
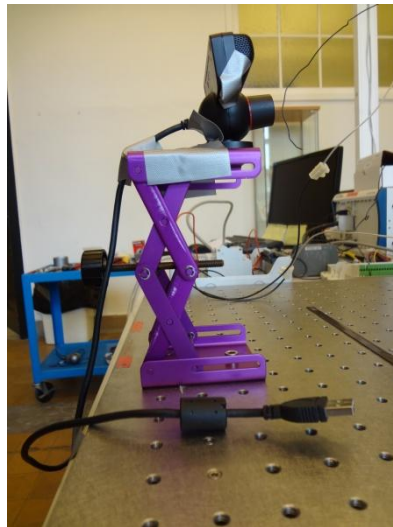
Figure 2.32. Common webcam manged trhough Python scripts

The possibility to follow the evolution of sample's elongation through the camera, is made possible by the wide optical access realized on climatic chamber's front door.

2.3.1.5.2 Software, calibration process and data processing

Python is a programming language, dynamic and object oriented which resulted particularly suitable for the present application. In particular four Python scripts were developed, each one dedicated to a different phase of the test. In particular, two scripts were dedicated to the calibration of the camera.
Camera calibration means to estimate parameters that are either internal or external to a camera [27] [28]. The internal (or intrinsic) parameters determine how the image coordinates of a point are derived, given the spatial position of the point with respect to the camera. Some of the resulting variables from this phase are camera's focal length and distortion coefficients. The existing techniques for camera calibration can be classified into object-based calibration and self calibration. Self-calibration techniques do not use any

calibration object. Using self calibration techniques, a large number of parameters need to be estimated. Hence, self-calibration creates mathematical complexity. The object-based calibration can be further classified into three categories according to the dimension of calibration objects. The calibration techniques can be summarized as follows.

3D object-based camera calibration is performed by observing a calibration object whose geometry in 3D space is known with very good precision. The calibration object usually consists of two or three planes orthogonal to each other. This approach requires an expensive calibration apparatus and an elaborate setup. 2D object-based camera calibration proceeds by observing a planar pattern shown at various orientations. A 2D pattern for calibration is easier to be set up than a 3D pattern. 1D calibration is achieved by observing a few pre-determined collinear points on a 1D calibration object. During the observation, the 1D object can be freely moved except that at least one point on the object must be at a fixed location all the time. Zhang's approach requests at least six observations of the 1D object for estimating only five intrinsic parameters and his approach does not estimate any extrinsic parameters.

The method used for the present work is 2D object based calibration. In particular, the reference object was a chessboard properly dimensioned (60x90mm; composed by 54 squares 10x10mm). The procedure followed by the first Python script is to receive as an input the dimensions characterizing the chessboard and then take several images of the 2D object from different angles. Starting from these information all the internal parameters of the adopted camera are estimated and memorized into '.txt' files (cameraMatrix.txt; distortionCoef.txt). Internal parameter are fixed, once evaluated, this script doesn't have to be repeated, it should be run just once.

The second script is aimed to get camera's external parameters. The external (or extrinsic) parameters describe the geometrical relation between the camera and the scene. This means that the script calculates the position and orientation of the camera, relative to the plane containing the chessboard. The script receives as input the specifications about chessboard dimensions and is designed to recognize the 2D object in the space. Once the object is recognized, the script plot a particular colored pattern on the framed image off the chessboard. This visual signal, reported in

Figure 2.33, means that camera recognized the chessboard and its orientation and position.
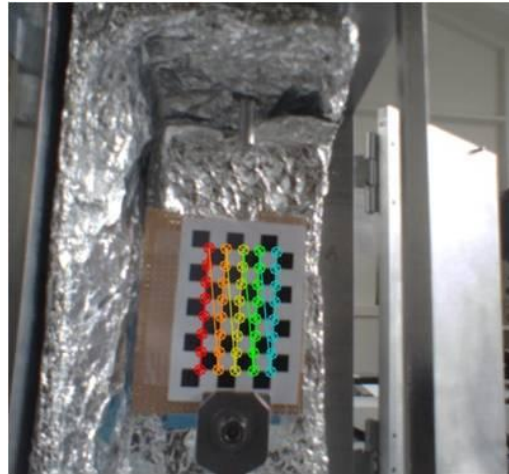
Figure 2.33. A colored pattern is used by Python script to confirm the recognition of chessboard position

When this signal appears, the user should give an input to the script through the keyboard. After this input, the script memorizes all the external parameters of the camera into two '.txt' files (rMat.txt; tvec.txt).

Using this two files, through third and fourth script, Python is able to provide the distance of every couple of points in the same plane in which chessboard was positioned during external parameters calibration. Obviously this phase should be performed after fixing the camera to the position assumed during test. The device shouldn't be touched anymore, at least until next calibration.

The following two Python scripts work in a similar way. In particular they provide the distance between two clicked pixels on the image framed by the camera. However, the third script takes photos with a frequency of 0,2 Hz, while the fourth provides the distance between two pixels but starting from the images memorized by third script and without taking any other photograph.

The third script was then adopted to monitor the evolution of the test, taking as already said an image of it every five seconds (a file containing the corresponding time of each photograph is produced at the end of the test). On the other hand, the fourth script was used to treat the images after the test. As a matter of fact, using this script it is possible to scroll through the memorized images and for each of them, just by clicking on sample's sensitive zone extremities, it is possible to get the elongation.

Furthermore, it is interesting to notice that the acquisition frequency of the camera is set to be pretty low. This is due to two simple reasons.

The first one is the fact that camera maximum acquisition frequency is lower than the one provided by the load cell. The second reason is related to the necessity to treat images manually at the end of the test. This leads not to exceed

with the acquisition frequency, which is proportional to the number of images to be treated. As a matter of fact, yet with a so low frequency the manual treatment of the images results very time expensive.

In conclusion, the camera resulted useful for a further reason. Indeed the thermocouple visual interface (multimeter main body) was positioned in front of the camera and through it, monitoring the evolution of temperature versus time was made possible.

2.3.1.6 Secondary components

Among the secondary components it is important to mention the transformer adopted for the power supply of the load cell. Indeed, in the laboratory, a transformer obtained from a computer was available. It receives as input 220 V coming from electricity network and returns two pretty stable voltage signals. One of 5 V and the other of 10 V. The latter was adopted for load cell's conditioning module.

Other important components to be mentioned are the gripping devices. Differently from what hypothesized in the first version of test bench, it was retained too much complicated and time expensive to manufacture this parts. As a matter of fact the time delay estimated by workshop staff was not compatible with the time frames of the project. It was then decided to find an alternative solution.

After a quick search a suitable couple of gripping devices was found in another laboratory. In particular, these components were used previously to perform traction tests on plastic films. It was then decided to borrow them. An image of one of the gripping devices is shown in
Figure 2.34.
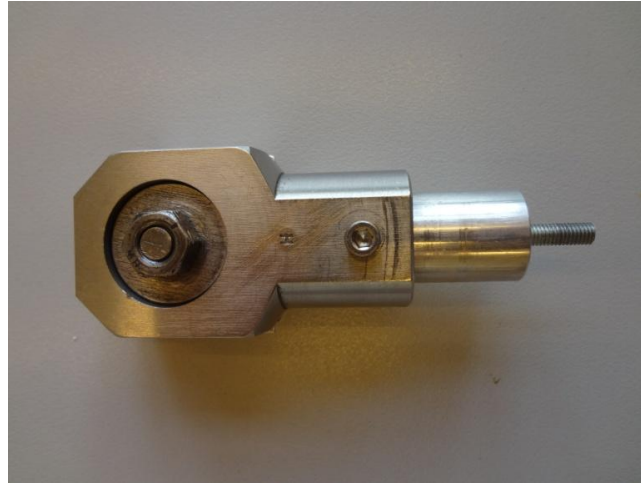
Figure 2.34. Gripping device

However, the inner surface of this jaw is strongly irregular. This kind of surface could damage the sample and exerted an irregular pressure on it. Two aluminum plates were then inserted in the gripping device in order to make the direct contact with polymer smoother and the exerted pressure more uniform. In this way, the risk of unexpected breakage of samples due to excessive pressure exerted by jaws was reduced.

Regarding gripping devices, several solutions can be found in literature. In particular in [6] and [7] pneumatic grippers are adopted. Using this kind of solution makes it difficult to regulate the pressure exerted on the polymer. This could imply a damage to the sample and undesired breakage during traction. The grippers adopted for the present project can be tightened manually by means of an internal screw.

In conclusion it is important to underline that several tricks were took for preventing the transmission of heat to sensitive components. In particular climatic chamber Teflon feet presented in Table 2.5 (number 3) were introduced to prevent heat to be transmitted directly to machine metallic basement which is exposed to the contact with people. Moreover a Teflon screw was used to connect load cell with motor shaft extension. As a matter of fact, the latter has a substantial part exposed to direct heat, inside the chamber. It is then normal that this component heats up quickly. Preventing load cell direct contact whit shaft extension is then important in order not to damage the measuring instrument.

With the present chapter, all machine's main features have been introduced and their functioning have been explained. The following chapter 3 will introduce all the aspects related to test procedures and methods adopted, while chapter 4 will make a broad overview about all results obtained.

Chapter 2

Chapter 3

Shape memory polymers thermo-mechanical characterization

In the following sections all the details about how tests were performed will be presented. In particular section 3.1 is a brief introduction to the types of tests performed while section 3.2 will focus on the physical and dimensional features of samples. In conclusion, section 3.3 will explain all the steps followed during each kind of test and the methods adopted while the last one section (3.4) will deepen the way in which the obtained data were processed and treated.

3.1 Strain and stress recovery cycle

The reference thermo-mechanical cycle for the present work is the one introduced at section 1.3.1.2. This particular cycle can be realized in two different ways. The difference between the two is the last part of the cycle. On the one hand it is possible to free one extremity of the sample, heat it above melting temperature and evaluate the ability of the material to recover the original shape. On the other, it is possible to keep the sample bonded while heating it above melting temperature and measure the force it is able to develop. The name associated during the present work to the first type of cycle is 'strain recovery cycle' while the name associated to the second one is 'stress recovery cycle'. The indexes obtained by both have been presented in section 1.3.1.2. From a practical point of view, sample is fixed to the machine through the gripping devices presented in section 2.3.1.6. One of these components is fixed to climatic chamber base and doesn't move. The other one is integral with motor shaft extension. Through this moving gripper, the motor exert a traction on the sample which results progressively elongated. This is what happens during traction phase (path 1➜2 of

Figure 1.1) which is performed while climatic chamber is closed and kept at a temperature above melting temperature. Obviously, before starting traction phase, a proper time delay should be respected in order to ensure that sample and thermocouple reached a condition of thermal equilibrium with the surrounding environment above melting temperature. Once the maximum stroke desired is reached, motor shaft is kept blocked and the cooling phase starts (path 2➜3 of

Figure 1.1). In particular it consists in switching off the climatic chamber and opening its doors in order to make sample and thermocouple reach the thermal equilibrium with ambient.

After cooling phase, sample is released from bottom gripper (path 3➔4 of Figure 1.1) and reaches zero stress condition.

Once this phase is completed, it is possible to switch to a strain recovery cycle or to a stress recovery one. If the first one is chosen, climatic chamber's doors are closed and temperature is lead above the melting one. In this way heated sample is free to recover its original shape and all the recovery phase is monitored through the contactless optical system as it is during the rest of the procedure. This type of test finishes some seconds later the reaching of the maximum established temperature (the latter is normally around 65°C). On the other side, stress recovery cycle previews to keep the sample bounded during heating phase. In particular, at the end of cooling phase, sample is released from bottom gripper in order to evaluate strain fixity rate (Equation 1.1). Afterwards it is bounded again, the climatic chamber is closed and temperature raised above melting temperature. Due to recovery properties the polymer exerts a certain force to grippers and this variable is monitored by the load cell.

3.2   Sample dimensions and materials

One essential aspect while testing a material are the dimensions and shape of samples. This feature should be defined in a unique way in order to promote the repeatability among tests' results. Moreover, this aspect is particular important while dealing with polymeric small samples that are particularly sensitive to scale effects. In the present work, it was then decided to adopt a unique shape for all the materials studied. ASTM D638 regulation [18] was took as reference regarding this feature (sample type V) as it was in [6] and [7]. In particular it suggests to adopt dogbone shaped samples characterized by the dimensions specified in

Figure 3.1 referred to sample type V, which is the one adopted for this study.
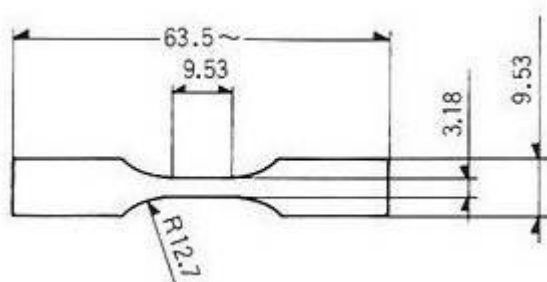
Figure 3.1. ASTM D638 sample type V

Figure 3.2 is an image of a sample cut according to the regulation.

Figure 3.2. Polymeric sample cut according to ASTM D638 regulation

The present work focuses on samples synthesized at Mons university (department of chemistry). Provided samples belong to six different typologies. In particular it is possible to distinguish two big families: Jera and FLPI. Between the two there are some differences in composition and synthesizing process but they both can provide good shape memory properties. Due to their composition, samples belonging to Jera family can't overtake too high temperatures, otherwise they undertake a composition change that compromises their properties. All the samples provided from Mons university were tailored in their composition in order to have a melting temperature T_m between 40 and 50 °C.

Indeed as explained in section 1.2, it is possible to tailor shape memory properties playing with their chemical structure. In particular modifying the composition of the polymer, it is possible to achieve different values for characteristic temperatures. For example it is possible to further decrease the values of melting temperature T_m by adding to the polymer some ordered and crystalline structures. However this would probably worsen shape memory properties. Indeed, the adding of a crystalline structure would surely decrease entropy of the polymer network and this is in contrast with shape memory properties. In the provided materials families, some different compositions were synthesized. One of the goal of the present work is to investigate the effects of composition differences related to material thermo-mechanical properties.

Overall, three different types of Jera (Jera G117c; Jera G117e; Jera G117f) and three different types of FLPI (FLPI A40; FLPI A46; FLPI) were provided.

3.3 Test procedure

The present section explains each single practical step followed during the test procedure normally adopted in this work. As it will emerge later, this procedure appears someway complex and articulated. However it has to be considered that project timeframes allowed just to develop a well functioning and reliable system, but not to optimize it. As it will be explained in the conclusions, the machine offers still several possibilities of optimization in order to make test procedure simpler and maybe more automated.

Regarding the actual test's procedure it will be described in the following points:

- Step 1, Motor positioning:
  As shown in
  Figure 2.11, motor is fixed to a horizontal column which in turn is mounted to a vertical one. This configuration provides the motor with the possibility to slide either horizontally or vertically and change orientation rotating. In this way, numberless points and orientation can be covered by the motor inside a two-dimensional frame. Taking advance of this, it is possible to use different stroke levels of the motor. In particular, as bottom gripper is stuck and sample length is fixed, the only degree of freedom is motor position. Displacing it vertically allows to use a larger or a shorter stroke for traction phase. Moreover the possibility to move it horizontally and rotate leaves more degree of freedom for machine setting optimization. In conclusion, depending on the desired stroke, motor's position is set during this phase.
- Step 2, sample preparation:
  before positioning the sample on the machine, it is submitted to a procedure aimed to relax all the residual internal stresses due to synthesis

process. It consists in immerging samples into an hot water bath ($T \approx 70°C$). Through this expedient all the fixed strains during synthesis process are recovered and sample results finally relaxed.

- Step 3, sample positioning on the machine:
  at the beginning of this phase, the upper gripping device is took off from the machine in order to facilitate a precise positioning and fixing of the sample on the machine. It is indeed important to ensure a precise orientation and position of the specimen in respect to traction direction. The axis of the sample should be as parallel as possible to the latter also to ensure a good repeatability of tests. Ensuring this precision in sample positioning would be particularly complicated if this phase should be performed while upper gripper is hanging from motor shaft inside climatic chamber. This justifies the disassembly of this component before each test.
  Regarding sample's positioning, as already said, its axis should be as parallel as possible to traction direction and its upper extremity should be in contact with gripper's internal screw. Once sample is fixed to the gripper, the latter is assembled again on the bench.

- Step 4, motor shaft extraction:
  at this point, Matlab script related to motor is launched. Once this script starts, it defines motor movements until the end of the test. The first part of the script makes the motor extract the shaft up to a defined level. The latter has to bring sample's second extremity exactly inside bottom gripper, with the ending in contact with gripper's internal screw. Once this position is reached, motor's script previews a 'waiting' phase which consists in keeping the shaft stuck along a period of time necessary for all the following operations.

- Step 5, sample fixing:
  This phase consist simply in fixing sample's second extremity to the bench, by simply tightening the bottom gripping device

- Step 6, sample heating:
  Once the sample is fixed properly to the machine, climatic chamber's doors are closed and the heating source is switched on. The power supply for halogen lamp during this phase is constant and set to a medium value, in order not to exceed with temperature and compromise material chemical and physical properties. The heating phase lasts about four minutes. This time interval could seem excessive, but it has been set with a large security margin, in order to be sure that sample and thermocouple are perfectly in a thermal equilibrium with the surrounding environment. This phase and the previous one are comprehended in motor script's waiting phase.

- Step 7, start of variables recording:

Fifteen seconds before the end of waiting phase, the two software related to variables recording (Python and Labview) are launched at the same time manually. This ensure that data coming from Labview (related to load cell) and data coming from Python (related to strain and temperature) at the end of the test are perfectly synchronized and they can be compared as they share the same beginning time. The recording process that starts at this step lasts until the end of the test. Indeed, all the following steps represent a fundamental phase of the thermo-mechanical cycle.

- Step 8, traction phase:
  At the end of the waiting phase, motor script previews a controlled retraction of the shaft up to zero position. The elongation imposed to sample is then defined by the position of the motor and shaft initial level of extraction. For motor movement phase it is possible to specify speed, acceleration and final position. In particular speed has been always set to a very low value ($0.5 \frac{mm}{s}$) and acceleration too ($10 \frac{mm}{s^2}$) in agreement with the assumption made for the load cell about the fact that no high frequency phenomenon are supposed to occur. It is important to ensure this condition in order to be sure that load cell is able to follow properly the development of the test, despite the time delay introduced by physical and software filters. At the end of this phase sample reaches a particular level of strain which will be expressed as a percent of its initial length and it is proportional to the stroke performed by motor.

- Step 9, cooling phase:
  once the desired stroke is reached, a new waiting phase starts. This one is longer than the previous and lasts until the conclusion of the test. The aim of this waiting phase is to keep motor and consequently the upper extremity of the sample stuck. Regarding shape memory properties, the cooling phase is performed in order to fix the deformed shape. From a practical point of view, the sample is cooled by simply switching off the lamp and opening the climatic chamber in order to expose sample to ambient temperature while it is still bound. As the aim of this phase is to bring the material to thermal equilibrium with the ambient as fast as possible, a fan was positioned close to one open side of climatic chamber. Temperature is continuously monitored through the thermo couple, in order to realize when the temperature of the environment surrounding the sample is equal to ambient temperature. After some minutes, it is possible to assume that sample is in a thermal equilibrium with the ambient, and cooling phase gets to a conclusion.

- Step 10, zero stress condition
  during this phase, sample is released from the bottom end. In this way it is reaches a zero stress condition because no bounds are applied and it

results hung from the upper extremity. After this step, it is possible to calculate strain fixity rate (equation (1.1)).

At this point tests splits into two different paths, depending on the type of test aimed. A distinction will be now made between:
a) Strain recovery cycle
b) Stress recovery cycle

- Step 11a, second heating phase:
  The sample is left free from the bottom extremity. The climatic chamber is closed and heating source switched on. The power supply of halogen lamp is kept constant and at an intermediate level, as it was during first heating phase. When temperature approaches melting temperature, sample starts to recover the original shape reducing its length. This evolution in sample's shape is recorded by mean of the camera and Python third script, while load cell signal is supposed to keep on being null. This phase finishes once temperature gets to a level close to the maximum which is set to 65°C. At the end of this phase it is possible to evaluate strain recovery rate (equation (1.2)).
- Step 11b, sample bound again:
  This step previews simply to tighten again the bottom gripping device in order to block sample's deformation.
- Step 12b, second heating phase:
  as in step 11a, climatic chamber is closed and halogen lamp switched on. When temperature approaches melting temperature, sample starts trying to recover its original contracted shape, but the bound exerted by gripping devices keep the shape unvaried. For this reason a force is applied by sample on the extremities and sensed by the load cell. Also this phase finishes once reached a temperature value around the maximum one (65°C). An important parameter observable during this step, is the maximum stress recovered, compared with the one reached during the first traction phase.

- Step 13, test conclusion: At this point both types of tests get to an end and the climatic chamber is switched off and the scripts managing measuring instruments are interrupted simultaneously and data stored in proper files.

3.4 Data processing

Chapter 3

Once test gets to an end it is necessary to treat the acquired data. As already said, this machine has several aspects that can still be optimized and maybe automated. One of these aspects is the treatment of data. As a matter of fact, the latter have to be performed manually and results particularly time expensive. There are basically two set of data to analyze. The first one is generated by Labview, related to load cell and consisting in two big arrays. One array containing the time instants in which a sample was took by load cell. The second array contains the relative load cell samples. The dimensions of these arrays are very big, as the acquisition frequency was set to 100 Hz and tests, starting from traction phase, have an average duration of seven minutes. The average number of samples stored during one of these tests is equal to 42000. This first set of data is stored when, at the end of the test, Labview script is interrupted. The format of the file is an internal format of Labview ('.lvm' file) but it is compatible with Microsoft Excel and other data managing softwares. '.lvm' file orders the two arrays and associates to them a particular header.

The second set of data to analyze is generated through Microsoft Excel manually, while treating (through Python's fourth script) the images took during test by Python's third script.

The first step of data treatment consists in opening '.lvm' file through Excel. The two arrays contained are automatically ordered into two columns of the Excel document. Each column has its header, one relative to time and the second to force. Afterwards, other two sheets are created into the document, one will be dedicated to elongation and the second to temperature. During test, python creates automatically a '.txt' file containing all the instants in which the camera took an image of the test. This array of values covers the same time range of the Labview's one, but has a length much lower. As a matter of fact, camera acquisition frequency is set to a lower value compared with load cell's one. At this point of data treatment, this column of time values is copied in the first column either of elongation dedicated sheet or of temperature dedicated sheet of the Excel document under construction. Afterwards Python fourth script is launched and it starts showing the first image took by camera (the one associated to the first time value). Python script returns the distance between two manually clicked pixels on the image. This double clicking procedure aimed to get the distance between two points can be repeated an infinite number of times for each image took. Once obtained the distance with sufficient precision, it is possible to switch to the following image. The procedure is repeated until last photograph. It is now worthwhile to specify the principle on which this measurement works. When camera external parameters were calibrated, through the aid of a 2D pattern, the position and rotation of the camera in respect with the plane containing the chessboard were fromalized in two '.txt' files ('cameraMatrix.txt' and 'tvec.txt') through which Python third and fourth script are able to calculate the length of the vector connecting the centre of the camera to a chosen point on the plane. Once a second point on the plane is selected by

clicking, the distance between the two points is simply calculated by Python as a difference between two vectors. This articulated principle is useful for sample's elongation measurement if during external parameters calibration the reference 2D pattern was positioned exactly in the plane that will be occupied by the sample during test. As a matter of fact, the specimen has a two-dimensional structure and during every kind of test it keeps on staying in the same plane (with a negligible exception for strain recovery phase, during which sample squirms slightly but can still be considered contained in the reference plane). In conclusion, in each image treated by means of Python fourth script, the photographed sample is in the reference plane. It is then possible to evaluate the distance between two points on sample's surface. This offers a great opportunity to track material's elongation and contraction during test. For this purpose, before performing the test, two black stripes were printed on sample's surface at the extremities of sensitive zone whose length is equal to 9.53 mm, as shown in Figure 3.1. A photo took to a sample after this procedure is reported in Figure 3.3

Figure 3.3. Black stripes printed at sample sensitive zone extremities

Moreover, thermocouple's visual interface, reporting the measured temperature, was positioned exactly in front of the camera during tests. In this way images took by camera contained not only the information related to elongation, but also the one related to temperature evolution in respect with time.

Going back to data treatment, once Python fourth script is launched, it is possible to evaluate sample's elongation and read temperature value image by image. The achieved values are then inserted in the Excel file next to the corresponding time value and in the right sheet (elongation or temperature one). This procedure is repeated for each image memorized. Afterwards elongation and force data were transformed respectively in strain and stress. For the elongation this means apply equation (2.3), while for the force it means to divide data by sample's normal section at sensitive zone as showed in equation (2.2).

The necessity to analyze each image manually explains why acquisition frequency of camera is kept to a so low value. Otherwise, manual treatment of the images would be extremely time expensive.

A consequence of this low acquisition frequency is the fact that, at the end of data treatment, the resulting arrays containing data have different dimensions. In particular they cover the same time range, as the instrumentation has been synchronized since the beginning, but load cell resulting array has much more samples, due to its higher acquisition frequency.

As it was retained interesting not just analyze the single arrays in respect whit time, but also try to plot the three variables in the same three-dimensional graph, a way to make arrays dimensions equal was necessary. The solution tough was to use Matlab 'interp1' function. In particular a simple Matlab script was developed. Through the latter, data were extracted from the Excel document and associated to a Matlab variable (an array was created for each measured variable). Furthermore an array was created either for time data of load cell or for time data coming from Python. 'interp1' improve the dimensions of the array related to strain and temperature, inserting the values of the linear interpolating line between two points of strain or temperature, evaluated at load cell time values. At the end of this procedure the three arrays have the same dimension and are comparable.

In conclusion, the final part of the same Matlab script produces a three-dimensional graph, whose axes are stress, strain and temperature. This kind of graph reproduces the theoretical trend introduced in section 1.3.1.2, Figure 1.1, and allows to evaluate the most significant indexes related to shape memory properties.

The following chapter is dedicated to the discussion of the results obtained during the study about shape memory polymers, which made reference to all the procedures and specifications explained in the present chapter.

Chapter 4

Results

In the present chapter all the results obtained during tests will be widely exposed. In particular a first explorative step consisted in studying the repeatability of results provided by the assembled machine. Afterwards, performing a first group of strain and stress recovery cycles on polymer samples, it was possible to identify some limits of the machine. Some improvement and optimizations were worked out and applied to the system and this represents the concluding part of this first approach which will be the object of section 4.1 Afterwards the study about shape memory properties was continued improving progressively the maximum elongation imposed to samples during thermo-mechanical cycles, until reaching their resistance limit. This phase will be discussed at section 4.2. In the final part of this study, described in section 4.3 the most promising materials were selected and submitted to a fatigue study, aimed to evaluate the decrease of mechanical and shape memory properties after several cycles.

4.1   First approach

Once machine assembly was concluded, its good functioning had to be verified. In particular, the ability of the machine to reproduce behaviors similar to the ones found in literature was investigated. Moreover, the reliability of the results provided and of machine functioning was analyzed.
All these steps were treated during a first approach in which some preliminary thermo-mechanical cycles were performed on samples.
It is now necessary provide some information about the setting of these first set of tests, which will be basically kept for the whole study about shape memory polymers.
A first important aspect is the temperature range. The latter was defined to go from ambient temperature (25÷28°C) up to a maximum level around 65°C.
The lower limit is imposed by ambient. As it was decided to cool down the material by making it exchange heat with the external environment, it is necessary to ensure a temperature difference between sample and ambient until the end of the process. It is then impossible to overtake this limit going to a lower temperature then the ambient one.
The upper limit is due to the assumption suggested by literature [5]-[9][17] that no particular differences can be sensed in sample behavior, improving the

level of temperature reached above the melting one. Moreover, at excessive temperatures, one of the two big families analyzed (Jera) suffers a change in its chemical composition that compromises it shape memory properties.

The maximum temperature of 65°C was then chosen as a good compromise between being sure to overtake melting temperature and not losing too much time and energy in heating with the risk of a permanent damage in the material.

Furthermore, it was tough that a not excessive temperature meant not to expose the whole machine to unnecessary rigid conditions.

Regarding the deformation imposed to the material, it can be related to the level of motor stroke used. As already explained in the previous chapters, once defined the position of the motor (which is tunable), the shaft is extracted in order to make sample's lower extremity get really close to bottom gripper's internal screw. This makes it possible to fix sample also from the lower ending. Afterwards, retracting the shaft up to zero level, the sample is pulled and a particular elongation is imposed to it. The latter will be then defined by the position assigned to the motor. The higher is motor's position, the larger is the imposed elongation, until a maximum level of 50 mm.

In conclusion, the force signal sensed by load cell is proportional to the elongation imposed to samples.

For this first approach, it was initially decided to adopt a low level of stroke (10 mm) in order to perform a first set of tests on the most part of the available materials families. As it will be explained later, this first set of data resulted very useful for the optimization of the system.

Afterwards, using an intermediate level of stroke (20 mm), this first step was concluded performing a group of stress recovery cycles on different samples of the same material. The aim of this last data set was to gather information about the repeatability of results produced by the developed system and evaluate the affecting parameters.

4.1.1 System reliability

For the data produced during this first phase of the study a low level of stroke was adopted (10 mm). The family of materials studied is composed by:

- FLPI
- FLPI A40
- FLPI A46
- Jera G117f

Unfortunately, dealing with FLPI A46 samples resulted impossible, due to some defects in the composition and in the manufacturing process. As a matter of fact, already during the preliminary hot bath, samples made up of FLPI A46 squirmed due to the fact that during manufacturing process, several temporary deformations were memorized and then recovered during hot bath.

For this reason, FLPI A46 specimens resulted deformed and not compatible with test bench's layout, after the preliminary set up. It was necessary to discard this materials and this reduced the range of the materials to be analyzed.

Moreover, among the materials provided by Mons university, Jera G117e was tailored in a way that makes it practically lacking of shape memory properties and more similar to a conventional polymer.

For this reason, it was decided not to analyze this material as unattractive and incompatible with timeframes available.

In conclusion the starting set of materials was reduced to three components: FLPI, FLPI A40 and Jera G117f.

The data set gathered at the end of this first group of tests resulted extremely useful, first of all to verify the reliability of the machine to provide results similar to the ones presented in literature. Moreover it allowed to start getting familiar with shape memory polymers and in particular with the provided types, underlining the positive and negative aspects related to each one of them and giving some tips that helped in the planning of the subsequent stages of the study.

As it will be further explained, from the achieved results some limits of the system emerged and were finally identified. This allowed to understand better the problems still present in the machine in order to work out some optimizing changes. The description of these changes will be the object of section 4.1.2.

Hereunder the achieved results will be presented accompanied by some shorts comments.

The first analyzed material was FLPI. The performed strain recovery and stress recovery cycles are presented respectively in
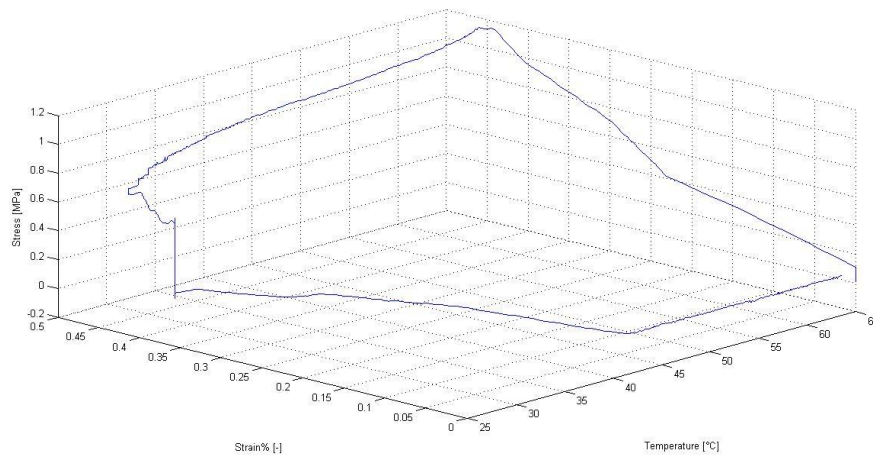
Figure 4.1 and

Figure 4.2.

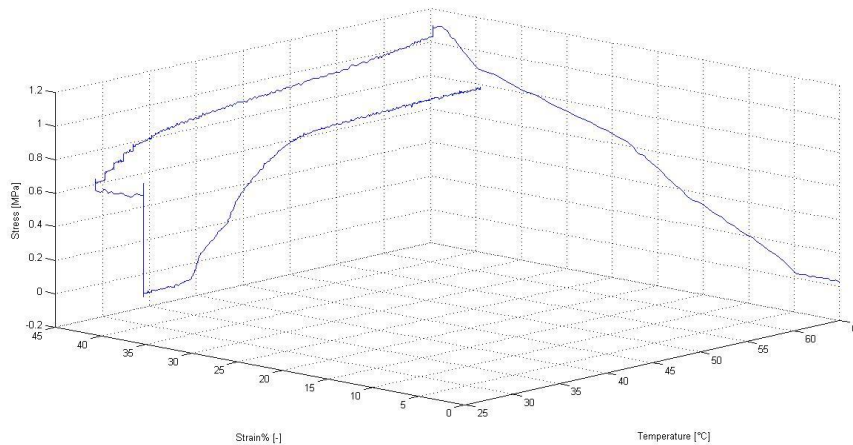**Figure 4.1. Strain recovery cycle performed on FLPI using a motor stroke of 10 mm**

Figure 4.2. Stress recovery cycle performed on FLPI using a motor stroke of 10 mm

This first set of results resulted particularly encouraging for the high similarity with the trends found in literature and for this reason it represented a first confirmation about the reliability of the machine in monitoring properly the actual behavior of these materials.

Moreover the quality of the signal was verified to be particularly good and this is an essential feature while working with very low force signals.

After performing each cycle the main indexes related to shape memory properties were calculated starting from the information provided by the test.

All these indexes are gathered and presented together at the end of this section in Table 4.1 which allows to compare the three materials studied.

The study was then continued performing the same couple of cycles on FLPI A40.

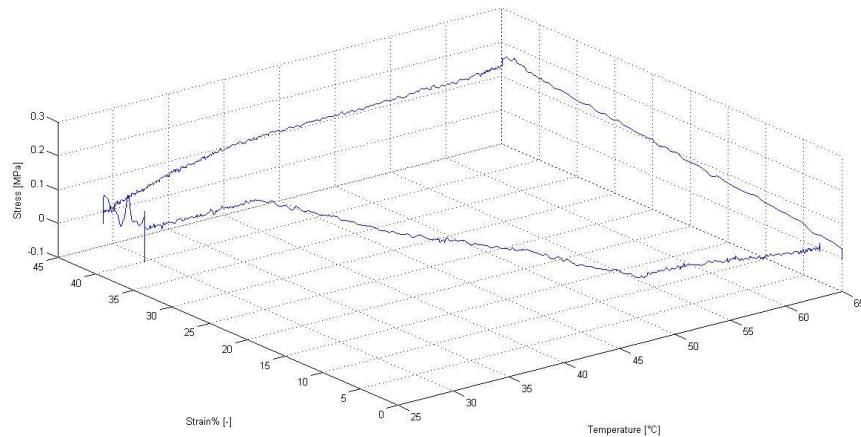The obtained results are presented in the following two figures.

Figure 4.3. Strain recovery cycle performed on FLPI A40 using a motor stroke of 10 mm
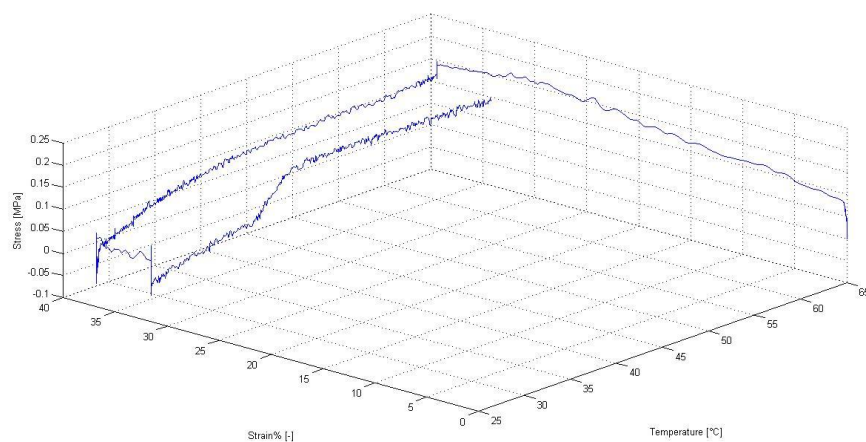

Figure 4.4. Stress recovery cycle performed on FLPI using a motor stroke of 10 mm

This second dataset is a further confirmation about machine's good functioning. From the obtained trends it is immediately possible to notice that, regarding the maximum stress achievable and recoverable by this material is definitely lower than the one provided by FLPI. This will be a fundamental criterion for the planning of the subsequent phases.

The last data set regards Jera G117f and it is presented in the two cycles reported in
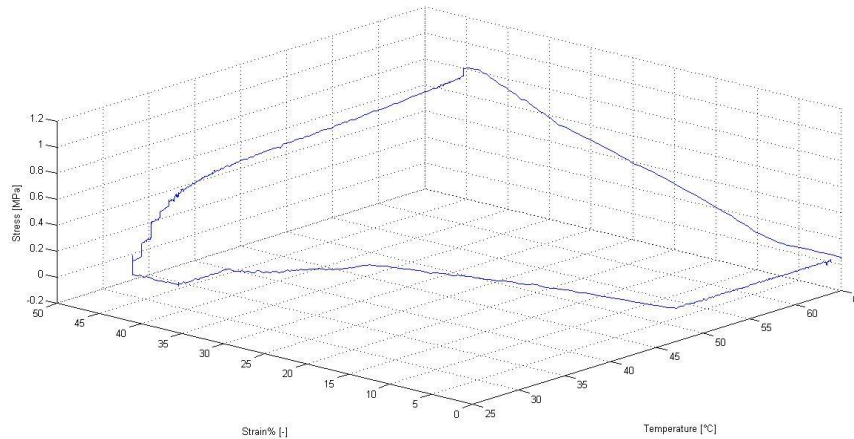
Figure 4.5 and
Figure 4.6.

Figure 4.5. Strain recovery cycle performed on Jera G117f using a motor stroke of 10 mm
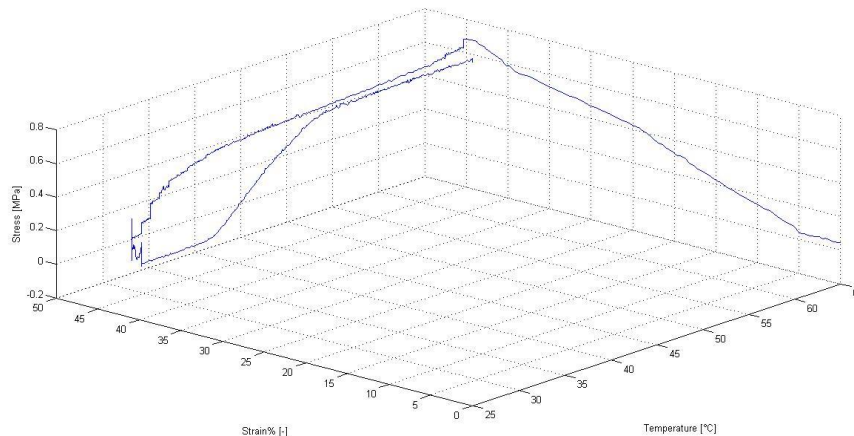

Figure 4.6. Stress recovery cycle performed on Jera G117f using a motor stroke of 10 mm

This last dataset suggest immediately that Jera G117f is able to provide performances which are comparable with the ones provided by FLPI in terms of maximum stresses. This couple of materials candidates itself already from this first dataset to be the most promising one.

In conclusion, the trends obtained reflect exactly what expected in terms of behavior of the material. Indeed they follow precisely what was achieved by other authors working on similar materials [5]-[9][17].

Furthermore the good quality of signals recorded, confirms the fact that despite the system is particularly complicated, it is well working and able to sense down to the slightest change in the involved variables.

The combination of these features confirms the system as suitable for the study of this family of materials.

As anticipated, Table 4.1 resumes the main indexes and values obtained during this first step. In particular R_f and R_r are calculated as exposed respectively in equations (1.1) and (1.2). The last column of the table lists the percent of the maximum stress reached during traction phase at high temperature that the material was able to recover. In particular it is calculated as follows:

$$\sigma_{rec(\%)} = \frac{\sigma_{recovery}}{\sigma_{max}} \cdot 100$$ (4.1)

The latter index is particularly important because, while the maximum stress reached is proportional to the elongation imposed and fundamentally bounded to material mechanical properties (Young's modulus, which is important too), the percentage of this stress that the material was able to recover is strongly related to its shape memory properties. The study of the latter is an important aim of this work.

Table 4.1. Main indexes and values achieved during the first step of the study

Material	ε_{max} %	ε_{fix} %	ε_{res} %	R_f	R_r	σ_{max} [MPa]	$\sigma_{recovery}$ [MPa]	$\sigma_{rec(\%)}$
FLPI	46.1	40.5	1.7	0.878	0.96	1.12	0.77	68.75
FLPI A40	44.85	39.32	2.91	0.877	0.93	0.165	0.1	60.6
Jera G117f	45.33	39.76	1.193	0.877	0.97	0.75	0.56	74.67

Starting from these values it is possible to conclude that, the three materials are very similar in terms of ability to keep the fixed temporary shape. As a matter of fact, strain fixity rate R_f assumes very similar values.

Regarding the recovered shape, Jera G117f offers the best performance. However, also FLPI is particularly interesting from this point of view and furthermore, it is able to reach very high values of stresses despite being above melting temperature.

However, the most interesting parameter for the purpose of the present work is represented by the percentage of the maximum stress the material is able to recover thanks to its shape memory properties.

Regarding this feature, FLPI recovers the 68,75% of the maximum stress reached while Jera G117f goes back to the 74,66% of the maximum stress which was already pretty high.

In conclusion FLPI A40 is confirmed to be the less performing material also in respect to this parameter. The recovered stress is indeed just the 60,6 % of the maximum, which was particularly low.

Despite all the encouraging aspects underlined, through this first group of results some issues emerged about test bench. As a matter of fact some little defects of the system compromised slightly the quality of results or made difficult to treat data. The description of these problems and their solution attempts will be the focus of next section.

In conclusion. This first step on the one hand resulted encouraging about machine's reliability, on the other, it allowed to identify some of the aspects that still limited the system.

4.1.2 Machine optimization

The issues identified after the first approach and the corresponding solutions are basically three and they will be exposed in the following sections.

4.1.2.1 Reflective shield

The first problem found is not directly deducible from the obtained trends. As a matter of fact it is related to the heating source.

At the end of tests, the sample showed on its surface something like the effects of aging typical of polymers when exposed to intense direct radiation.

Specimens appeared shrunken and more prone to breakage during traction.

The cause of this effect was immediately attributed to the direct exposition to halogen lamp radiation. As a matter of fact, the heating source was fixed to the inner side of one door. This means that nothing is interposed between sample and direct radiation. Moreover, after climatic chamber closure, the position of the lamp is really close to the specimen. The temperature of lamp's main body can go up to 800°C and the intensity of the emitted radiation is particularly high. These factors are probably the origin of sample's degradation process.

The solution though is really simple and intuitive and consists in interposing a thin layer made up of aluminum between sample and heat source. This component, observable in

Figure 2.30, was supposed to reflect the radiation emitted by lamp, in order to invest the sample with an indirect radiation which results less severe for the polymer.

This solution resulted particularly effective. The aging effect on samples was strongly reduced. Despite the exposition to high temperatures in the climatic

chamber, specimens were still able to perform several other cycles without any risk of breakage.

4.1.2.2 Glass paper

Observing all the first graphs obtained, it is possible to notice some unexpected steps during cooling phase. For example, considering the trend obtained during the strain recovery test performed on Jera G117f , some discontinuities are observable at the end of cooling phase, as underlined in

Figure 4.7. These irregularity can't be explained neither with some electrical interference nor with the behavior of the material.

As a matter of fact, it is normal that stress level decrease during cooling phase but it is supposed to do it in a continuous way. The temporary shape is progressively fixed through cooling. The material adapts itself to this new elongated shape and stronger links are created among polymer's chains. The latter prevent sample to go back to original contracted shape. This results in a progressive decrease of force exerted by sample at the extremities. The latter doesn't go to zero during this phase because it is impossible to fix all the deformation. As a matter of fact, after releasing one extremity of the sample a little percent of the strain is recovered. The described dynamics is supposed to cause a progressive continuous decrease in stress signal and not steps.

It was then tough that the origin of this effect was related to a loss of grip in the devices supposed to keep firmly the polymeric film. The latter grab the specimen by closing two plates with a smooth surface. It is then not surprising if a loss of grip occurs when polymer is cooled down and reduce slightly its dimensions.
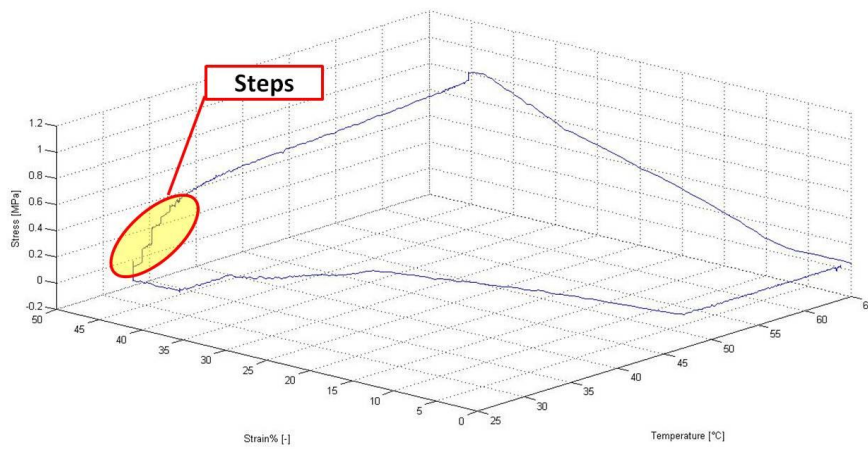
Figure 4.7. Unexpected steps at the end of cooling phase during a strain recovery cycle performed on Jera G117f using a stroke of 10 mm

It was then tough to provide the above-mentioned plates with a layer of glass paper glued on the inner side (the one in contact with sample).
Figure 4.8 is an image of the optimized component.
Once this solution was implemented the adherence between the polymer and gripping device's internal surface was effectively improved. However the problem was not completely eliminated. Little discontinuities occurred also in some subsequent test.
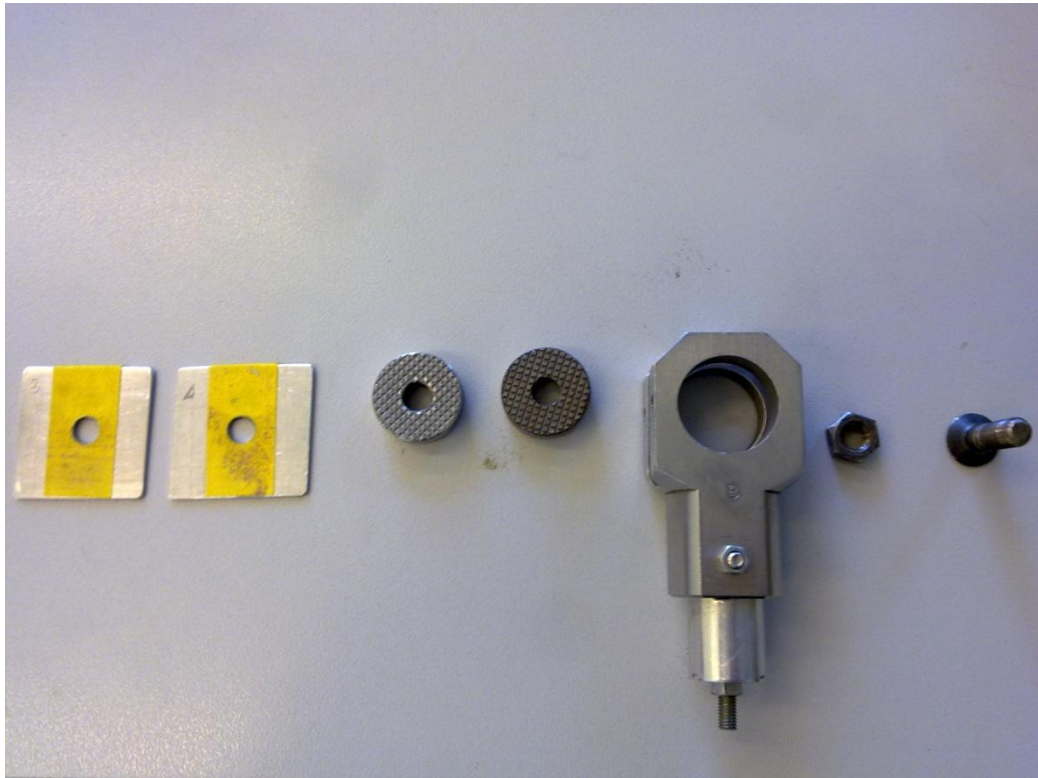
Figure 4.8. Gripping device after the application of glass paper on the inner side of aluminum plates

4.1.2.3   Opaque background

As explained in 63Chapter 3, the data related to elongation and temperature were manually extracted by the images took through Python. In particular, using Python fourth script, it is possible to get the distance between two stripes printed on the sample, defining its sensitive zone.

This procedure is repeated image by image and requires that black stripes are well distinguishable on sample's surface. During this first group of tests it was realized that the images took by the camera were not really clear due to the light reflected by insulating material's inner surface. This made really hard to process the first data sets because of the difficulty in identifying the black stripes.

The solution worked out for this problem was simple but effective. The latter consisted in attaching an opaque surface on the inner side of the insulating material, exactly behind the sample. This expedient improved the quality of the images and made simpler to identify the position of black stripes on sample's surface.

Figure 4.9 is one of the images took by the camera during a test after the application of the opaque background.

Figure 4.9. Image took by the camera during a test after the application of an opaque layer behind the sample

4.1.3   Results repeatability

Once machine's reliability and results' quality was improved through the expedient presented in the previous section, a study about the repeatability of results was retained necessary. This kind of analysis was aimed to evaluate the capability of the machine to provide similar results starting from the same initial conditions.

In practice, several tests were performed on the same material and every time using a new sample. The fact that the sample was new for each test ensured the equality in the initial conditions of the procedure. Obviously all the other conditions were kept constant from one test to another. In particular:

- Material: FLPI
- Temperature range: $25°C \div 65°C$
- Motor stroke: 20 mm
- Test type: stress recovery cycle

After the first group of results obtained, FLPI was retained particularly interesting due to its mechanical and shape memory properties. This material

was then retained a good candidate for this second step of the whole study. An intermediate stroke was adopted in this phase.

The following three images show the results of this repeatability study. Despite the trend around zero stress condition (which is always confused due to the disturb introduced by the operator opening gripping device), the graph obtained are strongly similar and surely comparable.
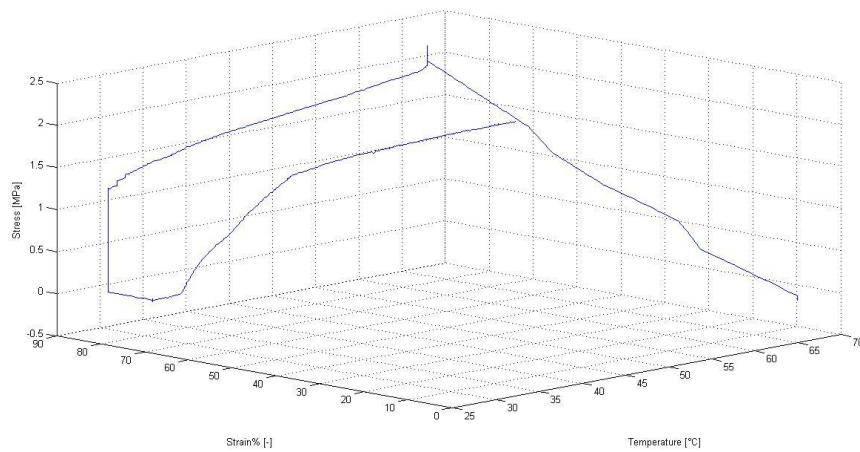

Figure 4.10. Repeatability study, first trend obtained: stress recovery cycle performed on FLPI with a stroke of 20 mm
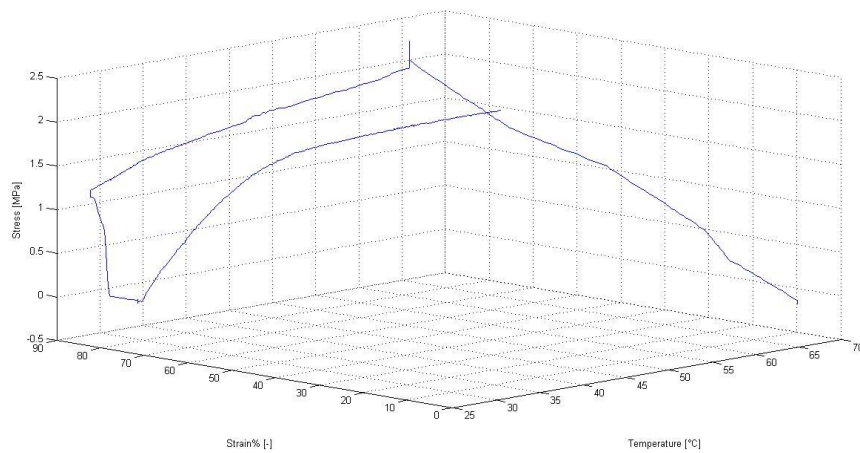
Figure 4.11. Repeatability study, second trend obtained: stress recovery cycle performed on FLPI with a stroke of 20 mm
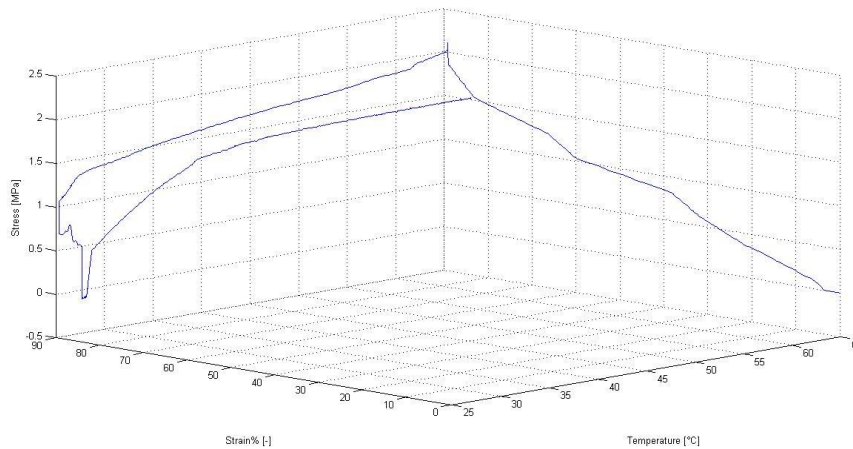
Figure 4.12. Repeatability study, third trend obtained: stress recovery cycle performed on FLPI with a stroke of 20 mm

Table 4.2 contains for each sample tested the value of the maximum stress reached during traction phase at high temperature, the stress recovered, the corresponding percentage of the maximum stress and finally strain fixity rate.

Table 4.2. Main results and indexes achieved during repetability study

Number of sample	σ_{max} [MPa]	$\sigma_{recovered}$ [MPa]	$\sigma_{rec(\%)}$	R_f
1	2,234	1,325	59.31	0.8788
2	2,246	1,363	61	0.8777
3	2,212	1,371	61.98	0.8799

Starting from the values listed in Table 4.2 and trends presented in the previous images, it is possible to conclude that test bench's results are characterized by a good repeatability.

The slight differences among the presented results could be associated to the fact that in some phases of a test the user have to get in contact with the sample and move the system. This causes a random effect in the results (human factor) which is particularly evident around zero stress condition (sample manually released from bottom gripper).

Another source of results dispersion are the differences in composition and shape of samples due to manufacturing process. The latter is not ideal and unable to avoid completely defects or differences among synthesized specimens.

4.2 Strain improvement and materials' features study

At this point of the work the machine resulted optimized and characterized in its features and limits. It was then possible to keep on with the study about shape memory polymers. The following step consisted in improving the elongation imposed to sample. Larger strokes of the motor were then investigated. In particular the following configurations were tested:
- Motor stroke: 30 mm
- Motor stroke: 40 mm
- Motor stroke: 50 mm

The first of the listed configurations (30 mm) was extended really to all six available families of materials. However it was not possible to bring to an end the analysis with all of them. As a matter of fact, due to the same problems introduced in section 4.1.1, it was impossible to carry out a study about FLPI A46. Moreover samples made up of FLPI and Jera G117e broke during the test. These three materials had to be discarded for the rest of the study. This was an important loss, because FLPI showed very promising properties until this point.

The number of families to be analyzed was then reduced to three:
- FLPI A40
- Jera G117c
- Jera G117f

For each family a strain recovery cycle and a stress recovery one were performed. The resulting graphs are presented in the following set of images.
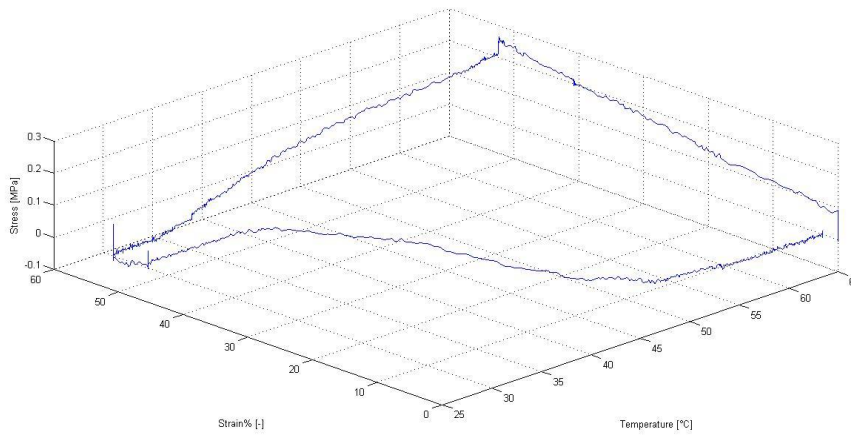The first couple of images is related to FLPI A40.

Figure 4.13. Strain recovery cycle performed on FLPI A40 using a motor stroke of 30 mm
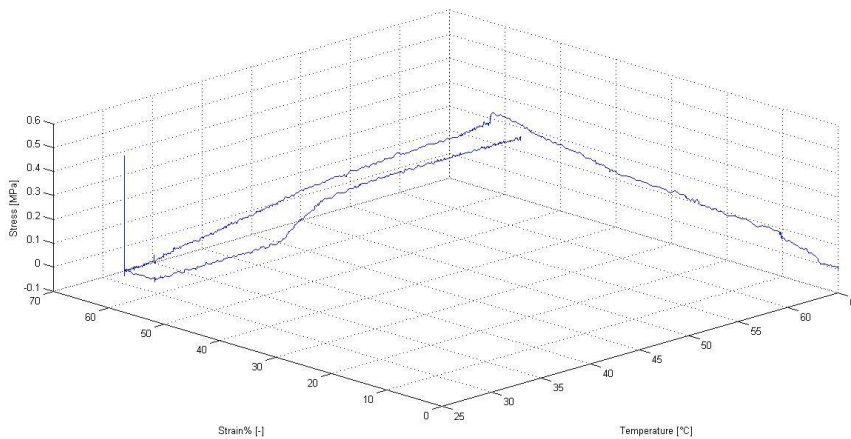

Figure 4.14. Stress recovery cycle performed on FLPI A40 using a motor stroke of 30 mm

Already from these graphs it is possible to notice that the maximum level of stress reached with this material is still low, despite the improvement of motor stroke. As a matter of fact this material results particularly soft at high temperatures.
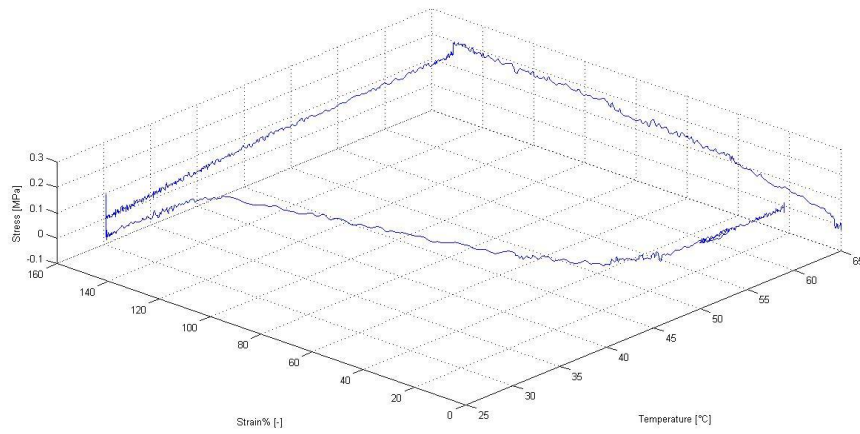The second set images are the trends obtained using Jera G117c.

Figure 4.15. Strain recovery cycle performed on Jera G117c using a motor stroke of 30 mm
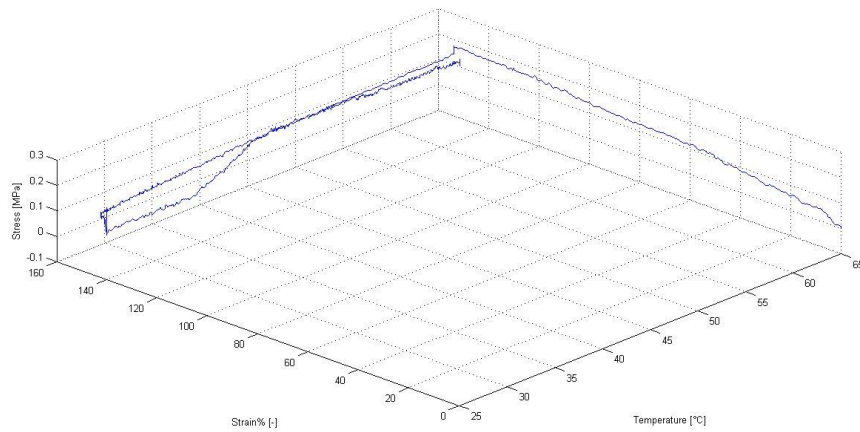

Figure 4.16. Stress recovery cycle performed on Jera G117c using a motor stroke of 30 mm

The results achieved in terms of maximum stress with this material are even worse than the ones obtained with FLPI A40.
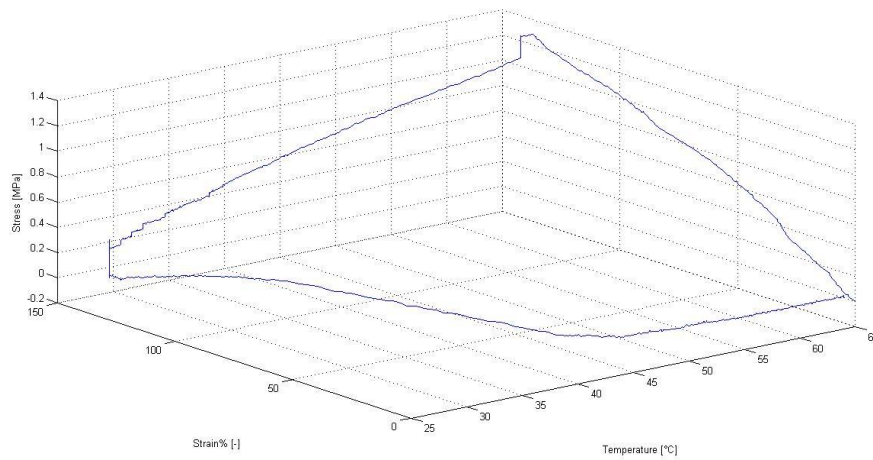The last couple of images are strain and stress recovery cycles performed on Jera G117f.

Figure 4.17. Strain recovery cycle performed on Jera G117f using a motor stroke of 30 mm
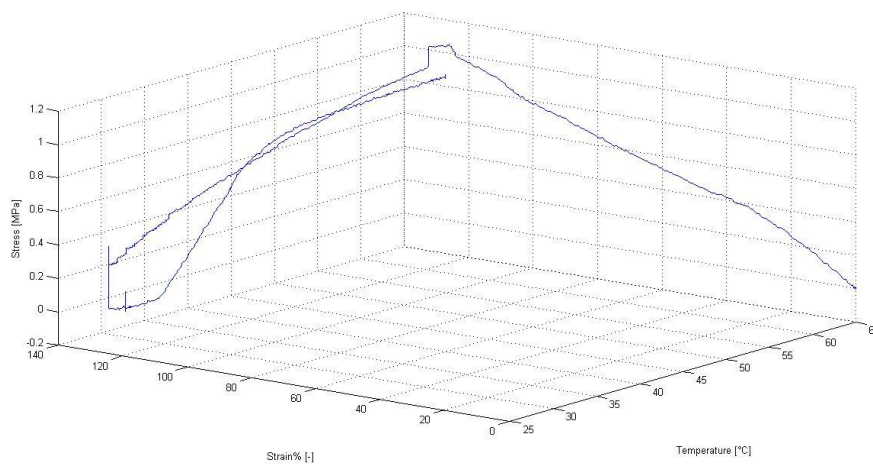

Figure 4.18. Stress recovery cycle performed on Jera G117f using a motor stroke of 30 mm

As it was during the first approach, Jera G117f is confirmed to be a very performing material in terms of maximum stress reached during traction. This material is indeed particularly hard, but at the same time able to undertake high deformations.

The following Table 4.3 resumes all the main indexes calculated starting from tests results and some of the values extracted by obtained trends.

Table 4.3. Main values and indexes extracted by strain and stress recovery cycles using a 30 mm stroke of the motor

Material	ε_{max} %	ε_{fix} %	ε_{res} %	R_f	R_r	σ_{max} [MPa]	$\sigma_{recovered}$ [MPa]	$\sigma_{rec(\%)}$
FLPI A40	145.38	130.12	8.11	0.895	0.94	0.23	0.154	66.95
Jera G117c	151.6	151.3	22.16	0.998	0.85	0.175	0.141	80.57
Jera G117f	142.3	137.4	5.159	0.965	0.96	1.054	0.849	80.55

Despite Jera G117f doesn't show the best performances in terms of shape fixity and recovery, it is able to reach and then recover very high values of stresses. This is what makes the material particularly appealing for the present project. As a matter of fact, in the final ARC PREDICTION project application, it is important to ensure a proper open and close mechanism through the activation of material contraction or elongation, but above all, it is essential to develop a force high enough to win the pressure exerted by human body internal tissues. From this point of view, the most interesting index is the maximum stress recoverable after fixing a particular elongation. Obviously the maximum reached and recovered stress are directly proportional to the imposed elongation. However as emerged up to now from tests, some materials have higher Young's modulus than others and they reach stress levels that are more than twice the one of other materials. It is the case of Jera G117f compared with FLPI A40 or Jera G117c.

Moreover it is important to consider the fact that sometimes, material's high Young's modulus is associated to an inability of the polymer to undergo large deformations. It is for example the case of FLPI.

All these aspects were considered in order to identify the most suitable material for the final application in ARC PREDICTION project bronchoscope.

At this point the following step consisted in improving the deformation imposed to sample until the limit of tensile strength at high temperatures. For this purpose motor stroke was increased by 10 mm for a total of 40 mm.

Unfortunately all the material tested with this configuration broke during test, exception made for Jera G117f. It is then possible to assume that this level of elongation represent an upper bound for the most part of the studied polymers.

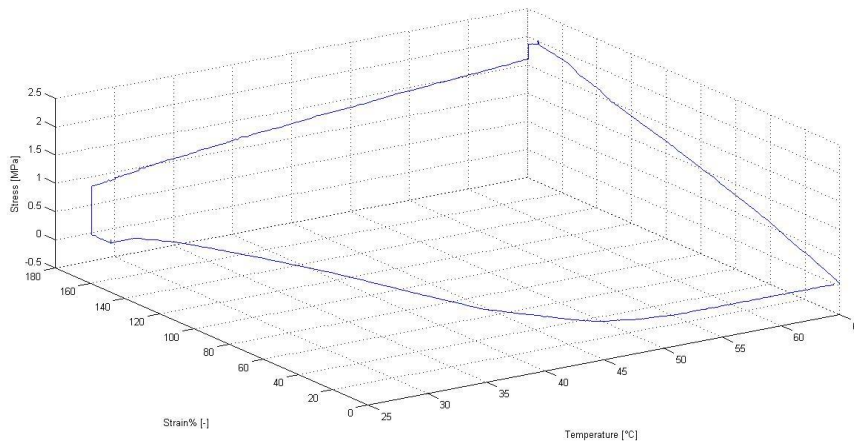Regarding Jera G117f the obtained results are listed in the following two images.

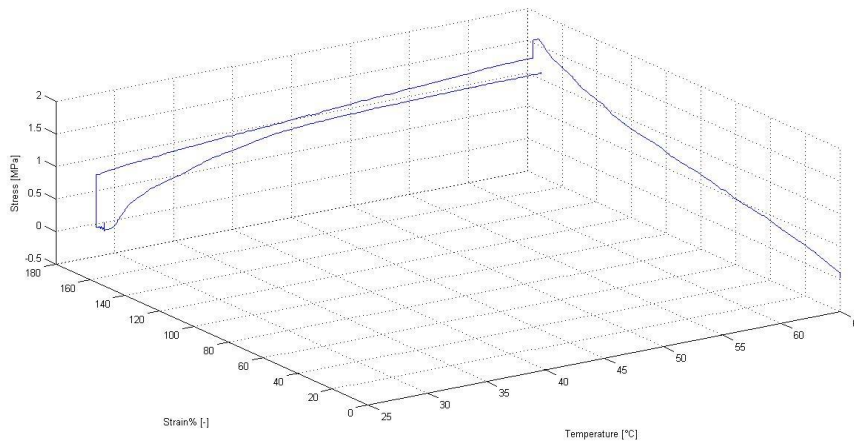**Figure 4.19. Strain recovery cycle performed on Jera G117f using a motor stroke of 40 mm**

Figure 4.20. Stress recovery cycle performed on Jera G117f using a motor stroke of 40 mm

The following Table 4.4 gathers the main indexes and values obtained during this phase.

Table 4.4

Material	ε_{max} %	ε_{fix} %	ε_{res} %	R_f	R_r	σ_{max} [MPa]	$\sigma_{recovered}$ [MPa]	$\sigma_{rec(\%)}$
Jera G117f	179.5	168.5	3.5	0.94	0.98	1.61	1.084	67.33

This last set of data confirms the high performances of Jera G117f. This material is indeed able to reach and recover very high stresses and despite its high Young's modulus, it is able to undergo very high strains. For example in this last couple of tests, the strain level reached is almost 200%.

It is noteworthy that, focusing on Jera G117f, while not big changes can be underlined in strain fixity rate R_f and strain recovery rate R_r from a data set to the other, in this last data set it is possible to observe a decrease in the percent of maximum stress recovered.

The last step of this section consisted in a further increase of the deformation imposed by adopting the maximum stroke available (50 mm).

None of the materials families get to undergo this maximum elongation without breaking.

In conclusion, this section of the study resulted very useful to identify the most performing materials in terms of:

- Ability to memorize a temporary shape
- Ability to recover completely the original permanent shape
- Ability to reach high levels of stress
- Ability to recover the maximum stress reached during traction phase
- Ability to undergo large elongations

As already introduced, the last two indexes are the most interesting for the present project because they determine strongly the suitability of the material for the final application. It is indeed impossible to think about adopting a material unable to provide large deformations and to win the forces exerted by the external environment.

Regarding these aspects Jera G117f showed surely the most performing behavior. It could then be assumed as suitable for the actual application.

4.3   Fatigue study

The last step of this work consisted in a study aimed to evaluate the eventual occurrence of a decrease in material's shape memory and mechanical properties after performing several cycles. As a matter of fact, during the previous study, dedicated to the analysis of different elongations, stress recovery cycle was always performed after strain recovery one using the same sample. In some of these couple of test, a slight difference between the maximum stress reached was observed between results. These aroused suspicion about the possibility of a decrease of shape memory properties of the material through the usage.

In order to verify this eventuality a tailored study was performed. The latter regarded three of the materials available in particular the ones that during the

first part of the study showed some appealing features in terms of shape recover, elongation underwent and maximum stress reached and recovered. The materials chosen were:

- FLPI
- Jera G117c
- Jera G117f

The configuration of the test adopted was the same for all the materials and previewed to use a 20 mm stroke of the motor performing three stress recovery cycles for each material. The sample used was obviously the same from a cycle to another (otherwise it would be impossible to evaluate the decrease of properties).

Hereunder all the graphical results achieved will be presented in a row. Afterwards some numerical results will be discussed.
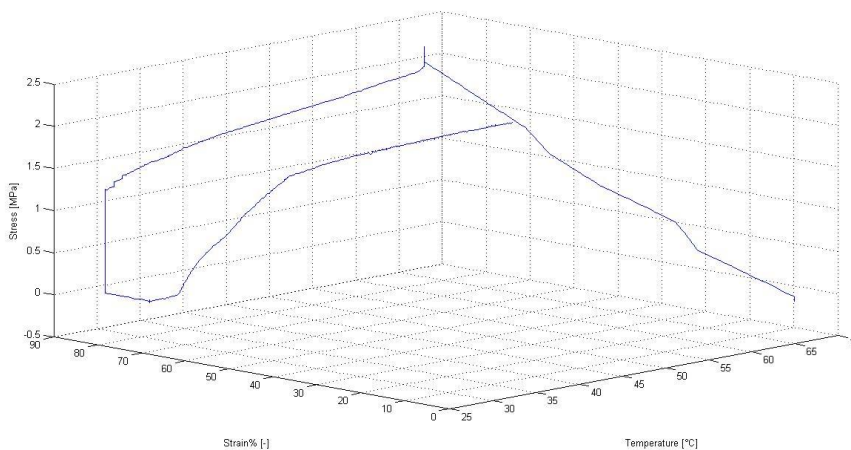
The first group of images is related to FLPI.

Figure 4.21. Properties decrease study: first stress recovery cycle performed on FLPI using a stroke of the motor equal to 20mm
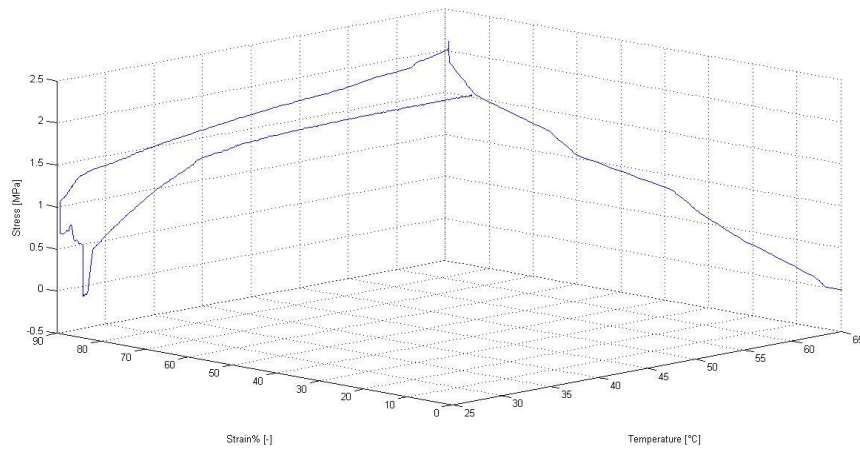
Figure 4.22. Properties decrease study: second stress recovery cycle performed on FLPI using a stroke of the motor equal to 20mm
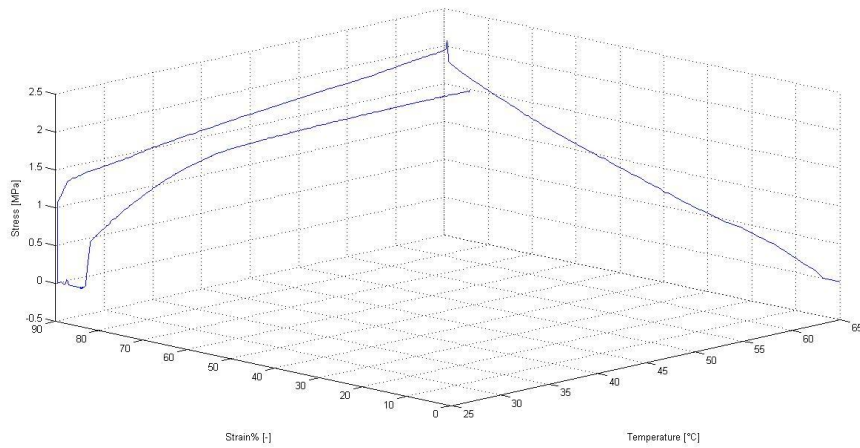

Figure 4.23. Properties decrease study: third stress recovery cycle performed on FLPI using a stroke of the motor equal to 20mm

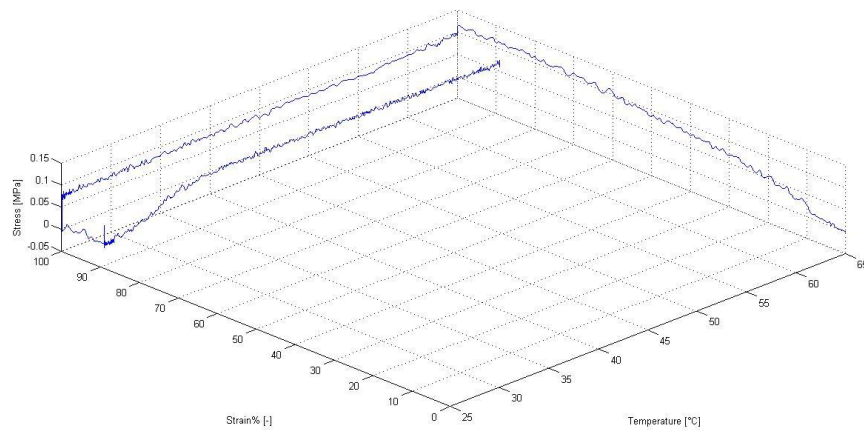The second set of graphs will start now and it is related to Jera G117c.

Figure 4.24. Properties decrease study: first stress recovery cycle performed on Jera G117c using a stroke of the motor equal to 20mm
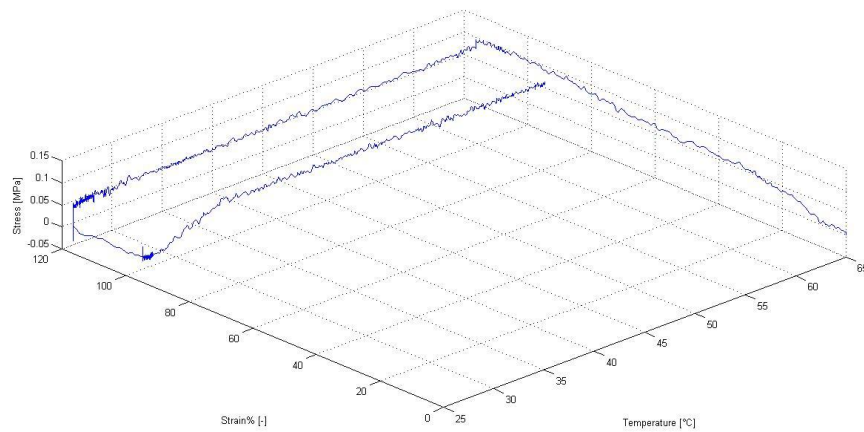

Figure 4.25. Properties decrease study: second stress recovery cycle performed on Jera G117c using a stroke of the motor equal to 20mm
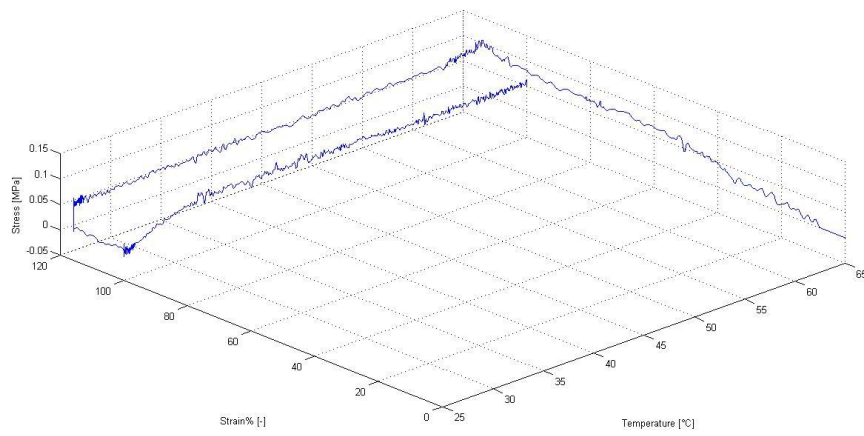
Figure 4.26. Properties decrease study: third stress recovery cycle performed on Jera G117c using a stroke of the motor equal to 20mm

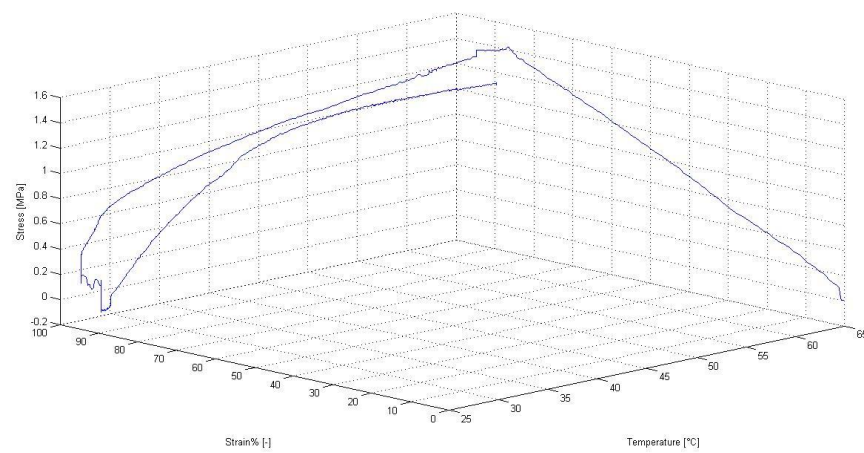The last dataset, related to Jera G117f, will be now presented.

Figure 4.27. Properties decrease study: first stress recovery cycle performed on Jera G117f using a stroke of the motor equal to 20mm
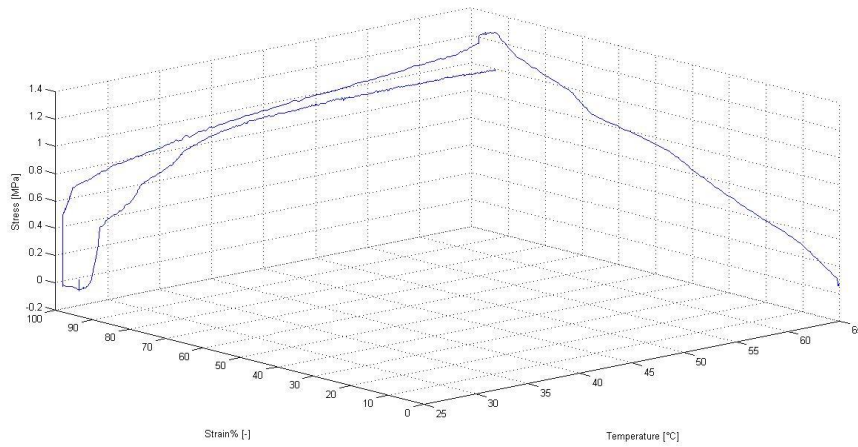
Figure 4.28. Properties decrease study: second stress recovery cycle performed on Jera G117f using a stroke of the motor equal to 20mm
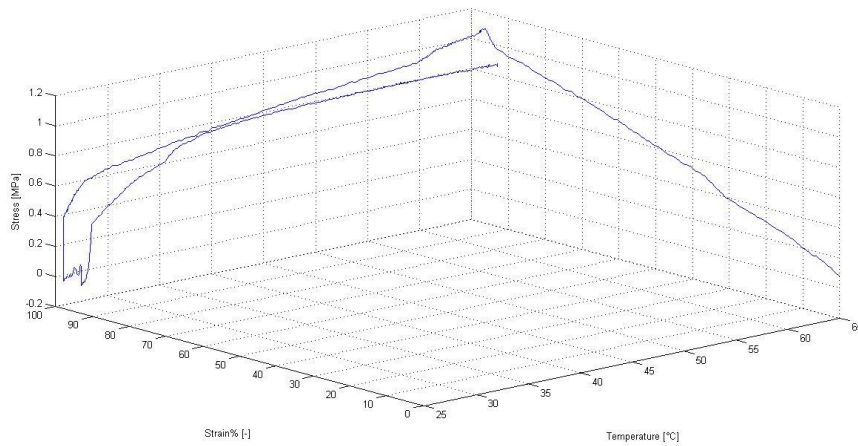
Figure 4.29. Properties decrease study: first stress recovery cycle performed on FLPI using a stroke of the motor equal to 20mm

The following phase of this study consisted in extracting from trends the values of maximum stress reached and the level of stress recovered. Afterwards, as already done in the previous sections, the percent of the maximum stress recovered was simply calculated as explained in equation (4.1).
The results are listed in the following Table 4.5.

Table 4.5. Main indexes obtained during fatigue study

Material	Index	1st cycle	2nd cycle	3rd cycle
FLPI	σ_{max} [MPa]	2.234	2.112	2.085
	σ_{rec} [MPa]	1.325	1.515	1.471
	$\sigma_{rec(\%)}$	59.31	71.73	70.50
Jera G117c	σ_{max} [MPa]	0.118	0.097	0.102
	σ_{rec} [MPa]	0.072	0.064	0.057
	$\sigma_{rec(\%)}$	61.02	65.43	56.18
Jera G117f	σ_{max} [MPa]	1.424	1.266	1.089
	σ_{rec} [MPa]	1.148	0.998	0.878
	$\sigma_{rec(\%)}$	80.62	78.83	80.62

We will now focus on $\sigma_{rec\,(\%)}$ observing its trend from a test to another, in order to identify the eventual presence of a decrease in polymer's shape memory properties. In the following images (
Figure 4.30,
Figure 4.31 and
Figure 4.32), the trend of $\sigma_{rec\,(\%)}$ during cycles is plotted for each sample. While Figure 4.33 is a three-dimensional histogram comparing the results obtained for the three materials in terms of $\sigma_{rec\,(\%)}$ in each cycle.

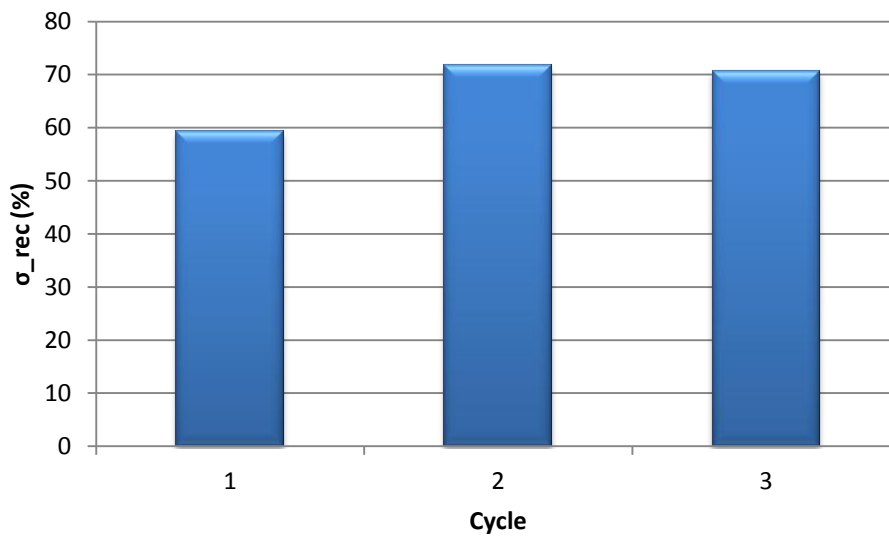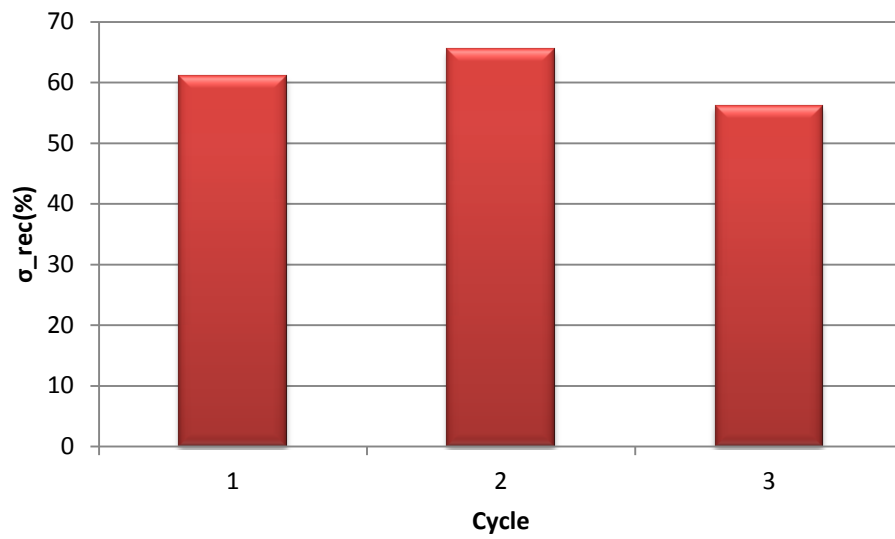**Figure 4.30. Trend of $\sigma_{rec(\%)}$ from cycle 1 to 3 related to FLPI**

Figure 4.31. Trend of $\sigma_{rec(\%)}$ from cycle 1 to 3 related to Jera G117c
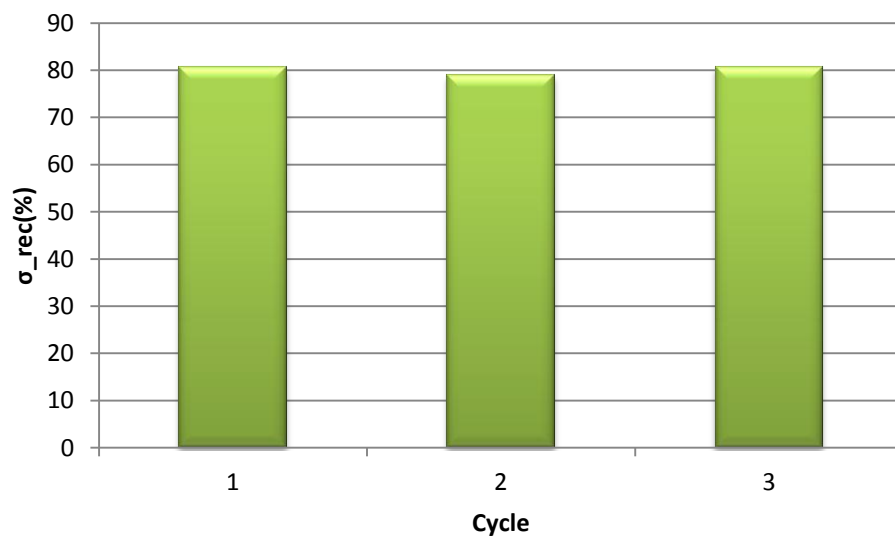

Figure 4.32. Trend of $\sigma_{rec(\%)}$ from cycle 1 to 3 related to Jera G117f
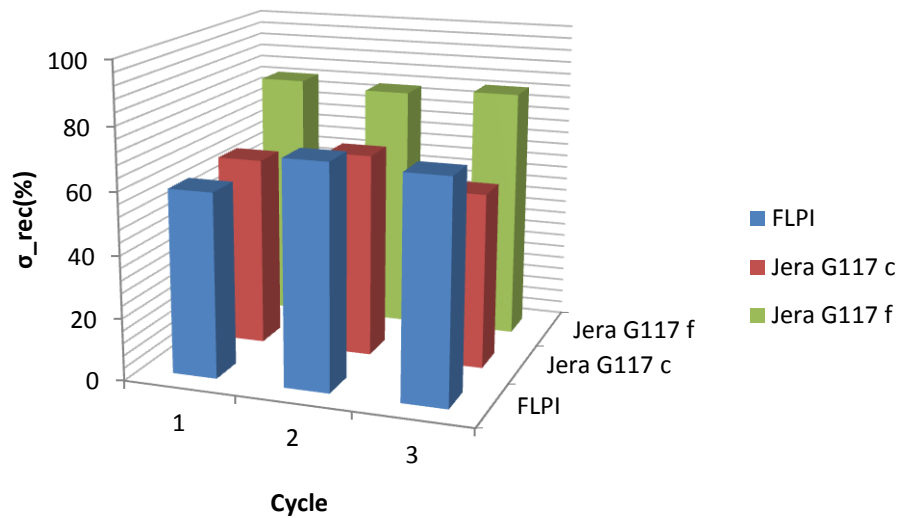
Figure 4.33. Comparison of $\sigma_{rec(\%)}$ values among FLPI, Jera G117c and Jera G117f obtained during fatigue study

 Starting from the last set of images, it is possible to observe that $\sigma_{rec\,(\%)}$ is subject to slight variations for all the materials analyzed. However these variations can't be associated to an actual decrease. As a matter of fact, $\sigma_{rec\,(\%)}$ values move around an average and do not decrease continuosly.

It is then possible to assume that shape memory properties, are not subjected to a deterioration in the short term. The data set analyzed is indeed significant just for the short term because only few cycles were performed with the same sample.

Furthermore Jera G117f, as happened for several other sections of this study, provides the most performing behavior. As a matter of fact, its $\sigma_{rec\,(\%)}$ values are the highest among the three materials and they are particularly stable during tests.

In conclusion, this section underlines the fact that shape memory polymers are not subjected to a decrease in their properties, at least when used for few cycles. Moreover this last data set confirms the really good properties provided by Jera G117f. Indeed this material provided the highest values of $\sigma_{rec\,(\%)}$ which moreover resulted particularly stable in the cycles performed.

Conclusions and possible optimizations

At the end of this path through the main steps of the present work, it is possible to come to the following conclusions.

The long and articulate design process that led until the last and actual version of the bench provided a really effective and reliable instrument for the analysis of heat actuated shape memory polymers. As a matter of fact, starting from a literature inspired solution, some innovative aspects were worked out in order to optimize this kind of system. The most important one is the adoption of a contactless measuring system that, through the usage of a conventional camera and a Python script, makes it possible to rebuild the elongation of samples' sensitive zone.

Starting from the obtained results, several information on shape memory polymers were gathered. In particular, it was possible to identify the most performing materials in terms of mechanical and shape memory properties. Among all, Jera G117f showed the best performances, especially in terms of maximum stress reached and recovered. Moreover, the latter was the only material able to undergo strains up to almost 200%.

All this information resulted particularly useful for the identification of the most suitable material for ARC PREDICTION project application.

In conclusion, it is important to underline the limits of the system assembled and the aspects that can further be optimized.

In particular, as explained in the previous chapters, the data processing is carried out manually. This implies that this phase is particularly time expensive. A possible improving solution could be the automation of a dedicated tracking system able to recognize the position of a moving object. Such a technology would, for example, allow following the displacement of the two stripes printed on sample's surface, in order to monitor and record the elongation of the material in real time.

Another aspect that could be optimized is the control of the climatic chamber temperature. In fact, up to now this operation is performed manually. It would be desirable to automate it through a proper control loop and synchronize it with the rest of the system.

Nomenclature and list of acronyms

ULB   Université Libre de Bruxelles
BEAMS   Bio Electro and mechanical systems
SMPs   shape memory polymers
IR   infrared

Bibliography

[1]   Yiping Liu, Ken Gall, Thermomechanics of shape memory polymers: Uniaxial experiments and constitutive modeling, *International Journal of Plasticity* (2004)

[2]   Y.C. Lu, J.T. Fulcher, Microscale thermomechanical characterization of environmentally conditioned shape memory polymers, *Polymer Testing* (2011)

[3]   A. Lendlein, H. Jiang, Light induced shape memory polymers, *Letters to Nature* (2005), pp. 879-882

[4]   T. S. Wilson, Ward Small IV, Shape memory polymer therapeutic devices for stroke (2005)

[5]   J.T. Fulcher, Y.C. Lu, Thermomechanical characterization of shape memory polymers using high temperature nanoindentation (2010)

[6]   B. Atli, F. Gandhi, Thermomechanical characterization of shape memory polymers. *Journal of Intelligent Material Systems and Structures* (2008)

[7]   B. Volk, Characterization of shape memory polymers

[8]   S. Passera, Characterization and tailoring of the shape memory behavior of polymeric materials for biomedical applications, PhD Thesis (2011)

[9]   Peixi Yuan, Biodegradable shape memory polymers, Literature Seminar (2010)

[10]   Andrew A Sharp, Hrishikesh V Panchawagh, Towards a self-deploying shape memory polymer neuronal electrode, *Journal of neuronal engineering* (2006)

[11]   W. Sokolowski, Medical applications of shape memory polymers, *Biomedical materials* (2007)

[12]   Ward Small, IV, Pooja Singhal, Biomedical applications of thermally activated shape memory polymers, *Journal of Materials Chemistry* (2010)

[13]   Christopher M. Yakacki, R. Shandas, Uncostrained recovery characterization of shape memory polymer network for cardiovascular applications, *Biomaterials,* (2007)

[14]   Patrick R. Buckley, Gareth H. McKinley, Inductively heated shape memory polymer for the magnetic actuation of medical devices (2006)

[15]   J.M. Ortega, W. Small, A Shape Memory Polymer Dialysis Needle Adapter for the Reduction of Hemodynamic Stress within Arteriovenous Grafts, *Institute of electrical engineers transactions in biomedical engineering* (2006)

[16]   J. Xu, J. Song, Thermal responsive shape memory polymers for biomedical applications (2011)

[17]   A.Lendlein, S. Kelch, Shape memory polymers, *Angewandte chemie*

[18]   ASTM International D638-10, Standard test method for tensile properties of plastic

[19]   F.M. Schmidt, Y. Le Maoult, S. Monteix, Modelling of infrared heating of thermoplastic sheet used in thermoforming process, *Journal of Materials Processing Technology* (2003)

[20]   F. Quadrini, L. Santo, V. Tagliaferri, F. Trovalusci, An IR molding system for direct shaping of thermoplastics, *Polimer Engeneering and ScienceI* (2010)

[21]   F. Quadrini, L. Santo, V. Tagliaferri, F. Trovalusci, Plastic shaping by means of IR heating and direct pellet molding, *Polimer Engeneering and Science* (2006)

[22]   A. Bernasconi, M. Filippini, M. Giglio, Fondamenti di costrizione di macchine, McGraw-Hill (seconda edizione)

[23]   E. O. Doeblin, Strumenti e metodi di misura, McGraw-Hill

[24]   A. Brunelli, Strumenti per la misura di grandezze meccaniche e fisiche, GISI

[25]   A. Cigada, L. Comolli, S. Manzoni, Appunti di estensimetria elettrica, Cittastudi/UTET

[26]   http://en.wikipedia.org/wiki/PEEK

[27]   B. Martens, B. De Leener, Robust structured light pattern for use with a spatial light modulator in 3-D endoscopy, *International Journal of Optomechatronics*, (2013)

[28]   MengChao Ma, XiangCheng Chen, Camera calibration by using fringe patterns and 2D phase-difference pulse detection, *Optik* (2013)